



Jasmin Handl BSc.

# **Optimization of organic/inorganic tin halide perovskite solar cells**

Master Thesis

to achieve the university degree

Diplom Ingenieur

Master program Technical Chemistry

submitted to

University of Technology Graz

Supervisor

Assoc. Prof. DI Dr. Gregor Trimmel

Institute for Chemistry and Technology of Materials

University of Technology Graz

## **AFFIDAVIT**

I declare under oath that I wrote the present thesis independently and I have not used any sources and aids other than stated with quotations duly marked as such. The uploaded thesis at TUGRAZonline is identical to the present Master Thesis.

## **EIDESSTATTLICHE ERKLÄRUNG**

Ich erkläre an Eides statt, dass ich die vorliegende Arbeit selbstständig verfasst, andere als die angegebenen Quellen/Hilfsmittel nicht benutzt, und die den benutzten Quellen wörtlich und inhaltlich entnommenen Stellen als solche kenntlich gemacht habe. Das in TUGRAZonline hochgeladene Textdokument ist mit der vorliegenden Masterarbeit identisch.

**Graz, am** \_\_\_\_\_

\_\_\_\_\_

## Abstract

Tin-based perovskite solar cells gained a lot of attention in the past few years, as they are a promising alternative to lead-based perovskite solar cells. Tin based perovskite materials have excellent optoelectronic properties and are structurally similar to lead based perovskite materials. However one main disadvantage of tin based perovskite materials is the easy oxidation of  $\text{Sn}^{2+}$  and low reproducibility of Sn-based perovskite solar cells. Therefore up to now the maximum power conversion efficiency with up to 9% for tin based perovskite solar cells is lower compared to lead based ones with up to 22%. This study deals with the optimization of tin-based perovskite solar cell fabrication to enhance the solar cell performance and make it more stable. Solar cells with an inverted device architecture (glass/ indium doped tin oxide/ poly(3,4-ethylenedioxythiophene)-poly(styrenesulfonate)(PEDOT:PSS)/ Sn-based perovskite/ [6,6]-phenyl-C61-butyric acid methyl ester ( $\text{PC}_{60}\text{BM}$ )/ Al) are prepared with a mixed organic-cation  $(\text{Methylammonium})_{0.75}(\text{Formamidinium})_{0.15}(\text{Phenylethyl ammonium})_{0.1}\text{SnI}_3$  perovskite. The easy oxidation from  $\text{Sn}^{2+}$  to  $\text{Sn}^{4+}$  is a major problem, as it leads to a higher probability of recombination and therefore to a worse solar cell performance. Hence the purchased  $\text{SnI}_2$  (purity 99.99%) is further purified using different purification methods, whereas purification in a tube furnace (sublimation) is the method of choice. Because of this high sensitivity towards oxidation and water as well as the fast crystallisation behaviour, the preparation of Sn-based perovskite solar cells is not well reproducible and the optimization of the preparation steps of the solar cell is a key issue and has a huge influence on the solar cell performance. First, an anti-solvent dropping is studied and optimized to enhance the formation of the perovskite films. Additional parameters that influence the solar cell performance are the film thickness of the perovskite layer as well as the  $\text{PC}_{60}\text{BM}$  layer. An optimization of these layers is achieved via variation of the spin coating rate, variation of the annealing step and different concentrations of the perovskite precursor solution. Through the optimization of the solar cell preparation a maximum power conversion efficiency of 6.4% can be achieved with a fill factor of 62.4%, an open circuit voltage of 0.48 V and a short circuit current of  $21.69 \text{ mA cm}^{-2}$ . In addition it was found that the introduction of a phenylethyl ammonium iodide layer between the PEDOT: PSS and perovskite layer can have a positive effect on the solar cell performance. The addition of  $\text{CuBr}_2$  to the perovskite was further investigated, which should lead to a better stability and an improved solar cell performance, however this positive effect was not observed in this study and the introduction of  $\text{CuBr}_2$  leads to a deterioration of the performance.

## Kurzfassung

In den letzten Jahren haben Zinn-basierte Perowskit-Solarzellen viel an Aufmerksamkeit gewonnen, da diese eine vielversprechende Alternative zu Blei-basierten Perowskit-Solarzellen sind. Zinn-basierte Perowskitmaterialien haben sehr gute optoelektronische Eigenschaften und sind Blei-basierten Perowskitmaterialien strukturell ähnlich. Jedoch stellen die leichte Oxidation von  $\text{Sn}^{2+}$  und die schlechte Reproduzierbarkeit einen großen Nachteil dar. Daher konnte bis jetzt nur eine maximale Effizienz von 9% für Zinn-basierte Perowskit-Solarzellen erreicht werden, welche deutlich niedriger ist als jene für Blei-basierte Perowskit-Solarzellen mit 22%. Daher beschäftigt sich diese Arbeit mit der Optimierung des Herstellungsprozesses von Zinn-Perowskit-Solarzellen, um diese in ihrer Performance und Stabilität zu verbessern. Die Solarzellen werden in einem invertierten Aufbau (Glas/ Indiumzinnoxid/ Poly-3,4-ethylendioxythiophen / Zinn-basierter Perowskit/ 1-[3-(Methoxycarbonyl)propyl]-1-phenyl-[6.6]C<sub>61</sub>/ Al) hergestellt, wobei  $\text{MA}_{0.75}\text{FA}_{0.15}\text{PEA}_{0.1}\text{SnI}_3$  ( $\text{MA}^+$  = Methylammoniumkation,  $\text{FA}^+$  = Formamidiniumkation,  $\text{PEA}^+$  = Phenylethylammoniumkation) als Perowskit-Material verwendet wird. Die schnelle und einfache Oxidation von  $\text{Sn}^{2+}$  zu  $\text{Sn}^{4+}$  stellt das größte Problem dar, da dies zu einer größeren Wahrscheinlichkeit einer Rekombination führt und dadurch die Performance der Solarzelle negativ beeinflusst wird. Deshalb wird das gekaufte  $\text{SnI}_2$  (Reinheit von 99,99%) weiter auf-gereinigt. Dies wird durch verschiedene Aufreinigungsmethoden erreicht, wobei die Aufreinigung im Rohofen (durch Sublimation) die Methode der Wahl darstellt. Durch die hohe Empfindlichkeit gegenüber Oxidation bzw. Wasser sowie bedingt durch die sehr rasche Kristallisation, stellt die Reproduzierbarkeit des Herstellungsprozesses von Perowskit-Solarzellen ein Problem dar. Daher ist die Optimierung des Herstellungsprozesses essentiell. Zuerst wird eine sogenannte „Antisolvent“-Methode für die Herstellung der Perowskitschicht untersucht und optimiert. Weitere Optimierungsparameter sind die Schichtdicke der Perowskitschicht und der PC<sub>60</sub>BM-Schicht. Dies wird durch die Veränderung der Spin-Coating-Parameter erreicht, aber auch durch Variation der Konzentration der Perowskitlösung und des Temperschnitts. Durch die Optimierung der Solarzellenherstellung kann eine Effizienz von 6,4% erreicht werden mit einem Füllfaktor von 62,4%, einer Leerlaufspannung von 0,48 V und einer Kurzschlussstrom von 21,69 mA cm<sup>-2</sup>.

Außerdem wurde herausgefunden, dass eine (Phenylethylammonium iodid)-Schicht zwischen der PEDOT:PSS und der Perowskit-Schicht einen positiven Effekt auf die Solarzellen Performance hat. Zusätzlich wurde die Zugabe von  $\text{CuBr}_2$  zur Perowskitschicht untersucht, da es zu einer Verbesserung der Stabilität und Performance der Solarzelle führen soll. Jedoch kann dieser positive Effekt nicht beobachtet werden und die Zugabe von  $\text{CuBr}_2$  hat zu einer Verschlechterung der Solarzellenperformance geführt.

## **Acknowledgement**

At this point I want to thank Assoc. Prof. Dr. techn. Dipl. Ing. Gregor Trimmel for his supervision, for providing this interesting topic for my master thesis and giving me the opportunity to do my master thesis at the Institute for Chemistry and Technology of Materials.

In addition I want to thank Dr. techn. Dipl. Ing. Thomas Rath, Dipl. Ing. Sebastian Höfler BSc, Dipl. Ing. Stefan Weber and MSc. Jimmy Mangalam BSc. for their help and input during my master thesis and the whole working group of Prof. Trimmel for the kind and good atmosphere.

I also want to thank Mrs. Birgit Kunert for doing the XRD measurements and Dr. Theodoros Dimopoulos for doing the SEM measurements.

Further I want to thank the PERMASOL Project in cooperation with Austrian Institute of Technology, Johanneum Research and the University of Patras.

Additionally I want to thank my family for supporting me during my whole academic education and especially I want to thank my father Günther Handl who made it possible for me doing my studies in Chemistry in Graz and always supported me.

Finally I want to thank Pia Hofmann for the good time as a student and her support and of course my friends for the good time in Graz.

## Abbreviations

AS	anti-solvent
CB	chlorobenzene
DMF	N,N – dimethyl formamide
DMSO	dimethyl sulfoxide
DSSC	dye sensitized solar cell
$E_g$	band gap energy
ETL	electron transport layer
FAI	formamidinium iodide
FF	fill factor
FTO	fluorine doped tin oxide
HOMO	highest occupied molecular orbital
HP	heating plate
HTL	hole transport layer
$I_{mpp}$	current at maximum power point
$I_{sc}$	short circuit current
ITO	indium doped tin oxide
$IV$	current-voltage
$J_{mpp}$	current density at maximum power point
$J_{sc}$	short circuit current density
$JV$	current density-voltage
LUMO	lowest unoccupied molecular orbital
MAI	methyl ammonium iodide
MPP	maximum power point
P3HT	poly-(3-hexylthiophen-2,5-diyl)
PC <sub>60</sub> BM	[6,6]-phenyl-C <sub>61</sub> -butyric acid methyl ester
PCE	power conversion efficiency
PEAI	phenylethyl ammonium iodide
PEDOT:PSS	Poly(3,4-ethylenedioxythiophene)-poly(styrenesulfonate)
PMMA	poly(methyl methacrylate)
PSC	perovskite solar cell
PV	photovoltaic
RT	room temperature
SC	spin coating
Spiro-MeOTAD	2,2',7,7'-Tetrakis[N,N-di(4-methoxyphenyl)amino]-9,9'-spirobifluorene
TCO	transparent conductive oxide
$V_{mpp}$	voltage at maximum power point
$V_{oc}$	open circuit voltage

## Table of contents

1	Introduction.....	1
1.1	Global Energy Demand.....	1
1.2	Solar Photovoltaics.....	2
1.3	Theoretical Background of Solar Cells .....	2
1.3.1	Solar cell working principle.....	2
1.3.2	Characterisation of solar cells.....	6
1.4	Dye Sensitized Solar Cell.....	8
1.5	Perovskite materials for solar cells .....	10
1.6	Lead-based perovskites .....	12
1.7	Lead free based perovskite solar cells.....	14
1.8	Germanium based perovskite solar cells.....	14
1.9	Bismuth based perovskite solar cells .....	15
1.10	Antimony based perovskite solar cells.....	15
1.11	Tin based perovskite solar cells .....	16
2	Aim of the thesis .....	21
3	Results.....	22
3.1	Comparison of the SnI <sub>2</sub> purification methods .....	22
3.2	XRD analysis of SnI <sub>2</sub> and MA <sub>0.75</sub> FA <sub>0.15</sub> PEA <sub>0.1</sub> SnI <sub>3</sub> perovskite .....	25
3.3	Optical Characterisation.....	27
3.4	Optimization of the solar cell preparation steps.....	28
3.4.1	Optimization of the perovskite layer .....	28
3.5	Optimization of the anti-solvent dropping .....	32
3.5.1	Influence of the anti-solvent dropping distance.....	32
3.5.2	Influence of the anti-solvent dropping speed and application number on the solar cell performance.....	35
3.5.3	Influence of the annealing step of the perovskite layer on the solar cell performance .....	36
3.6	Optimization of the PC <sub>60</sub> BM layer.....	40
3.7	Influence of a PEAI-interlayer between the PEDOT:PSS and perovskite layer 42	
3.8	Investigation of the influence of CuBr <sub>2</sub> .....	44
4	Best solar cell performance & investigation of the stability.....	47
5	Experimental.....	50
5.1	Chemicals.....	50
5.2	Characterisation.....	50
5.2.1	XRD analysis .....	50

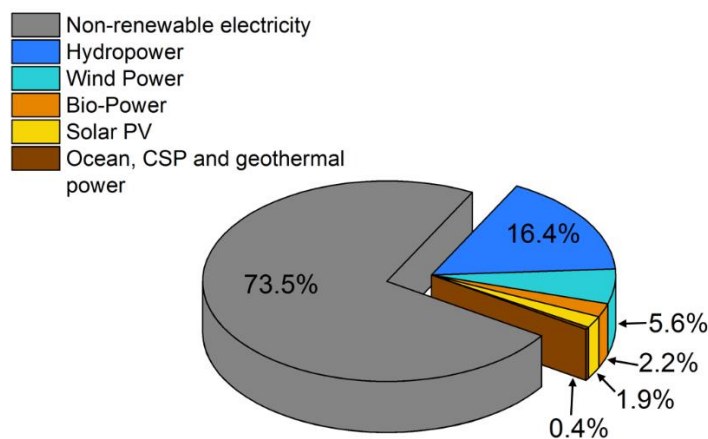
5.2.2	Optical characterisation of perovskite MA <sub>0.75</sub> FA <sub>0.15</sub> PEA <sub>0.1</sub> SnI <sub>3</sub> .....	51
5.2.3	<i>JV</i> - measurements .....	51
5.2.4	Layer Thickness .....	51
5.2.5	SEM .....	51
5.2.6	Optical Microscopy.....	52
5.3	Purification of SnI <sub>2</sub> .....	52
5.3.1	Sublimation .....	52
5.3.2	Bulb-to-bulb distillation.....	53
5.3.3	Recrystallization - SnI <sub>2</sub> (DMF) complex .....	53
5.3.4	Tube furnace .....	54
5.4	General solar cell preparation .....	54
5.4.1	Device Fabrication .....	54
5.5	General solar cell preparation .....	54
5.6	Perovskite precursor solution preparation.....	55
5.7	Optimization of the solar cell performance.....	56
5.7.1	Optimization of the perovskite layer .....	56
5.7.2	Optimization of the AS dropping.....	56
5.7.3	Optimization of the PC <sub>60</sub> BM layer .....	57
5.7.4	PEAI interlayer between the PEDOT: PSS and perovskite layer .....	58
5.7.5	Influence of CuBr <sub>2</sub> on the solar cell performance .....	58
6	Conclusion and Outlook .....	59
7	Index of Schemes.....	61
8	Index of Figures .....	61
9	Index of Tables .....	63
10	References.....	65

# 1 Introduction

## 1.1 Global Energy Demand

In 2017 the global energy demand increased by 2.1 %, which is ascribed to the steady global economic growth. More than 70 % of the global electricity was produced by non-renewables like oil, natural gas and coal, whereas the rest was accounted to renewables (see Scheme 1). Overall in the year of 2017 the carbon dioxide emissions that are related to the global energy increased by 1.4 %. However this rise was not the case for every country, as in the United States for example the emissions dropped due to an increase in renewables usage. The increase in carbon dioxide emissions shows that more effort has to be put not only in the improvement of global energy efficiencies, but also in the deployment of renewables. The energy efficiency improved only by 1.7 % in 2017 while over the past three years it improved with 2.3 % (caused by slowdown in efficiency policy coverage and stringency and lower energy prices).

Due to the expansion of wind, solar and hydropower the electricity generation based on renewables rose to 6.3 %.<sup>1</sup> In the next 25 years it is forecasted that the world energy demand is met by renewables and natural gas, as for example a drop in costs makes solar power a cheap electricity source.<sup>2</sup>



*Scheme 1: Renewable Energy Share of global electricity production (End – 2017); data used from reference<sup>3</sup>*

The net additions to global electrical power capacity accounted to renewable energy rose from 63% in 2016 up to 70% in 2017. The renewable electrical power capacity reached 2195 GW, which is enough supply about 26.5% of the global electricity.<sup>3</sup>

## **1.2 Solar Photovoltaics**

Sunlight can be converted into usable energy forms with well-established solar technologies like solar photovoltaics (PV), solar heating/cooling and solar thermal electricity. These systems are advantageous as there is no air, water and noise pollution, in addition there are no greenhouse gas emissions during operation. The net capacity additions from solar PV was higher than from any other power generating type in the year 2017. As solar PV is a modular technology it is possible deploying it in small quantities like using it for calculators or in off-grid applications. Large plants of these modules can be manufactured, which allows the construction of utility scale solar energy facilities. Therefore solar cells can be employed for a wide range of applications. These systems can be installed in single households and mounted on buildings or form part of a building like on rooftops. However there are also some disadvantages to be mentioned like the electricity is only produced in sunny periods, so storage is required. Therefore, these systems are only effective in cost when they are installed in sunny locations.<sup>4</sup> The solar PV capacity increased from 300 GW in 2016 up to 402 GW in 2017.<sup>5</sup>

In 2017 the main source for the new power capacity includes the major markets like China, the United States, Japan and India.

The increasing competitiveness of solar PV leads to a globally market expansion, in addition to the fact that this technology has the potential to reduce carbon dioxide emission, to alleviate pollution and to provide an access to energy.

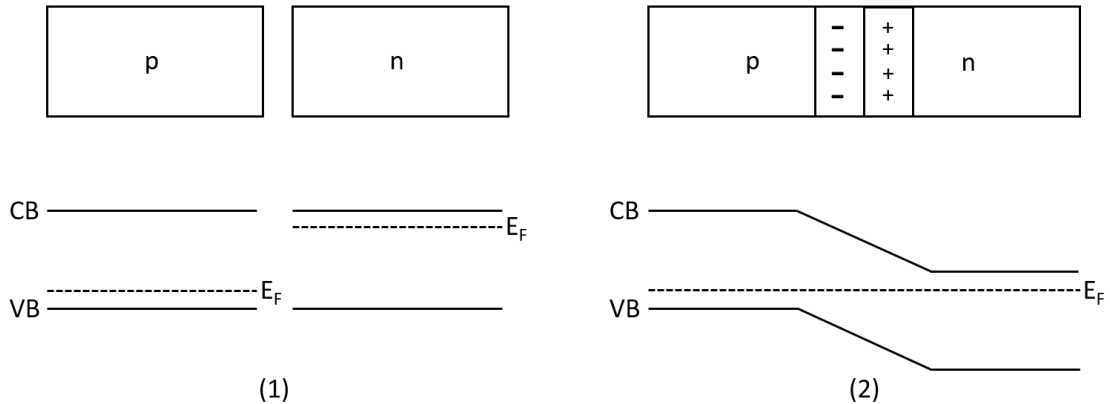
## **1.3 Theoretical Background of Solar Cells**

### **1.3.1 Solar cell working principle**

In solar cell devices a conversion from the energy of light to electrical energy through the photovoltaic effect occurs. These devices consist of semiconducting materials. The main principle of solar cells is the light induced generation of charge carriers, followed by transport and the collection of those carries by the electrodes.<sup>6,7</sup> The generation of current via light takes place through the absorption of incident photons in the semiconducting material.<sup>8</sup> If the photon energy is equal or higher than the energy difference of the valence band and the conduction band (=band gap) of the semiconducting material, electron/hole carriers can be generated.

This occurs as the electron is excited from the valence band to conduction band and leaves a void in the valence band, which can be termed as a “hole” and is similar to a positive charge and the electron is similar to a negative charge. In this process the radiative energy of the photon is converted into a chemical energy of those electron/hole carriers. In a semiconducting material the electrons can either populate the energy levels below the so-called valence band or above the conduction band, but in between those bands no energy state exists, which is allowed to be populated by electrons.<sup>9</sup> However the produced electron/hole carriers are meta-stable and only exist for a short time which is mostly equal to the minority carrier lifetime, they will then recombine again. If a recombination of the carrier occurs immediately after they are produced, the electron/hole carrier which is generated via light gets lost and no current or power will be produced. Electron/hole carriers are extracted via doping of the semiconducting material to avoid such recombination. So a p-n junction is received, which is formed when a n-type semiconducting material and a p-type material are joined. Through the p-n junction the electrons and holes are spatially separated and recombination processes get minimized. An external connection of the emitter and the base results in an external circuit through which the light generated carriers can flow.<sup>10</sup> Chemical energy is converted into electrical energy, when the electrons pass through the external circuit and then recombine with the holes.<sup>9</sup> The joining of a p-type and n-type semiconducting material leads to the formation of a charge concentration gradient. The p-type semiconducting material has a high concentration of holes and the n-type semiconducting material has a high concentration of electrons. For a p-doping, “impurities” which have fewer valence electrons are added, for example Al in the case of Si as semiconducting material. This leads to an electron deficit in the valence band and creates a “hole” in the valence band, where electrons can move. On the other hand n-doping is achieved via adding “impurities” with more valence electrons, like P to Si as semiconducting material. These additional electrons go then into the conduction band, as the valence band is already filled. So electrons can now easily move between the orbitals of the conduction band. Through this joining the excess electrons from the n-type material will diffuse to the p-type material and if there is an excess of holes in the p-type region, they will diffuse to the n-type material. So a movement of the electrons to the p-type side, produces positive ion cores in the n-type side and a movement of holes to the n-type side produces negative ion cores on the p-type side.

This results in an electric field and a junction where a depletion region is formed.<sup>11</sup> The produced drift current of the electrons and holes has the opposite direction of the initial diffusion current, so holes will drift from the n-region towards the p-region and vice versa, electrons will drift from the p-region to the n-region. The Fermi level is constant.<sup>12</sup> The joining of a p-type and n-type material and the formation of the depletion region is shown in Scheme 2.



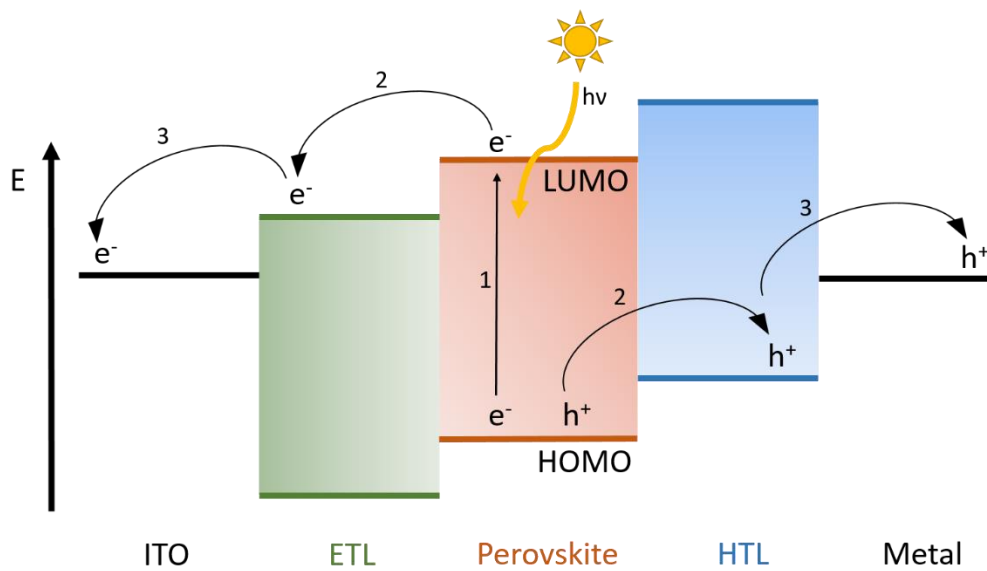
*Scheme 2: Illustration of the Fermi levels and energy levels of a p- and n-doped material (1); formation of a depletion region via joining the p- and n-doped material and the corresponding energy levels and Fermi level (2); drawn based on reference 12*

When photons reach the pn-junction region electron/hole pairs are created. The electrons will sweep to the n-region and the holes to the p-region. Because of this pn-junction a voltage is produced which forces the electrons through the external circuit which connects the n- and p-region externally. Therefore electrons will diffuse through the n-region and the external circuit to the p-region. At the p-region the electrons recombine with the holes, which closes the circuit and electricity is produced from the energy of incident photons.<sup>13</sup>

The formation of light induced charge carriers in solar cell is based on a similar principle as of the above described pn-junction. Depending on the solar cell type, the device architecture differs and with that the formation of the charge carriers and the transport of it (Note: as this work focusses on perovskite solar cells, only this topic is discussed in more detail). In perovskite solar cells an active layer is used, which is placed in between an electron transport layer and a hole transport layer as it is shown in Scheme 3. The perovskite material is the active layer, where the formation of electron/hole carriers occurs when light is absorbed.

Electron transport layers are usually n-type semiconductors that can effectively transport electrons. ETL have a high electron mobility and the hole transport in the direction of the electron motion is prevented, so that a recombination of electrons and holes gets reduced. This applies in the reverse way for hole transport layers.<sup>14</sup>

As already mentioned when light reaches the absorber material free electron/hole carriers are produced, through the electron transport layer and the hole transport layer those electron/hole carriers are transferred to the corresponding electrode. So the electrons are transported via the ETL and the holes are transported via the HTL. At the interface of the ETL/HTL and the electrode an extraction of the charge carrier occurs.



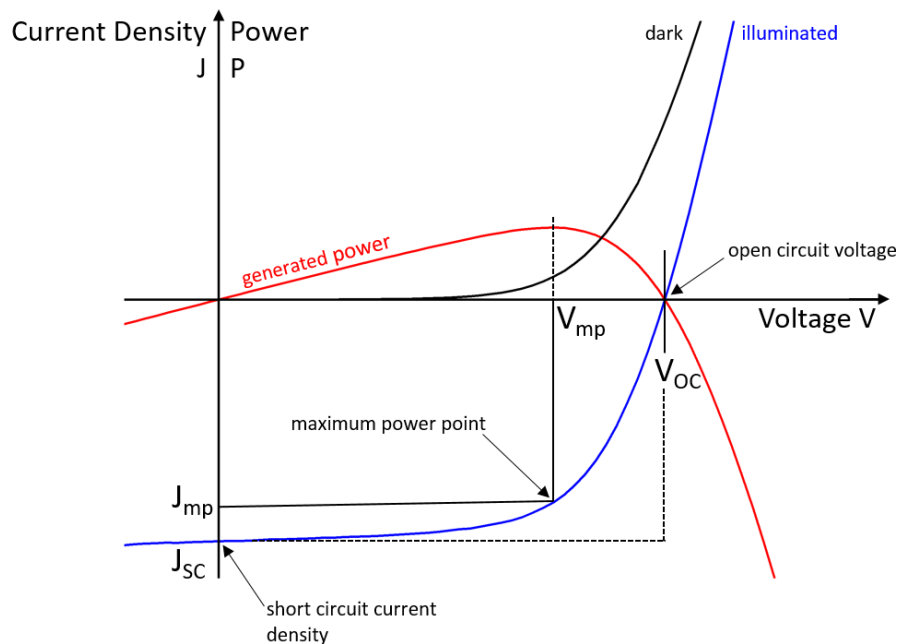
*Scheme 3: Charge carrier formation for perovskite solar cells: 1 Free charge generation via absorption of light 2. Transport of charges 3.Extraction of charges*

### 1.3.2 Characterisation of solar cells

The measurement of the electrical performance of a solar cell gives essential information about the output of the solar cell. Measuring the  $IV$ - curve at defined conditions is a common technique to gain information about the solar cell characteristics. Therefore the electrical parameters are measured at Standard Test conditions and via applying a voltage at the terminals of the solar cell an electrical current and power are created and measured.<sup>15</sup> Those standard conditions are a temperature of 25 °C, an Air Mass 1.5 spectrum (AM 1.5) with an intensity of 100 mW/cm<sup>2</sup>.<sup>16</sup> The  $IV$ - curves give information about the ability of the solar cell to convert sunlight into electricity.

It is common to record an  $IV$ - curve under illuminated conditions of the solar cell and under dark conditions to study the diode behaviour of the solar cell. The following parameters can be derived from the  $IV$ - curve: the  $I_{SC}$  (current at short circuit), the  $V_{OC}$  (voltage at open circuit), the  $P_{mpp}$  (maximum power point), the  $I_{mpp}$  and  $V_{mpp}$  (current and voltage at the maximum power point) and the FF (fill factor).<sup>15</sup>

As the  $I_{SC}$  depends on the solar cell area, it is often replaced by the short circuit current density  $J_{SC}$  (mA cm<sup>-2</sup>) and  $JV$ - curves are recorded. Scheme 4 shows a characteristic  $JV$ -behaviour for a solar cell measured under illuminated (blue curve) and dark conditions (black curve). The received parameters are marked in this graphic.



Scheme 4: Illustration of a characteristic  $JV$ - curve with corresponding parameters like the  $J_{SC}$ ,  $V_{OC}$ ,  $J_{mpp}$  and  $V_{mpp}$ , this schematic contains the curve resulting from illuminated (blue curve), dark conditions (black curve) and the generated power curve (red); self-designed based on reference 17

The power curve (red curve, Scheme 4) which is obtained, is the current density multiplied with the voltage and it is done point for point.<sup>18</sup>

$$P_{mp} = J_{mpp} * V_{mpp} = FF * J_{SC} * V_{OC}$$

The power curve is obtained when doing this from short-circuit to open circuit conditions. So the power curve ranges from short-circuit to open circuit conditions. Open circuited means, that the solar cell is not connected to any load, at this point the current is zero (minimum) and the voltage is at its maximum, this is called the open circuit voltage  $V_{OC}$ . The  $V_{OC}$  is limited by recombination, these recombination processes changes the rate of electron-hole production.

In contrast to this, the short circuit current density ( $J_{SC}$ ) occurs when the solar cell is short circuited, where the voltage is at zero (minimum) and the current density is at its maximum. The light-generated carriers which are generated and collected lead to the short-circuit current density. The  $J_{SC}$  depends directly on the light intensity, as well as on the diffusion length of the carriers.<sup>19</sup> Power can be generated where the  $JV$ - curve spans from the  $J_{SC}$  to the  $V_{OC}$ . At both points no power is generated, however the maximum power point lays in between. This point, the maximum power point MPP, is reached, when the solar cell produces maximum electrical power. The  $J_{mpp}$  and  $V_{mpp}$  are the corresponding values to this point.

Further information which can be gained out of the  $JV$ - curves are the fill factor FF and the power conversion efficiency PCE. The fill factor gives information about the quality of the cell, in an ideal case the fill factor is 1. The FF factor is strongly affected by parasitic resistances, whereas both the series and shunt resistance influence the FF. An ideal FF can be received if the series resistance is as small as possible and the shunt resistance as large as possible.<sup>20</sup> Typically the fill factor will range from 0.5 to 0.81.<sup>21</sup>

The FF is calculated via the following formula:

$$FF = \frac{V_{mpp} * J_{mpp}}{V_{OC} * J_{SC}}$$

The power conversion efficiency  $\eta$  is mostly used for the comparison of solar cells and is characterised as follows:

$$\eta = \frac{P_{MP}}{P_{in}} = \frac{FF * V_{OC} * J_{SC}}{P_{in}}$$

$P_{mp}$  ... maximum power point

$P_{in}$  ... incoming power

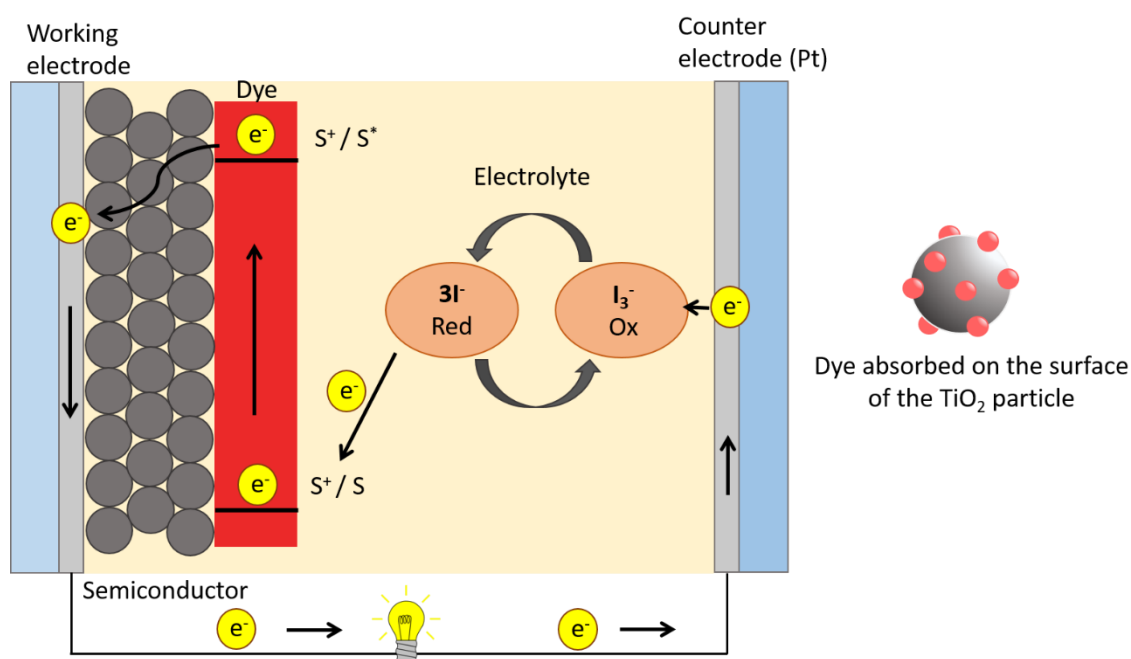
The PCE is defined by the incident power which is converted into electricity. The efficiency of a solar cell depends on the intensity of the sunlight and the spectrum of it, as well as on the temperature of the solar cell. This is why it is important to measure the solar cell under standard conditions.<sup>22</sup>

## 1.4 Dye Sensitized Solar Cell

The dye sensitized solar cell was invented by Michael Graetzel and Brian O'Regan at Ecole Polytechnique Federale de Lausanne (EPFL) in 1991. The dye sensitized solar cell converts visible light into electrical energy.<sup>23</sup> This type of solar cell mainly consists of three components: a material like glass which is coated with a transparent conductive oxide layer that serves as a current collector, like ITO (indium-tin oxide), FTO (fluorine-doped tin oxide) or TCO (transparent conductive oxide).<sup>24</sup> In addition it consists of a semiconductor, mostly of a mesoporous oxide layer, using sintered nanoparticles, like  $\text{TiO}_2$  (anatase).  $\text{TiO}_2$  is used as semiconductor as it has many advantages, like it is widely available, low in cost and non-toxic. The charge transfer dye sensitizer is absorbed on the surface of the semiconductor. A ruthenium complex (like  $[\text{Ru}(4,4\text{-dicarboxy-2,2\text{-bipyridine ligand})}_3]$ ) is commonly used as sensitizer. Organic solvents which contain a redox couple (ex. iodide/triiodide) are used as electrolyte. The counter electrode (Pt) regenerates the redox mediator.<sup>25</sup>

Differently to the silicon solar cell, in the DSSCs the semiconductor is mainly responsible for the charge transport, whereas the photoelectrons are provided by the sensitizer dye. The separation of the charges occurs at the surface between the semiconductor, the electrolyte and the dye.<sup>26</sup> The working principle is the following: when the photoactive material is illuminated by light, it produces electricity.<sup>23</sup>

Via illumination of the dye sensitized solar cell, a photon is absorbed by the sensitizer  $S$ , which leads to excitation  $S^*$  and an electron is injected in the conduction band of the semiconductor. The sensitizer is then in an oxidized state  $S^+$ . The electron flows through the semiconductor to the front contact and through an external load to the counter electrode. There it reduces the redox mediator, through which then the sensitizer is regenerated, which closes the circle.<sup>25</sup> Energy is created through the movement of the electrons, which can be harvested in a rechargeable battery for example.<sup>23</sup> The device set up of a dye sensitized solar cell and its working principle is illustrated in Scheme 5.



*Scheme 5: Illustration of the device set up and working principle of a dye-sensitized solar cell; self-designed based on reference 24*

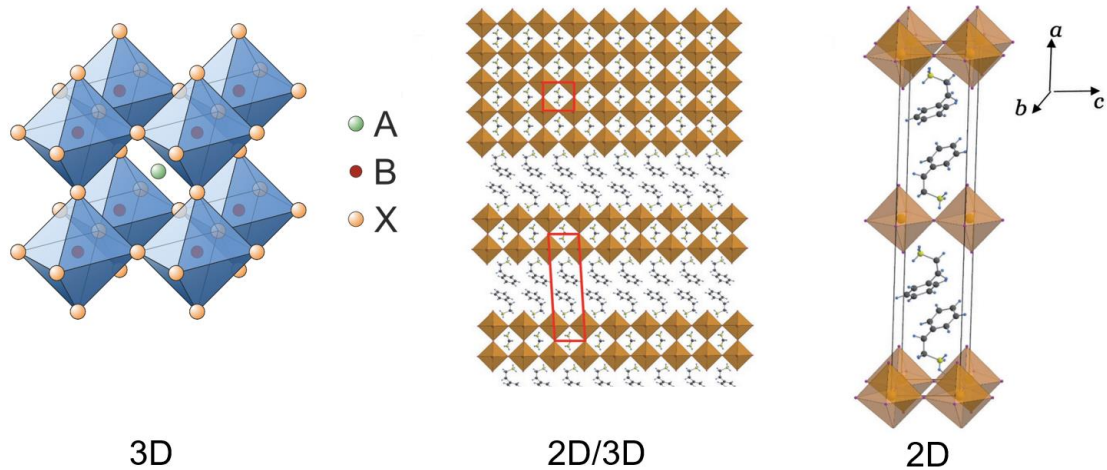
The advantages of dye sensitized solar cells are the inexpensive materials and the simplicity of the fabrication process. Furthermore the platinum catalyst can be replaced by cheaper materials like carbonaceous materials. In addition they can be fabricated in a roll-to-roll process, where the dye sensitized solar cells can be printed on flexible substrates via a low-cost continuous manufacturing method. Moreover, DSSCs also work in darker conditions like during cloudy weather, this makes it interesting for indoor applications like sunroof or windows.<sup>27</sup>

A major disadvantage for DSSC is the liquid electrolyte, as the stability is not given with varying temperatures. Lower temperatures lead to freezing of the electrolyte, so no power can be generated and there might be physical damages. Or higher temperatures can cause an expansion of the liquid. In addition the liquid electrolyte contains volatile organic solvents, so the DSSCs have to be sealed carefully. To avoid these disadvantages the liquid electrolyte can be replaced by a solid electrolyte, which might be a major field for the future research.<sup>26</sup>

The best solar cell performance of a dye sensitized solar cell was reported by Kakiage et al. where under simulated light intensity of  $100 \text{ mW cm}^{-2}$  a PCE of 14.3 %, a FF of 77.1%, a  $V_{OC}$  of 1.01 V and a  $J_{SC}$  of  $18.27 \text{ mA cm}^{-2}$  was reached.<sup>28</sup>

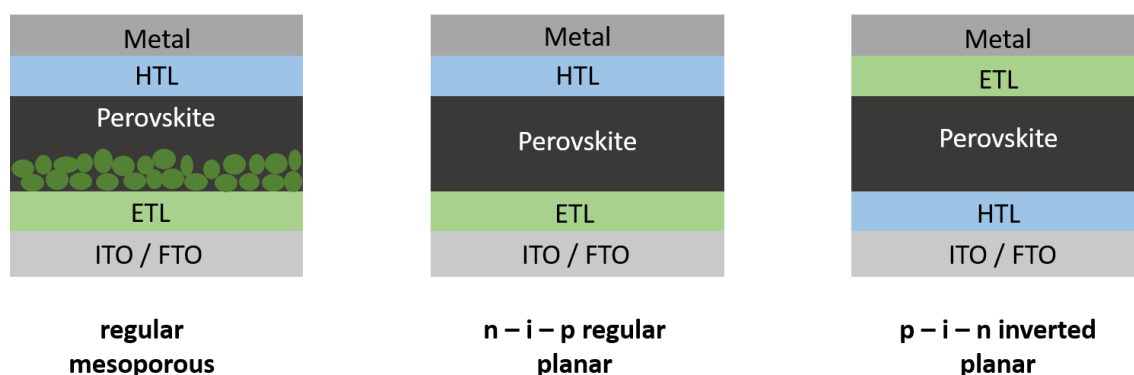
## 1.5 Perovskite materials for solar cells

The perovskite solar cells have their origin in dye-sensitized solar cells.<sup>29,30</sup> In 2006 the first perovskite solar cells have been discovered. The power conversion efficiencies for organic-inorganic-metal-halide perovskite materials increased very fast from 3.8%<sup>31</sup> in 2009 up to 22.1%<sup>32</sup> in 2016. Over the past few years the interest in hybrid organic-inorganic perovskites increased a lot and they caused a revolution in the field of photovoltaics, as they achieved power conversion efficiencies comparable to thin film technologies with thin films (CdTe or CIGS) or silicon. This fast evolution of perovskite solar cells led to more than 2000 publications only after some years. The optoelectronic properties are remarkable. The general perovskite structure has the composition  $ABX_3$ . In an ideal case the perovskite has a cubic symmetry, where the  $BC_6$ -octahedra are connected via the corners and the cuboctahedral voids are occupied by the A-cations. In the  $ABX_3$  structure A is in general either a small organic or an inorganic molecular cation, B is a metal ion such as lead, germanium, antimony or tin and X is a halide such as iodide, bromide or chloride.<sup>33,34,41</sup> Scheme 6 shows the 3D structure of  $ABX_3$  where A occupies the centre of the cubic cell, whereas B occupies the corners of the cell and X lays in the mid-points of the edges.<sup>35</sup> The structure can be changed to an orthorhombic, rhombohedral or tetragonal structure if there is a small A-ion and a large B-ion, this is because the tolerance factor gets smaller than 1. However the size of the A-ion can also have an influence on the dimensionality, so with a large A cation it is gained a 2D structure<sup>36,37</sup> or a 1D chain material.<sup>38</sup> The interest in mixtures of 2D and 3D (shown in Scheme 6) structures increased, due to resistivity against moisture compared to 3D structures alone.<sup>39,40</sup>



Scheme 6: 3D structure of  $ABX_3$ <sup>41</sup>; mixture of 2D/3D structure of perovskite with smaller and bigger cations; 2D structure of perovskite<sup>101</sup>

There are three main configurations for the device architecture, which are used for perovskite solar cells that are illustrated in Scheme 7. One possibility is a planar configuration with a stack either in a regular or an inverted form. In addition to the regular planar device stack the device can also be built in a regular mesoporous architecture, where for the regular mesoporous scaffold a mesoporous ETL is used. For example mesoporous  $TiO_2$  is mostly used as ETL in the regular mesoporous device architecture, often used with Spiro-MeOTAD as HTL. For the regular planar architecture it is either used an FTO or ITO layer, an ETL like  $TiO_2$  or ZnO, the perovskite as active material, the HTL like Spiro-MeOTAD and a metal contact. The inverted stack has the following design: FTO, ITO/HTL/Perovskite/ETL/metal, here PEDOT:PSS or NiO are often used as HTL and  $PC_{60}BM$  as ETL.<sup>42, 43, 44</sup>



Scheme 7: Device architecture of perovskite solar cells; regular set up perovskite solar cell with mesoporous (left) or planar (middle)  $TiO_2$  scaffold; inverted device set up with planar  $TiO_2$  scaffold (right); self-designed based on references 42, 43, 44

A huge advantage of metal halide perovskite solar cells is that their optoelectronic properties can be tuned via the substitution of ions. It is reported that a decrease in ionic size of the halide leads to an increase of the bandgap.

As cation A for example MA, FA or Cs can be used. However depending on the cation used the lattice and the structure are influenced, when using larger cations like FA compared to MA the lattice expands, which slightly decreases the band gap.<sup>42</sup> As already mentioned the band gap gets smaller when the ionic size of the halide gets bigger, so for the perovskite with Cl, Br and I the bandgap is 2.97eV, 2.24 eV and 1.53 eV.<sup>45</sup>

A major issue of perovskite solar cells is the low stability that depends on factors of potential degradation for certain perovskite materials, because of this also more studies towards the improvement of the stability are necessary.<sup>44</sup>

## 1.6 Lead-based perovskites

Only within 7 years there was a fast increase in power conversion efficiency from 3.8% to 22.1% for lead based perovskite solar cells with mesoporous scaffold configurations (as already mentioned above). Lead based perovskite materials have beneficial properties like for example long carrier diffusion lengths<sup>46,47</sup>, small exciton binding energy<sup>48,49</sup> and high absorption coefficient<sup>50,51</sup>. The first work was published in 2009 by Kojima and coworkers<sup>31</sup>, where the first PSCs were prepared in a dye-sensitized solar cell (DSSC) architecture with mesoporous TiO<sub>2</sub> (layer thickness of 8-12 μm) and an infiltration in the perovskite material, additionally a liquid electrolyte was used. The second work was published in 2011 on PSC, where also a DSSC configuration was used with a liquid electrolyte with an efficiency of 6.5%.<sup>52</sup>

However the breakthrough in PSCs was reached by using solid state HTL, like spiro-MeOTAD, with the advantage that it does not dissolve the perovskite layer. This was introduced by Lee et al.<sup>53</sup> and Kim et al.<sup>54</sup>. So records in efficiency were published, nevertheless it is to keep in mind that efficiencies published until 2013, do not take into account the hysteretic effect of perovskite materials (the recorded efficiencies depend on the scan direction, forward or backward). The most extensively investigated lead based perovskite material for solar cell has been methyl ammonium lead iodide MAPbI<sub>3</sub>.<sup>45</sup> However the attention shifted from MAPbI<sub>3</sub> to mixed ion perovskites (ex. FA<sub>x</sub>MA<sub>1-x</sub>PbBr<sub>y</sub>I<sub>3-y</sub>). The Seok group achieved efficiencies of 16.2% in 2014 which is reported in the publication of Jeon and coworkers.<sup>55</sup>

An anti-solvent treatment was introduced, where a non-polar solvent like toluene causes a faster precipitation of the perovskite material from  $\text{PbI}_2$  and MAI in a polar solvent during the spin coating process.

In 2015 the same group reached efficiencies of 18.5% and 20.1% by Jeon<sup>56</sup> et al. and Yang et al.<sup>57</sup>. The high performance of these PSCs with FA/MA Pb-based I/Br perovskites (1.6 eV bandgap) is ascribed to improved  $V_{\text{OC}}$  values. In the same year Bi and coworkers<sup>58</sup> used a polymer-templated crystal growth technique for perovskite materials with different cation/halogen mixtures. In addition crystallographic properties in MA/FA perovskites can be improved via incorporation of inorganic cations.<sup>59,60,61,62,63</sup> High efficiencies were reached via incorporation of Cs into FA/MA perovskites with efficiencies of 21.1% or for quadrupole perovskites with Rb in Cs/FA/MA perovskite mixture with 21.6%.<sup>63</sup>

But also planar PSCs have up to now made a large progress and reached values up to 20%. The first publication of solar cells with planar device configuration was in 2012 by Lee and coworkers.<sup>53</sup> However at the beginning only low efficiency values of 1.8% were reached with these planar devices. In 2013 Liu et al. deposited evaporated perovskite films in a planar configuration and reached a power conversion efficiency of 15%.<sup>64</sup> Again this work did not take hysteretic effects into account. The publication of Zhou and coworkers, who reached an efficiency of 19.3% and reported no hysteresis due to doping of  $\text{TiO}_2$ . However in their supporting information an efficiency difference of 17% for the backward scan and 13% for the forward scan can be observed so although neglected in their discussion PSCs show hysteretic effects as revealed in the supporting information.<sup>65</sup> Later on stabilized efficiencies, that take hysteretic effects into account were observed. Like in the work of Correa-Baena et al. who reached values of 18.2% via using  $\text{SnO}_2$  and mixed ion perovskites.<sup>66</sup> In 2016  $\text{SnO}_2$  was used in an inverted stacking configuration which yielded efficiencies of 18.8%.<sup>67</sup> Higher values of 19.5% were reached via a normal device architecture and the usage of  $\text{SnO}_2$  ETL by ALD.<sup>68</sup>

The highest efficiency reached with a planar device set up is a PCE of 20.8% with 1.2 V of  $V_{\text{OC}}$  with a solution-processed  $\text{SnO}_2$  as ETL prepared at low temperature.<sup>69</sup>

## 1.7 Lead free based perovskite solar cells

Due to toxicological and legalizing reasons, there is an ongoing search for more environmentally friendly alternatives to lead in perovskite solar cells.<sup>42</sup> A contamination of lead in the environment due to a strong enrichment causes problems for both human and animal health. Lead is a cumulative toxicant. Through the intake of contaminated food, water, etc. it is distributed to organs where it has a toxic effect.<sup>70,71</sup>

So far there were different attempts to replace lead in the perovskite structure including the following atoms: germanium, bismuth, antimony and tin.<sup>129</sup> Germanium, bismuth and antimony based perovskite materials for solar cells will only shortly be discussed in the following, whereas it is taken a closer look on tin based perovskite solar cells as this work focusses on those perovskite materials for solar cells.

## 1.8 Germanium based perovskite solar cells

Germanium is one possible candidate to replace lead in the perovskite structure, as it is also a group 14 element. Compared to lead, germanium has a higher electronegativity, so a more covalent character and a smaller ionic radius.<sup>72,73</sup> However so far there was only little research on germanium based perovskite solar cells which might be ascribed to the easy oxidation from  $\text{Ge}^{2+}$  to  $\text{Ge}^{4+}$ . The first reported germanium based solar cells were by Krishnamoorthy et al. in 2015.

They studied different A cations in the perovskite structure and investigated  $\text{CsGeI}_3$  and  $\text{MAGeI}_3$  based solar cells with PCE values reached of 0.11% and 0.2% respectively.<sup>74</sup> In the same year Stoumpos et al. studied different hybrid organic/inorganic germanium perovskites with respect to the A cation.<sup>75</sup> They found that the variation of the cation leads to a change of the bandgap, as with an increase of the cation size the band gap increases as well. Kopacic et al. investigated the influence of the substitution of the halide on the performance of the solar cell and its degradation. It was found that the incorporation of bromide in the perovskite structure leads to significant solar cell improvement and with  $\text{MAGeI}_{2.7}\text{Br}_{0.3}$  as absorber layer a PCE of 0.57%, a FF of 51%, a  $J_{\text{SC}}$  of  $2.43 \text{ mA cm}^{-2}$  and a  $V_{\text{OC}}$  of 0.46 V was obtained.<sup>76</sup> Further research on germanium based solar cells is essential for the enhancement of performance for this type of solar cell.

## 1.9 Bismuth based perovskite solar cells

Another interesting candidate for the replacement of lead, is the group 15 metal bismuth with a similar electronegativity and ionic radius.<sup>41</sup> Compared to lead it is environmentally friendlier.<sup>80</sup> MA<sub>3</sub>Bi<sub>2</sub>I<sub>9</sub> perovskites as absorber material have been extensively studied. They have been studied in a planar normal device architecture (glass/FTO/TiO<sub>2</sub>/MA<sub>3</sub>Bi<sub>2</sub>I<sub>9</sub>/P3HT/Au) by Lyu et al. with a PCE of 0.08%, FF of 44.4%, a V<sub>OC</sub> of 0.51 V and a J<sub>SC</sub> of 0.36 mA cm<sup>-2</sup>.<sup>77</sup>

In a planar inverted structure (glass/ITO/PEDOT:PSS/MA<sub>3</sub>Bi<sub>2</sub>I<sub>9</sub>/C<sub>60</sub>/BCP/Ag) Ran et al. reached a PCE of 0.39%, a FF of 34%, a V<sub>OC</sub> of 0.83 V and a J<sub>SC</sub> of 1.39 mA cm<sup>-2</sup>.<sup>78</sup> Zhang et al. used MA<sub>3</sub>Bi<sub>2</sub>I<sub>9</sub> in a mesoporous structured configuration (glass/ITO/c-TiO<sub>2</sub>/m-TiO<sub>2</sub>/MA<sub>3</sub>Bi<sub>2</sub>I<sub>9</sub>/Spiro-MeOTAD/MoO<sub>3</sub>/Ag) and reached a PCE of 0.42%, a FF of 62.5%, a V<sub>OC</sub> of 0.67 V and a J<sub>SC</sub> of 1 mA cm<sup>-2</sup>.<sup>79</sup> The best solar cell performance up to now was reached by Park et al. who used Cs instead of MA with a maximum PCE value of 1.09%, a FF of 60.0%, a V<sub>OC</sub> of 0.85 V and a J<sub>SC</sub> of 2.15 mA cm<sup>-2</sup> with a mesoporous structured device set up (glass/FTO/c-TiO<sub>2</sub>/m-TiO<sub>2</sub>/Cs<sub>3</sub>Bi<sub>2</sub>I<sub>9</sub>/Spiro-MeOTAD/Ag).

Although there has been up to now some research done on bismuth based perovskite solar cells, the overall PCEs are still low, which is mostly due to poor surface morphology.<sup>80</sup> Therefore further research has to be done to improve performance of bismuth based perovskite solar cells.

## 1.10 Antimony based perovskite solar cells

Beside germanium and bismuth, antimony is another promising alternative to lead based perovskite solar cells. Antimony has a similar electronic configuration as lead, as it is in the periodic table in the nearest group of it and the 3+ ions of antimony are similar in the electronic configuration as those of Pb<sup>2+</sup>.<sup>77,80,81</sup> Antimony forms A<sub>3</sub>Sb<sub>2</sub>X<sub>9</sub> perovskites with either a dimer structure or a layered structure.<sup>83</sup> Sapore et al. studied Cs<sub>3</sub>Sb<sub>2</sub>I<sub>9</sub> perovskite with a 2D-layered structure in solar cells. However with this perovskite material and the following device architecture: glass/FTO/c-TiO<sub>2</sub>/Cs<sub>3</sub>Sb<sub>2</sub>I<sub>9</sub>/PTAA/Au only low values for the solar cell performance are reached (PCE below 1%, a V<sub>OC</sub> of 0.3 V and a J<sub>SC</sub> below 0.1 mA cm<sup>-2</sup>).<sup>82</sup> Harikesh et al. investigated Rb as an alternative cation to Cs in the perovskite structure, as this leads to a layered antimony perovskite structure with better charge transport properties compared to the dimer structure.

They report a solar cell performance for  $\text{Rb}_3\text{Sb}_2\text{I}_9$  perovskite solar cells with a PCE of 0.66%, a FF of 56.97%, a  $V_{\text{OC}}$  of 0.55 V and a  $J_{\text{SC}}$  of  $2.11 \text{ mA cm}^{-2}$  with the following device architecture: glass/FTO/c-TiO<sub>2</sub>/m-TiO<sub>2</sub>/Perovskite/Poly-TPD/Au (poly-TPD: poly[N,N0 -bis(4-butylphenyl)- N,N0 -bisphenylbenzidine]).<sup>83</sup>

So far there was only little research in the application of antimony based perovskite solar cells<sup>84</sup>, however these materials have been more observed from an experimental<sup>85,86,87,88,89,90</sup> and theoretical<sup>91</sup> point of view. Solar cells based on  $\text{Rb}_3\text{Sb}_2\text{X}_9$  seem to be a promising antimony based perovskite in regard of  $J_{\text{SC}}$  higher than  $2 \text{ mA cm}^{-2}$  and  $V_{\text{OC}}$  of 0.55 V.

### 1.11 Tin based perovskite solar cells

An interesting alternative to lead based perovskite materials are tin based perovskite materials, which are structurally similar to the lead ones, as tin is in the same group in the periodic table like lead and has similar ion radii. Tin based perovskites have excellent optoelectronic properties comparable to lead-based perovskite materials.<sup>92</sup> The bandgap of Sn based perovskites has a smaller value of 1.3 eV<sup>93,94</sup> than for Pb based perovskites with 1.4 eV. According to Shockley Queisser the ideal bandgap for a single absorber material would be 1.34 eV to achieve the highest PCE value with 33%.<sup>95,96</sup> So Sn-based perovskites are close to this optimum band gap and higher short-circuit current densities are expected. However, with Sn-based materials the performance is not as good as with Pb based materials up to now.

One reason for this is the easy oxidation from  $\text{Sn}^{2+}$  to  $\text{Sn}^{4+}$ , which is due to a lack of the inert pair effect, contrary to  $\text{Pb}^{2+}$ . As the formation energy of Sn vacancies is very low, there is a high concentrations of holes<sup>97,98</sup>, which can lead to a high carrier recombination. Despite the easy oxidation of tin there are other challenging issues like the fast crystallization of tin based perovskites that makes the fabrication of uniform and compact film difficult.<sup>99,100</sup> Furthermore the formation energy of Sn vacancies is low, therefor charge carrier recombination occurs as the hole concentration is high.<sup>101,102</sup>

So over the past few years it was tried to overcome these challenges via optimization of the solar cell preparation that includes: varying the cations and anions to optimize the optoelectronic properties<sup>103,104,105</sup>, suppress the oxidation of  $\text{SnI}_2$  via addition of additives<sup>106,107,108</sup>, optimization of the fabrication process<sup>99, 109, 110,111</sup> and using ETL and HTL in a way that the charge recombination is reduced as it matches the band gap of the perovskite material.<sup>112,113</sup>

CsSnI<sub>3</sub> (1.3 eV bandgap) is one possible candidate to replace lead based perovskite solar cells, which was utilised by Graetzel's group.<sup>106</sup> SnF<sub>2</sub> was introduced to reduce the background carrier density and improve the performance of the photovoltaic system. Best PCE values were achieved with 20% SnF<sub>2</sub> in CsSnI<sub>3</sub> with a PCE of 2.02%.

Via the addition of SnF<sub>2</sub> the probability for the formation of Sn<sup>4+</sup> is reduced. Too high amounts of SnF<sub>2</sub> lead to phase separation in the film as well as to micrometre-sized aggregates which have a negative impact on the efficiency.<sup>107</sup> In the same year 2014 methyl ammonium tin halide perovskites were studied by Feng and Xiao<sup>114</sup> concerning that the effective masses and bandgaps decrease from chlorine to iodine. Formamidinium cation (FA<sup>+</sup>) is another possible A cation in the tin perovskite structure resulting in solar cells with a relatively good stability in air.<sup>115</sup> The material has a bandgap of 1.41 eV, for which it can be achieved a maximum photocurrent density of about 30 mA cm<sup>-2</sup>.<sup>116</sup>

Lee et al. have achieved in 2016 a PCE of 4.8% with FASnI<sub>3</sub> and with SnF<sub>2</sub> pyrazine with a long term stability for over 100 days (the solar cells were encapsulated and stored under ambient and dark conditions). The surface morphology got better with pyrazine, as well as the Sn oxidation gets reduced. Using pyrazine with SnF<sub>2</sub> gives better results, as it complexes with SnF<sub>2</sub>.<sup>107</sup> Recently PCE values of 6.22% were reached with an inverted p-i-n device structure by Yan and co-workers.<sup>99</sup> In 2017 and 2018 there was a fast increase in efficiencies.

In 2017 it was reported by Liao et al. that via reduction of the dimension of the perovskite structure, the thermodynamic stability gets improved and with this the degradation under air exposure is reduced. A source of decomposition of perovskite solar cells, is the adsorption of water and oxygen molecules on the perovskite.<sup>117,118,119,120,121</sup> The stability of three dimensional perovskites is reported to be lower than that of the two-dimensional film.<sup>122,123</sup> Low dimensional Sn perovskites are highly oriented. However due to the quantum well structure the carrier transport properties for two dimensional tin perovskite are poor.<sup>40,123,124</sup> But there is the assumption that the photovoltaic performance can be improved, if the perovskite films are grown vertically, through which the carrier transport is not hindered.<sup>39</sup> Further the stability of Sn-based perovskite solar cells can be improved via the incorporation of PEA<sup>+</sup> molecules into the boundaries and the pinhole-free perovskite films through which the diffusion of oxygen can be hindered.

The solar cells were built in the device architecture: glass/ITO/NiO<sub>x</sub>/Sn-perovskite/PCBM/Al. The tin perovskite layer consisted of SnI<sub>2</sub>, SnF<sub>2</sub>, FAI and varying amounts of PEAI, dissolved in a DMF and DMSO mixture. The tin perovskite films are grown with a one-step spin coating method. Via the addition of PEA<sup>+</sup> to FASnI<sub>3</sub> a mixture of 2D/3D nanolayers are formed. The following structure PEA<sub>2</sub>FA<sub>n-1</sub>SnI<sub>3n+1</sub> was obtained with n as the number of tin iodide layers. The number of layers can be changed by the variation of the stoichiometric ratio from 0-100% of PEA<sup>+</sup> to FA<sup>+</sup>. PEA<sup>+</sup> is used as an organic separating interlayer, to produce low dimensional tin halide perovskites. The orientation is changed via variation of the PEA<sup>+</sup> ratio. Using 20% PEA<sup>+</sup> a perovskite film was achieved with a high orientation of two dimensional perovskite layers perpendicular to the substrate, which led to a PCE of 5.94%, a FF of 69%, V<sub>OC</sub> of 0.59 V and a J<sub>SC</sub> of 14.44 mA cm<sup>-2</sup>.<sup>125</sup>

The perovskite structure has also an influence on the stability in solar cells, as it was reported by Liao et al. Instead of PEA<sup>+</sup>, ethylenediammonium {en} was used to have a positive influence on the perovskite structure. Due to the oxidation of Sn<sup>2+</sup> to Sn<sup>4+</sup> self-doping in the material is happening, where Sn<sup>4+</sup> is a p-type dopant, which leads to low V<sub>OC</sub> values or short circuits. Low V<sub>OC</sub> values in tin-perovskites can also have its origin in high dark carrier density. It is reported that by changing the perovskite structure the dimensionality and performance can be influenced in a positive way. It has been indicated that the cations butylammonium and phenylethylammonium change the 3D structure to a 2D structure, which leads to a better stability. In this work it is reported that ethylenediammonium {en} was incorporated into 3D FASnI<sub>3</sub> perovskite structure. With those {en}FASnI<sub>3</sub> solar cells (with 10% {en} loading) a PCE of 7.14% was achieved that is further described below.<sup>126</sup> Similar to {en}FASnI<sub>3</sub> perovskite materials, {en} can also enter the MASnI<sub>3</sub> crystal structure, but does not lower the dimensionality to a 2D structure. {En} leads to a 3D perovskite with SnI<sub>2</sub> vacancies, as {en} replaces MA<sup>+</sup> and the cages of the 3D structure are not that dense, and the electron trap state density gets reduced thereby increasing the charge carrier lifetime. The incorporation does not show any changes in dimensionality but it improves the optical and electronical properties of these perovskite films. The performance of solar cells with {en}MASnI<sub>3</sub> absorber can achieve high reproducible efficiencies of up to 6.63%, a FF of 63.72%, a V<sub>OC</sub> of 0.43 V and a J<sub>SC</sub> of 24.28 mA cm<sup>-2</sup>. The solar cells were built in the device architecture: glass/FTO/c-TiO<sub>2</sub>/m-TiO<sub>2</sub>/ {en}MASnI<sub>3</sub>/PTAA/Au.<sup>105</sup>

As above mentioned {en} was also incorporated in the FASnI<sub>3</sub> perovskite by Ke et al.<sup>112</sup> However the main idea behind this research was to replace the expensive organic HTL like Spiro-MeOTAD and PTAA, with a suitable HTL that has a high hole mobility, which effectively transports holes and blocks electrons. The problem with these organic HTL is the addition of additives and dopants which is necessary to improve the performance leads not only to higher costs, but it is also often a peroxidation step with atmospheric O<sub>2</sub> necessary for the manufacturing step, which can lead to a faster degradation of the perovskite film.<sup>127</sup> Therefore, tetrakis(triphenylamine) TPE was used as a hole transport layer. TPE consists of a tetraphenylethene core with four end-capped triphenylamine units. The results which are reached with TPE as a HTL are similar to those solar cell devices which use PTAA as HTL and better than those using Spiro-MeOTAD. The HOMO and LUMO level are closer together for tin based perovskites than for lead based perovskites, ETL and HTL are needed with narrower HOMO and LUMO levels.<sup>113,128</sup> The benefit of TPE is its effective charge transfer and favourable band alignment. The solar cells were prepared in the following device architecture: glass/FTO/TiO<sub>2</sub>/ {en}FASnI<sub>3</sub>/HTL/Au.

Using this dopant free TPE as HTL in addition to the hollow perovskite {en}FASnI<sub>3</sub> a solar cell performance with a PCE of 7.23%, a FF of 69.74% , a V<sub>OC</sub> of 0.46 V and a J<sub>SC</sub> of 22.54 mA cm<sup>-2</sup> were achieved.<sup>112</sup>

Zhao et al. reports the huge influence of cation mixing on the power conversion efficiency. Due to the mixing of the cations the film morphology can be improved, which reduces the charge carrier recombination. The work of Zhao et al. contains the optimization of the FA and MA ratio of the FA<sub>x</sub>MA<sub>1-x</sub>SnI<sub>3</sub> perovskite. The highest PCE value was reached with FA<sub>0.75</sub>MA<sub>0.25</sub>SnI<sub>3</sub> and additionally 10% SnF<sub>2</sub> with the following device architecture glass/ITO/PEDOT:PSS/FA<sub>0.75</sub>MA<sub>0.25</sub>SnI<sub>3</sub>/C<sub>60</sub>/BCP/Ag with a maximum PCE of 8.12% and average PCE 7.48% ± 0.52%, a FF of 61.9 ± 1.8%, a V<sub>OC</sub> of 0.58 ± 0.03 V and a J<sub>SC</sub> of 21.0 ± 0.5 mA cm<sup>-2</sup>.<sup>104</sup>

Up to now the best performance was reached in 2018 by Shao et al. with 2D/3D based hybrid FASnI<sub>3</sub> perovskite solar cells. Low power conversion efficiency can be attributed to high background carrier density, because the density of intrinsic defects is high, like Sn vacancies and the oxidized species Sn<sup>4+</sup>. The main problem is that the formation of Sn vacancies has a low formation energy and the easy oxidation of Sn<sup>2+</sup> to Sn<sup>4+</sup>.

These two main challenges lead to self-p-doping in the tin based perovskite that ends up in recombination losses of the charge carriers. The addition of SnF<sub>2</sub> should fill the tin vacancies and the oxidation of Sn<sup>2+</sup> should be suppressed. A high PCE of 9% was achieved via using a combination of 2D and 3D FASnI<sub>3</sub> in a planar p-i-n device structure (too much of SnF<sub>2</sub> would deteriorate the perovskite film morphology and the device performance). As reported by Zhao et al. PCE of 8.12% using mixed cation tin perovskites were reported, however the resistance to moisture is limited, as the organic cations FA<sup>+</sup> and MA<sup>+</sup> are hydrophilic. The substrates are built in an inverse device architecture as follows: glass/ITO/PEDOT: PSS/2D,3D FASnI<sub>3</sub>/C<sub>60</sub>,BCP/Al. PEAI was mixed to the FAI and SnI<sub>2</sub> perovskite solution to achieve 2D structure. A maximum PCE of 9%, a FF of 71%, a V<sub>OC</sub> of 0.53 V and a J<sub>SC</sub> of 24.1 mA cm<sup>-2</sup> were reached with a 0.08 M of layered 2D structure and 0.92 M of 3D perovskite.<sup>101</sup>

In addition to the improvement of the solar cell performance via variation of the perovskite composition, Chen et al. investigated the interfacial modification of the tin based perovskite solar cells. Therefore they introduced a PEABr layer between the HTL and the perovskite.

The following device set up was used: glass/ITO/PEDOT:PSS/PEABr/FASnI<sub>3</sub>/C<sub>60</sub>/BCP/Cu. It was reported that this interlayer leads to an improvement in morphology and to a reduction of trap states of the perovskite films and the interface. Best solar cell performance was with a PCE of 7.05%, a FF of 63%, a V<sub>OC</sub> of 0.45 V and a J<sub>SC</sub> of 24.87 mA cm<sup>-2</sup>.<sup>129</sup>

## 2 Aim of the thesis

This thesis focuses on the investigation and optimisation of tin based perovskite solar cells as alternative to lead based perovskite. Based on the Master Thesis of Bastian Friesenbichler<sup>130</sup> different strategies to improve the solar cell performance are envisaged. Therefore MA<sub>0.75</sub>FA<sub>0.15</sub>PEA<sub>0.1</sub>SnI<sub>3</sub> was chosen as perovskite starting material with an inverted device architecture (glass/ITO/PEDOT: PSS/MA<sub>0.75</sub>FA<sub>0.15</sub>PEA<sub>0.1</sub>SnI<sub>3</sub>/PC<sub>60</sub>BM/Al). One major problem of these systems is the easy oxidation of Sn<sup>2+</sup>, which causes stability problems and a poor solar cell performance. Additionally, it is described in literature that purchased “pure” SnI<sub>2</sub> often also contain SnI<sub>4</sub><sup>139</sup>, a fact which was already observed by B. Friesenbichler in his thesis. Therefore the first goal of this work is to find a suitable purification method for the purchased SnI<sub>2</sub>. A second goal is set on the optimisation of the fabrication process as it was found that the preparation of tin based perovskite solar cells has a poor reproducibility.<sup>132</sup> Apart from that tin based perovskites have a much lower solubility than lead based perovskites, so the crystallization process is much faster and hence it is more difficult to receive smooth tin based perovskite films.<sup>128</sup> Therefore the spin coating steps and the anti-solvent dropping of the layers should be optimized as well as the crystallization step of the perovskite film via annealing should be improved. Furthermore the influence of the addition of CuBr<sub>2</sub> to enhance the stability of the solar cell should be investigated as it is reported for example in the work of Li et al. that an addition of CuBr<sub>2</sub> of Pb-Sn perovskites leads to an improvement of the perovskite crystallization with improved charge transport properties.<sup>131</sup> As well as it is mentioned in the work of Lee et al. that the introduction of bromide in the perovskite structure leads to an improved air stability, as the defect concentration is lowered through which the carrier density is lowered.<sup>132</sup>

As it is also reported that the interface between the perovskite and the HTL/ETL has a crucial influence on the solar cell performance, an interlayer between the PEDOT:PSS layer and the perovskite layer should be investigated based on the recently published work of Chen et al.<sup>129</sup>

# 3 Results

## 3.1 Comparison of the SnI<sub>2</sub> purification methods

The easy oxidation from Sn<sup>2+</sup> to Sn<sup>4+</sup> can cause Sn vacancies in the perovskite structure which would lead to carrier recombination losses. This has a negative effect on the solar cell performance, therefore it was tried to purify the purchased SnI<sub>2</sub>. Different purification methods were used based on two main principles. It was tried to purify SnI<sub>2</sub> via sublimation, bulb-to-bulb distillation and purification in the tube furnace (modified sublimation method). These methods are based on the principle to remove SnI<sub>4</sub> from SnI<sub>2</sub> due to different boiling points of these two. The melting and boiling point of SnI<sub>4</sub> is with 144 °C and 364 °C<sup>133</sup> significantly lower than for SnI<sub>2</sub> with 320 °C and 714 °C<sup>134</sup>.

The other method used was to recrystallize the purchased SnI<sub>2</sub> to receive a SnI<sub>2</sub>(DMF) complex as pure crystals. Solar cells were then built with the purified SnI<sub>2</sub> and the impact of the purification on the solar cell performance was investigated.

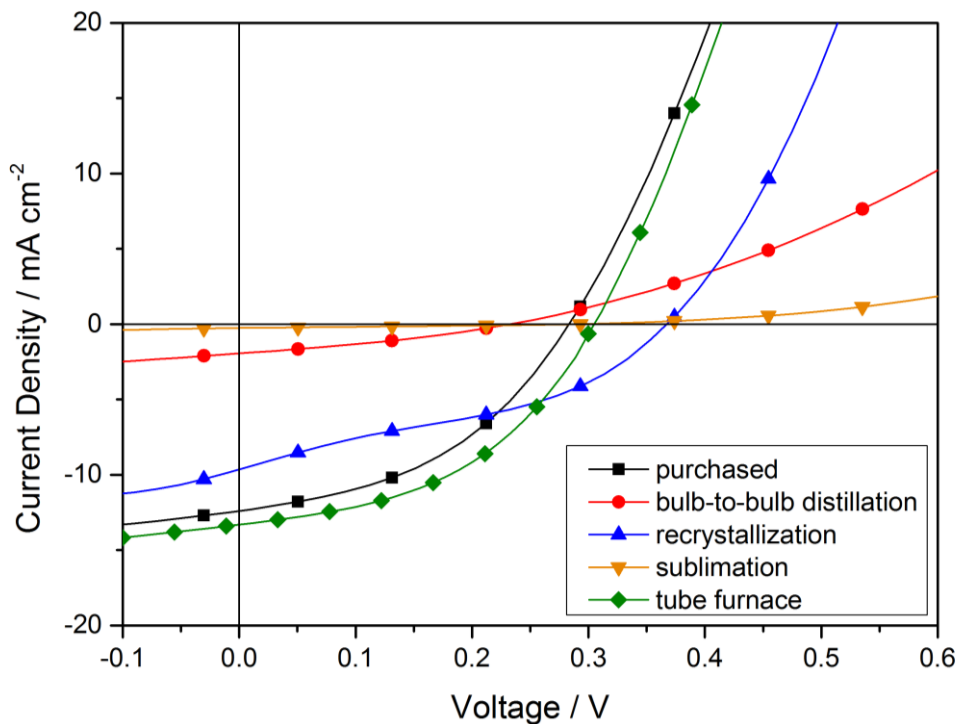


Figure 1: JV- curves of the best solar cell performance when using the purchased SnI<sub>2</sub> and SnI<sub>2</sub> of each purification method for the preparation of the solar cells

It can be observed that for those solar cells built with purified SnI<sub>2</sub> via bulb-to-bulb distillation, sublimation and recrystallization the solar cell performance got worse compared to those with the purchased SnI<sub>2</sub>. Although the  $V_{OC}$  is with 370 mV the highest value for the recrystallization compared to the other values, all the other values of the  $J_{SC}$ , the FF and the PCE are higher for the purchased SnI<sub>2</sub> and the SnI<sub>2</sub> purified in the tube furnace.

The overall best performance was achieved with SnI<sub>2</sub> purified in the tube furnace. The best performance within this study was with solar cells prepared with purified SnI<sub>2</sub> in the tube furnace with a PCE of 1.83 %, a FF of 45.5 %, a  $V_{OC}$  of 0.3 V and a  $J_{SC}$  of 13.3 mA cm<sup>-2</sup>. Therefore ongoing solar cells were built with SnI<sub>2</sub> purified in the tube furnace. The received performance values are listed in Table 1 and an illustration via a boxplot is shown in Figure 2.

*Table 1: Mean values and standard deviation of the  $V_{oc}$ ,  $J_{sc}$ , FF and PCE for differently purified SnI<sub>2</sub>, purified via sublimation, bulb-to-bulb distillation, recrystallization and tube furnace, the values are calculated out of five values*

Method	$V_{OC} / V$	$J_{SC} / \text{mA/cm}^{-2}$	FF / %	PCE / %
Purchased	$0.28 \pm 0.003$	$8.71 \pm 2.66$	$43.6 \pm 2.6$	$1.05 \pm 0.28$
<b>Best cell</b>	<b>0.29</b>	<b>12.29</b>	<b>41.8</b>	<b>1.49</b>
Sublimation	$0.23 \pm 0.09$	$0.85 \pm 1.73$	$30.7 \pm 7.6$	$0.11 \pm 0.24$
<b>Best cell</b>	<b>0.29</b>	<b>0.24</b>	<b>27.7</b>	<b>0.02</b>
Bulb-to-to distillation	$0.11 \pm 0.232$	$0.437 \pm 1.88$	$30.5 \pm 3.3$	$0.032 \pm 0.14$
<b>Best cell</b>	<b>0.23</b>	<b>1.88</b>	<b>32.7</b>	<b>0.14</b>
Recrystallization	$0.378 \pm 0.0123$	$6.42 \pm 2.04$	$37.7 \pm 1.39$	$0.88 \pm 0.273$
<b>Best cell</b>	<b>0.37</b>	<b>9.43</b>	<b>37.7</b>	<b>1.31</b>
Tube furnace	$0.243 \pm 0.043$	$11.8 \pm 1.56$	$41.9 \pm 2.6$	$1.23 \pm 0.41$
<b>Best cell</b>	<b>0.3</b>	<b>13.3</b>	<b>45.9</b>	<b>1.83</b>

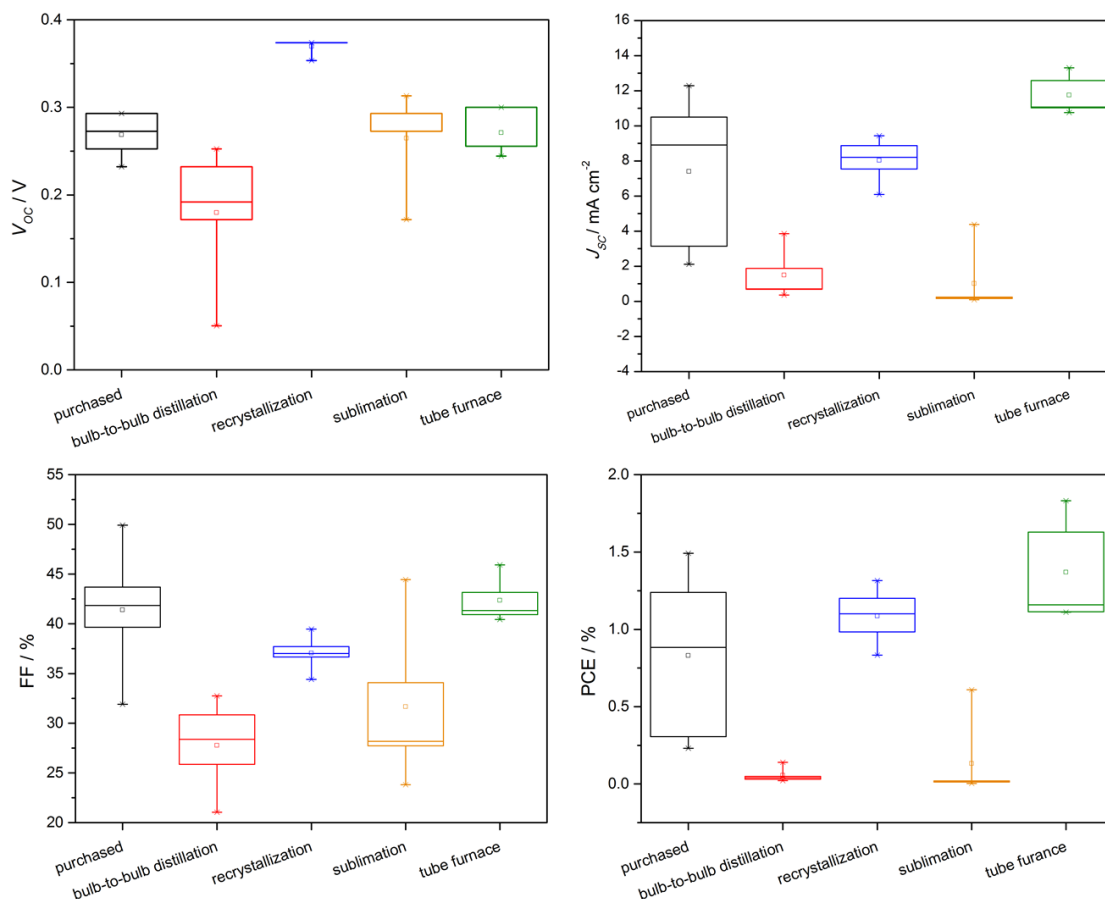


Figure 2: Boxplot of the mean values and standard deviation of the  $V_{OC}$ , the  $J_{SC}$ , the FF and the PCE for the purchased  $\text{SnI}_2$  and the purified  $\text{SnI}_2$  via bulb-to-bulb distillation, recrystallization, sublimation and purification in the tube furnace

It is assumed for the purification methods like bulb-to-bulb distillation and sublimation that the purification was not successful. In case for the bulb-to-bulb distillation it is assumed that the vacuum was not high enough and therefore the temperature which can be reached with the bulb-to-bulb distillation apparatus was not sufficient to separate  $\text{SnI}_4$  from the  $\text{SnI}_2$  fraction. The sublimation did not seem to be successful as in the first attempts the entire purchased  $\text{SnI}_2$  fraction to be cleaned was on the sublimation finger instead of having a separation. This leads us to the assumption that maybe a disproportionation reaction of  $2 \text{SnI}_2 \rightarrow \text{Sn} + \text{SnI}_4$  occurs. This disproportionation is an exothermic process. The stability of the oxidation state +II increases within the IV main group from C to Pb, the opposite is the case for the oxidation state +IV, which decreases. The equilibrium for the exothermic disproportionation of tin iodide lays at the side of the dihalogenide with increasing temperature. Tindiiodide is kinetically stable at room temperature.<sup>135</sup> We assumed that if there was  $\text{SnI}_4$  in the purchase  $\text{SnI}_2$ , it was turned into  $\text{SnI}_2$  at higher temperature and we removed it with the thought to be  $\text{SnI}_4$  fraction in the case for the sublimation purification.

Based on this assumption the purification via the tube furnace was carried out in a closed Schlenk tube, so that  $\text{SnI}_4$  would be changed to  $\text{SnI}_2$  through the disproportionation reaction and a purer  $\text{SnI}_2$  fraction is received.

### 3.2 XRD analysis of $\text{SnI}_2$ and $\text{MA}_{0.75}\text{FA}_{0.15}\text{PEA}_{0.1}\text{SnI}_3$ perovskite

A powder XRD was recorded of the purchased and purified (in tube furnace)  $\text{SnI}_2$  (purity 99.99%). The comparison of the XRD patterns received for the purchased and purified  $\text{SnI}_2$  with references of  $\text{SnI}_2$  and  $\text{SnI}_4$  should show if there are any residues of  $\text{SnI}_4$ . Figure 3 shows the XRD patterns of purchased/purified  $\text{SnI}_2$  and the references of  $\text{SnI}_2$ <sup>136</sup> and  $\text{SnI}_4$ <sup>137</sup>. The XRD patterns of the purchased and purified  $\text{SnI}_2$  are not completely similar; however there are almost no differences. Comparing the XRD patterns of the purchased and purified  $\text{SnI}_2$  leads to the conclusion that both show the same characteristic XRD patterns as the reference of  $\text{SnI}_2$ . Whereas the characteristic XRD patterns of the reference  $\text{SnI}_4$  cannot be found in the XRD patterns in both the  $\text{SnI}_2$  samples. Therefore it is assumed that neither the purchased nor the purified  $\text{SnI}_2$  contain significant amounts of  $\text{SnI}_4$ . However the XRD patterns do not completely match especially in the region of  $27.5^\circ$ , where more patterns can be observed for purified and purchased  $\text{SnI}_2$  compared to the reference patterns of  $\text{SnI}_2$ . So for  $\text{SnI}_2$  (purified and purchased) it is assumed that other unidentified residues are contained and further research would be necessary for their identification.

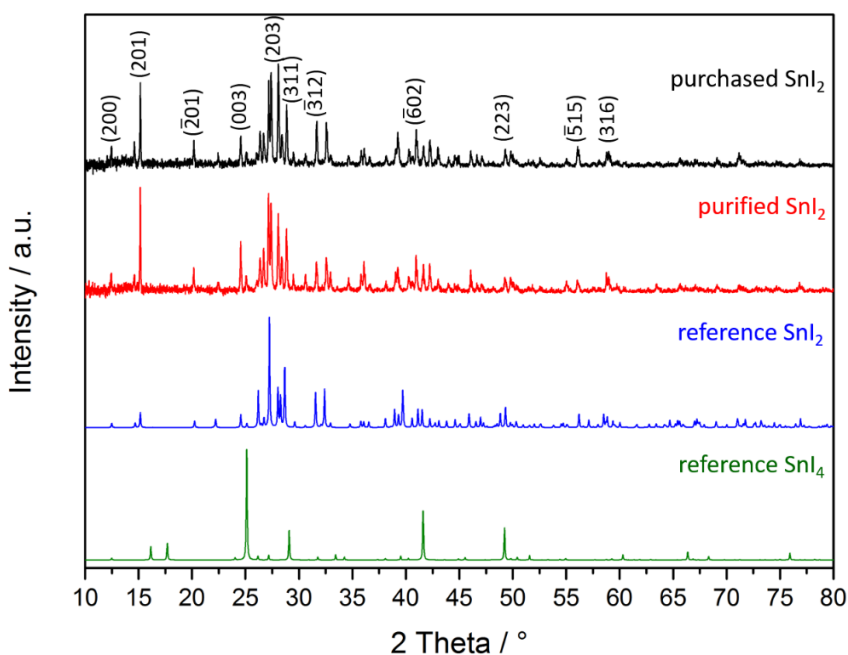


Figure 3: XRD diffractograms of the purchased  $\text{SnI}_2$  (black), purified  $\text{SnI}_2$  (red), reference  $\text{SnI}_2$  (blue) and reference  $\text{SnI}_4$  (green); the Miller indices are assigned to the corresponding diffraction patterns of the purchased  $\text{SnI}_2$ ; the reference for  $\text{SnI}_2$  and  $\text{SnI}_4$  are obtained from ICSD ID 1749 and 69631

In addition XRD measurement of the  $\text{MA}_{0.75}\text{FA}_{0.15}\text{PEA}_{0.1}\text{SnI}_3$  perovskite was performed to characterize the formed perovskite.

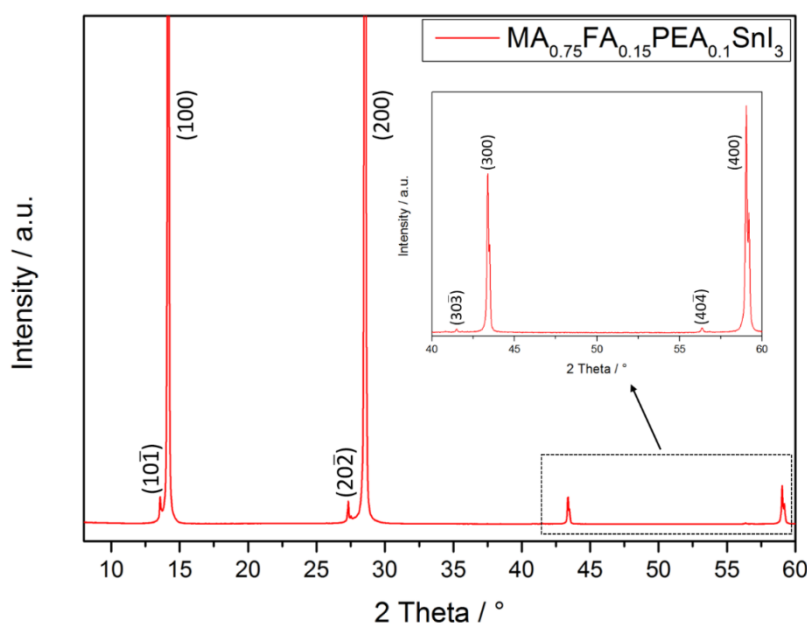


Figure 4: XRD diffractogram of the perovskite with the assigned Miller indices to the corresponding diffraction patterns

The addition of PEA to the tin based perovskite leads to a reduction of the dimensionality from pure 3D structure to a mixture of 2D/3D structure. The XRD pattern shows dominant diffraction peaks at  $14.2^\circ$ ,  $28.5^\circ$ ,  $43.4^\circ$  and  $59.1^\circ$ , which are assigned to the lattice planes (100), (200), (300) and (400), that are in agreement with literature.<sup>125, 101</sup> This indicates an orthorhombic 3D crystal structure, as it is also reported for a  $\text{FASnI}_3$  perovskite. However for a  $\text{FASnI}_3$  perovskite there are also reported peaks at  $24.4^\circ$ ,  $31.65^\circ$  and  $40.37^\circ$  for the crystallographic planes at (120)/(102), (122) and (222), which are totally suppressed in the diffraction pattern of the  $\text{MA}_{0.75}\text{FA}_{0.15}\text{PEA}_{0.1}\text{SnI}_3$ , that indicates the change from a 3D dimension to a 2D/3D dimension. The (h00) lattice planes indicate either that the crystallization occurs in a preferential direction or that the orientation is preferentially.

The smaller peaks at lower angles  $13.6^\circ$ ,  $27.3^\circ$ ,  $41.5^\circ$  and  $56.3^\circ$  can be attributed to the  $(10\bar{1})$ ,  $(20\bar{2})$ ,  $(30\bar{3})$  and  $(40\bar{4})$  planes, which originate from a distortion of the in-plane lattice parameters (a and c) due to the incorporation of  $\text{PEA}^+$ .

### 3.3 Optical Characterisation

Further the  $\text{MA}_{0.75}\text{FA}_{0.15}\text{PEA}_{0.1}\text{SnI}_3$  perovskite was optically characterized to investigate its absorption behaviour. Purchased  $\text{SnI}_2$  (99.99% purity) purified in the tube furnace was used for the preparation of  $\text{MA}_{0.75}\text{FA}_{0.15}\text{PEA}_{0.1}\text{SnI}_3$  perovskite. The band gap energy  $E_g$  of  $\text{MA}_{0.75}\text{FA}_{0.15}\text{PEA}_{0.1}\text{SnI}_3$  was calculated via the Tauc-Plot. Therefore a UV-VIS spectrum of  $\text{MA}_{0.75}\text{FA}_{0.15}\text{PEA}_{0.1}\text{SnI}_3$  (Figure 5) was recorded as well as the film thickness of these perovskite layers was determined. According to the following formula the absorption coefficient was calculated:

$$\alpha = 2.3026 * \frac{A}{t}$$

$\alpha$  ... absorption coefficient [ $\text{m}^{-1}$ ]

A ... absorbance []

T ... film thickness [m]

The band gap energy  $E_g$  was determined via plotting  $(\alpha h\nu)^2$  against the photon energy ( $h\nu$ ). The extrapolation of the linear part of the received curve leads to a line that intersects with the x-axis. The intersection point gives the band gap energy of the perovskite.

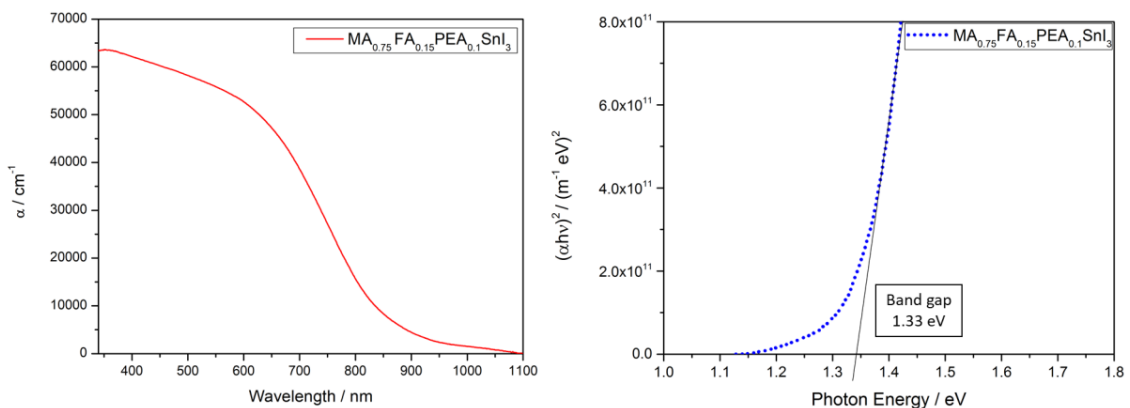


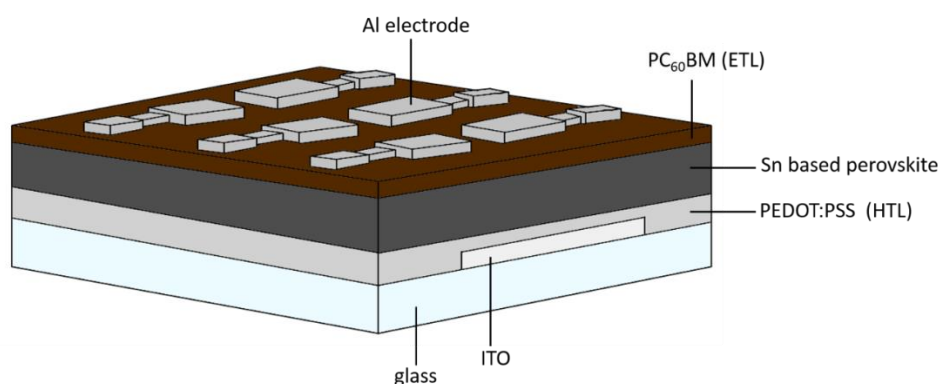
Figure 5: Absorption spectrum of  $\text{MA}_{0.75}\text{FA}_{0.15}\text{PEA}_{0.1}\text{SnI}_3$  perovskite (left graph); Calculation of the band gap for  $\text{MA}_{0.75}\text{FA}_{0.15}\text{PEA}_{0.1}\text{SnI}_3$  perovskite via the Tauc-Plot with a band gap energy of 1.33 eV (right graph)

An onset in absorption can be observed in Figure 5 (left graph) at about 930 nm, from where on an increase of absorption occurs up to an absorption coefficient of  $63315 \text{ cm}^{-1}$ . The band gap of the  $\text{MA}_{0.75}\text{FA}_{0.15}\text{PEA}_{0.1}\text{SnI}_3$  perovskite material was determined via the Tauc-plot with the received data from the absorption measurement and a layer thickness of  $323 \text{ nm} \pm 14 \text{ nm}$ .

The determined band gap for this perovskite material is 1.33 eV, which is nearly the ideal band gap of 1.34 eV for a photovoltaic absorber material according to the Shockley Queisser limit at which a maximum PCE of 33.7% can be reached in theory.<sup>96</sup>

### 3.4 Optimization of the solar cell preparation steps

As former experiments have shown that the preparation of tin based perovskite solar cells is not really reproducible and the fabrication parameters play a huge role, the solar cell preparation was tried to be optimized. Therefore the preparation of the different layers was varied according to their layer thickness and the concentrations of the applied perovskite precursor solution, as well as the annealing step of the perovskite layer was investigated and optimized. All solar cells were prepared in the same device architecture (glass/ITO/PEDOT:PSS/MA<sub>0.75</sub>FA<sub>0.15</sub>PEA<sub>0.1</sub>SnI<sub>3</sub>/PC<sub>60</sub>BM/Al) illustrated in Scheme 8.



*Scheme 8: Illustration of the device architecture for the prepared solar cells; glass/ITO/PEDOT:PSS/Sn based perovskite/PC<sub>60</sub>BM/Al*

#### 3.4.1 Optimization of the perovskite layer

The influence of the film thickness of the perovskite layer and the influence of the perovskite precursor solution concentration on the performance of the solar cell was investigated. Therefore, the spin coating rate of the perovskite layer was varied and in addition, different concentrations for the perovskite precursor solution were investigated.

The spin coating rate for the perovskite layer was varied from 4500, 5000, 5500 and 6000 rpm. The film thickness was determined via contact profilometer and the results show that with increasing spin coating rate the film thickness of the perovskite layer decreases as expected (Table 2).

Table 2: Mean values and standard deviation of the film thickness and roughness for the differently spin coated perovskite layers

SC rate perovskite	Film Thickness / nm	Roughness / nm
4500 rpm	378.6 ± 26.9	6.3 ± 3.3
5000 rpm	323.5 ± 45.1	3.4 ± 1.0
5500 rpm	246.0 ± 23.5	3.9 ± 1.0
6000 rpm	228.6 ± 11.6	3.4 ± 0.5

The received solar cell performances of the *JV*- measurement are shown in Figure 6 and Table 3. The best solar cell performance was reached with a spin coating rate of 5000 rpm with a layer thickness of 323.5 nm ± 45.1 nm. The highest values for this solar cell were a PCE of 3.68%, a FF of 63.3%, a  $V_{OC}$  of 0.42 V and a  $J_{SC}$  of 13.96 mA cm<sup>-2</sup>.

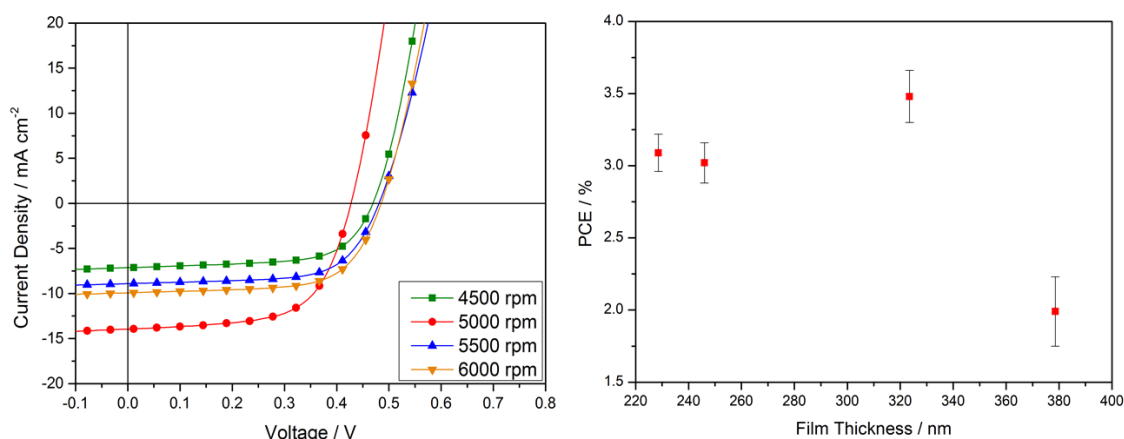


Figure 6: Left: solar cell performance of differently spin coated perovskite layers, with spin coating rates of 4500, 5000, 5500 and 6000 rpm; it is shown the best solar cell performance of each spin coating rate; right: variation of the PCE in dependence of the film thickness

It can be observed in Figure 6 (right) that if the film thickness is too low or too high the PCE decreases and the maximum PCE is at about 323 nm. The optimum thickness of the perovskite layer is a balance between absorption and recombination.<sup>138</sup> So it is maybe the case that for too thick films the diffusion length of the generated carriers is too short, therefore recombination can occur, whereas too thin films do not absorb efficiently and therefore the solar cell performance can decrease. Table 3 shows that the FF as well as the  $V_{OC}$  are relatively similar for the different spin coating rates with about 64% and 0.46 V. The  $J_{SC}$  is most affected by the film thickness change, consequently also the PCE values vary.

Table 3: Mean value and standard deviation for the performance parameters  $V_{OC}$ ,  $J_{SC}$ , FF and PCE calculated out of the best 5 values for the different spin coating rates of the perovskite layer

Spin coating rate	$V_{OC}$ / V	$J_{SC}$ / $\text{mA cm}^{-2}$	FF / %	PCE / %
4500 rpm	$0.47 \pm 0.05$	$6.68 \pm 0.68$	$63.3 \pm 1.41$	$1.99 \pm 0.24$
<b>Best cell</b>	<b>0.46</b>	<b>7.14</b>	<b>64.6</b>	<b>2.16</b>
5000 rpm	$0.44 \pm 0.1$	$12.45 \pm 0.88$	$64.4 \pm 1.1$	$3.48 \pm 0.18$
<b>Best cell</b>	<b>0.42</b>	<b>13.96</b>	<b>63.3</b>	<b>3.68</b>
5500 rpm	$0.48 \pm 0.06$	$9.71 \pm 0.29$	$64.9 \pm 1.66$	$3.02 \pm 0.14$
<b>Best cell</b>	<b>0.49</b>	<b>9.9</b>	<b>65.3</b>	<b>3.14</b>
6000 rpm	$0.47 \pm 0.05$	$10.12 \pm 0.51$	$65.0 \pm 2.13$	$3.09 \pm 0.13$
<b>Best cell</b>	<b>0.46</b>	<b>10.22</b>	<b>64.1</b>	<b>3.14</b>

Furthermore the solar cell performances were investigated of solar cells prepared with differently concentrated perovskite precursor solutions.

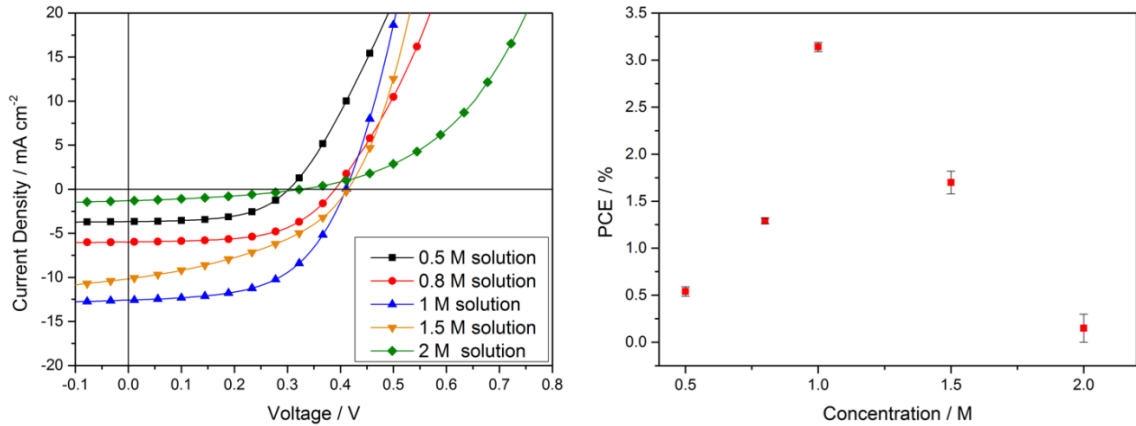


Figure 7: Left: JV- curves of the best performance of the solar cells built with differently concentrated perovskite precursor solutions, with a concentration range from 0.5, 0.8, 1, 1.5 and 2 M; right: PCE in dependence of differently concentrated perovskite precursor solutions

It can be observed that the best solar cell performance was reached with a 1 M perovskite precursor solution. An increase of the concentration from 0.5 M to 1 M leads to an increase in the  $V_{OC}$  as well as in the  $J_{SC}$  (Table 4), with the highest values reached with a concentration of 1 M. By further increasing the concentration to 2 M a decrease in these values occurs. Using lower concentrations the perovskite layer was more transparent which leads obviously to less absorption and therefore to a worse solar cell performance.

The concentration of the perovskite precursor solution is directly related to the film thickness of the perovskite layer. Therefore it is assumed that an ideal film thickness is reached with a 1M perovskite precursor solution, whereas for too high concentrated solutions the film thickness is too thick or for too low concentrated solutions the film thickness is too thin.

The maximum PCE value was reached with a concentration of 1M with a PCE of 3.14%, a FF of 47.5, a  $V_{OC}$  of 0.4 V and a  $J_{SC}$  of 16.56 mA cm<sup>-2</sup> (Figure 7), too low or too high concentrated perovskite precursor solutions have a negative impact on the performance of the solar cell.

*Table 4: Mean values, standard deviation and best performance of the solar cells with differently concentrated perovskite precursor solutions with 0.5, 0.8, 1, 1.5 and 2 M solutions, the mean values and the standard deviation were calculated with the best five performance values*

Concentration	$V_{OC} / V$	$J_{SC} / \text{mA cm}^{-2}$	FF / %	PCE / %
0.5 M	0.29 ± 0.01	3.38 ± 0.27	55.1 ± 1.7	0.54 ± 0.05
<b>Best cell</b>	<b>0.3</b>	<b>3.66</b>	<b>55.9</b>	<b>0.61</b>
0.8 M	0.39 ± 0.01	5.63 ± 0.31	58.5 ± 1.2	1.29 ± 0.03
<b>Best cell</b>	<b>0.38</b>	<b>5.89</b>	<b>57.5</b>	<b>1.32</b>
1 M	0.42 ± 0.01	13.99 ± 1.51	52.4 ± 0.03	3.06 ± 0.05
<b>Best cell</b>	<b>0.4</b>	<b>16.56</b>	<b>47.5</b>	<b>3.14</b>
1.5M	0.39 ± 0.02	9.35 ± 0.48	42.4 ± 0.88	1.56 ± 0.12
<b>Best cell</b>	<b>0.41</b>	<b>10.16</b>	<b>41.2</b>	<b>1.7</b>
2M	0.31 ± 0.02	1.26 ± 0.07	34.9 ± 1.32	0.13 ± 0.01
<b>Best cell</b>	<b>0.32</b>	<b>1.29</b>	<b>35.7</b>	<b>0.15</b>

### 3.5 Optimization of the anti-solvent dropping

It was found in previous experiments that the anti-solvent dropping has a huge influence on the perovskite film formation and the morphology. Therefore the AS dropping step was optimized with regard to the distance (between the pipette and the solar cell) the AS was applied, the speed of the dropping and the annealing step after the AS dropping. Either toluene or CB was used as anti-solvent. However some experiments showed that CB is more suitable as AS than toluene, as the performance of those solar cells using CB as AS was better than for those using toluene (see Table 5). Therefore chlorobenzene is the anti-solvent of choice for the optimized solar cell preparation.

*Table 5: Mean values and standard deviation for the performance of solar cells prepared with an anti-solvent either with chlorobenzene or toluene; the values were calculated out of the five best cells*

<b>Anti-solvent</b>	<b><math>V_{OC} / V</math></b>	<b><math>J_{SC} / mA\ cm^{-2}</math></b>	<b>FF / %</b>	<b>PCE / %</b>
<b>toluene</b>	$0.29 \pm 0.02$	$13.75 \pm 1.17$	$45.0 \pm 2.8$	$1.78 \pm 0.35$
<b>chlorobenzene</b>	$0.38 \pm 0.02$	$19.44 \pm 2.85$	$55.8 \pm 2.8$	$4.06 \pm 0.34$

#### 3.5.1 Influence of the anti-solvent dropping distance

The application of the anti-solvent with three different dropping distances from the pipette to the solar cell were investigated and the influence on the solar cell performance. Either the pipette dip was directly held above the solar cell (near), about 2.5 cm away from the solar cell (middle) or about 4.5 cm away from the solar cell (far) when the anti-solvent was applied. As the dropping distance was varied all other spin coating parameters remained the same.

The performance of the best cells for each method are shown in Figure 8 as well as the mean value and the standard deviation of these experiments, which were calculated out of the five best results shown in Table 6.

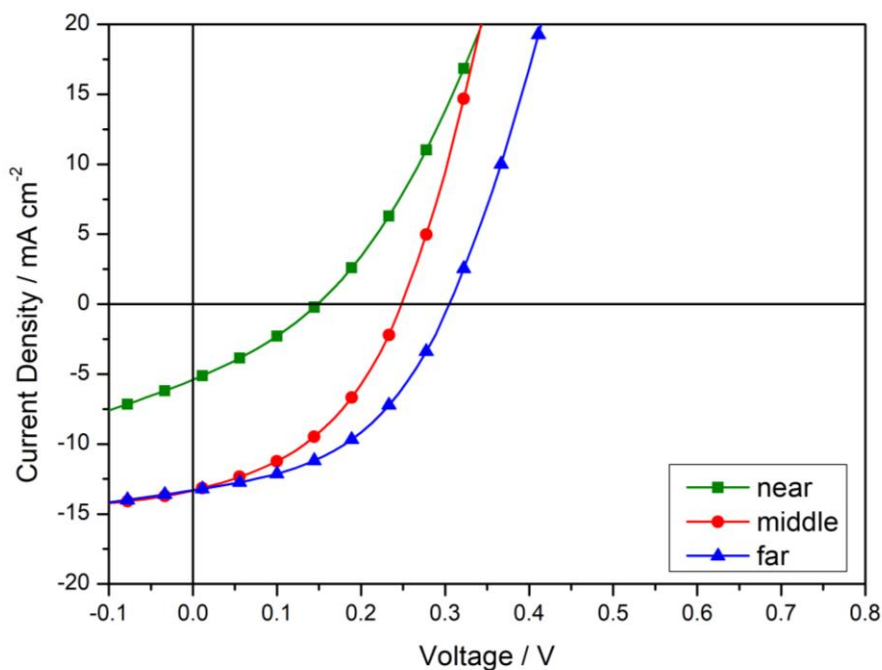


Figure 8: Best solar cell performance of solar cells prepared with different anti-solvent dropping distances (near, middle & far)

It can be observed that with increasing the distance from the solar cell to the pipette tip, the performance gets better regarding the PCE, FF,  $V_{OC}$  and  $J_{SC}$ .

The best performance was reached with an anti-solvent dropping distance of about 4.5 cm (far) with a PCE of 1.83%, a FF of 45.9%, a  $V_{OC}$  0.3 V and a  $J_{SC}$  of 13.3 mA cm<sup>-2</sup>. Therefor the anti-solvent dropping for ongoing experiments was carried out with a distance of 4.5 cm.

Table 6: Mean values and standard deviation of the solar cell performance with three different anti-solvent dropping distances (near, middle & far); the mean values and standard deviations were calculated out of the best five values

	$V_{OC}$ / V	$J_{SC}$ / mA cm <sup>-2</sup>	FF / %	PCE / %
Near	0.13 ± 0.01	4.15 ± 0.77	28.5 ± 0.017	0.15 ± 0.05
<b>Best cell</b>	<b>0.14</b>	<b>5.39</b>	<b>31.1</b>	<b>0.24</b>
Middle	0.22 ± 0.01	12.19 ± 0.74	41.5 ± 0.02	1.12 ± 0.16
<b>Best cell</b>	<b>0.24</b>	<b>13.3</b>	<b>42.4</b>	<b>1.38</b>
Far	0.28 ± 0.02	13.0 ± 1.4	43.9 ± 0.02	1.57 ± 0.28
<b>Best Cell</b>	<b>0.30</b>	<b>13.3</b>	<b>45.9</b>	<b>1.83</b>

Additionally it can be seen by the naked eye that when the AS is applied too near, the surface is not that smooth and grey streaks can be observed on the black surface (Figure 9; image D) compared to a smooth black surface (mirroring) when the AS dropping is applied from a distance farther apart (Figure 9, image E). Hence the surfaces were investigated via optical microscopy. Figure 5 shows the perovskite layers that were formed when applying the AS from a near, a middle and a far dropping distance via optical microscopy investigation.

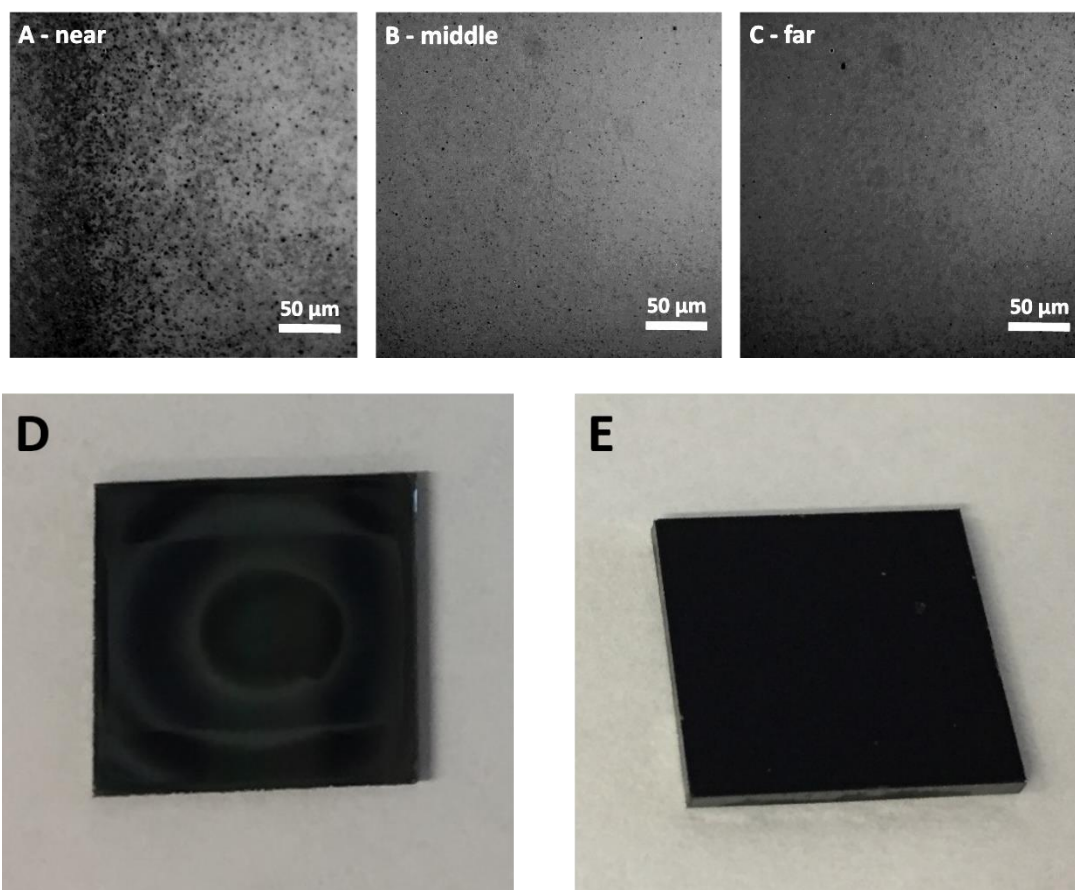


*Figure 9: Optical microscope images of glass substrates spin coated with the perovskite layer with different AS dropping distances between the pipette tip and the substrate; magnification 50 times onlight; image **A** with a near distance, **B** with a middle distance and **C** with a distance far; image **D** and **E** show prepared glass/TiO substrates with the perovskite layer on it with a near AS dropping distance in **D** and a far distance for image **E***

The optical microscopy investigation (image A-C, Figure 5) shows that for too near AS dropping black pinholes can be investigated whereas when the distances of the application increases less pinholes can be observed, which is might be the reason for the better solar cell performance.

### 3.5.2 Influence of the anti-solvent dropping speed and application number on the solar cell performance

The influence of AS dropping speed on the performance of the solar cells was investigated. Therefore the anti-solvent was either dropped fast in one step or dropwise on the solar cell. In addition it was investigated if there is a difference in applying the anti-solvent dropping only one time or two times. For this the spin coating and AS dropping procedure was repeated, so overall twice the volume and time was used for this spin coating step.

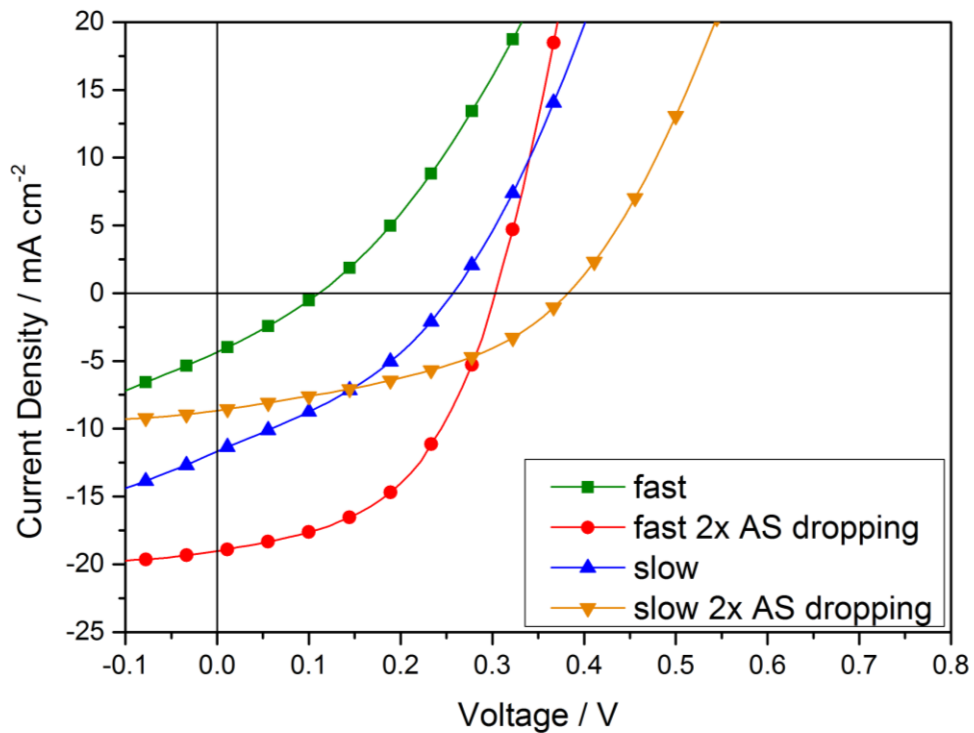


Figure 10: Best solar cell performance of solar cells prepared with different AS dropping speed (fast or slow) and number (one time or two times AS dropping)

The received *JV*- curves for those solar cells with one time AS dropping show a better performance, for the ones with a slower AS dropping than those with a fast AS application (Figure 10). Comparing the solar cells prepared with two times AS dropping, the two times and fast AS dropping leads to the best overall performance.

Although the  $V_{OC}$  is higher for the solar cells prepared with two times slow AS application, the  $J_{sc}$  values are much higher in the case for the ones with a two times fast AS dropping, therefore also the PCE is more than two times higher. The best solar cell performance was reached with two times AS dropping and a fast AS application with a PCE value of 2.78%, a FF of 49.2%, a  $V_{OC}$  of 0.3 V and a  $J_{SC}$  of 19.02 mA cm<sup>-2</sup> (see Table 7).

Table 7: Mean values and standard deviation of the  $V_{oc}$ ,  $J_{sc}$ , FF and PCE for the different AS dropping speeds (fast or slow) and one time or two time AS dropping

Technique	$V_{OC} / V$	$J_{SC} / mA\ cm^{-2}$	FF / %	PCE / %
Fast	$0.09 \pm 0.01$	$4.25 \pm 0.52$	$27.6 \pm 1.1$	$0.11 \pm 0.023$
<b>Best cell</b>	<b>0.11</b>	<b>3.99</b>	<b>28.9</b>	<b>0.14</b>
Fast, 2x AS dropping	$0.29 \pm 0.01$	$15.56 \pm 2.12$	$41.8 \pm 4.93$	$1.87 \pm 0.55$
<b>Best cell</b>	<b>0.30</b>	<b>19.02</b>	<b>49.2</b>	<b>2.78</b>
Slow	$0.23 \pm 0.05$	$9.21 \pm 1.51$	$32.8 \pm 2.14$	$0.71 \pm 0.25$
<b>Best cell</b>	<b>0.25</b>	<b>11.67</b>	<b>34.9</b>	<b>1.04</b>
Slow, 2x AS dropping	$0.30 \pm 0.08$	$5.43 \pm 1.52$	$34.6 \pm 3.87$	$0.59 \pm 0.32$
<b>Best cell</b>	<b>0.38</b>	<b>5.39</b>	<b>38.7</b>	<b>0.75</b>

### 3.5.3 Influence of the annealing step of the perovskite layer on the solar cell performance

The influence of the annealing step of the perovskite layer on the solar cell performance was investigated. It makes a difference if the solar cell with the perovskite layer was put on the hot heating plate (70 °C) immediately after the spin coating process or on the heating plate at RT and was then heated up to 70 °C, as the layer formation is different. Therefor also the solar cell performance will be different, as the carrier transport will be influenced. The perovskite layer was investigated via SEM measurements carried out by Dr. Theodoros Dimopoulos (AIT) of solar cells put directly on the hot heating plate or put on the heating plate after some time at RT, as well as one sample was put directly on the heating plate and two times AS dropping was applied.

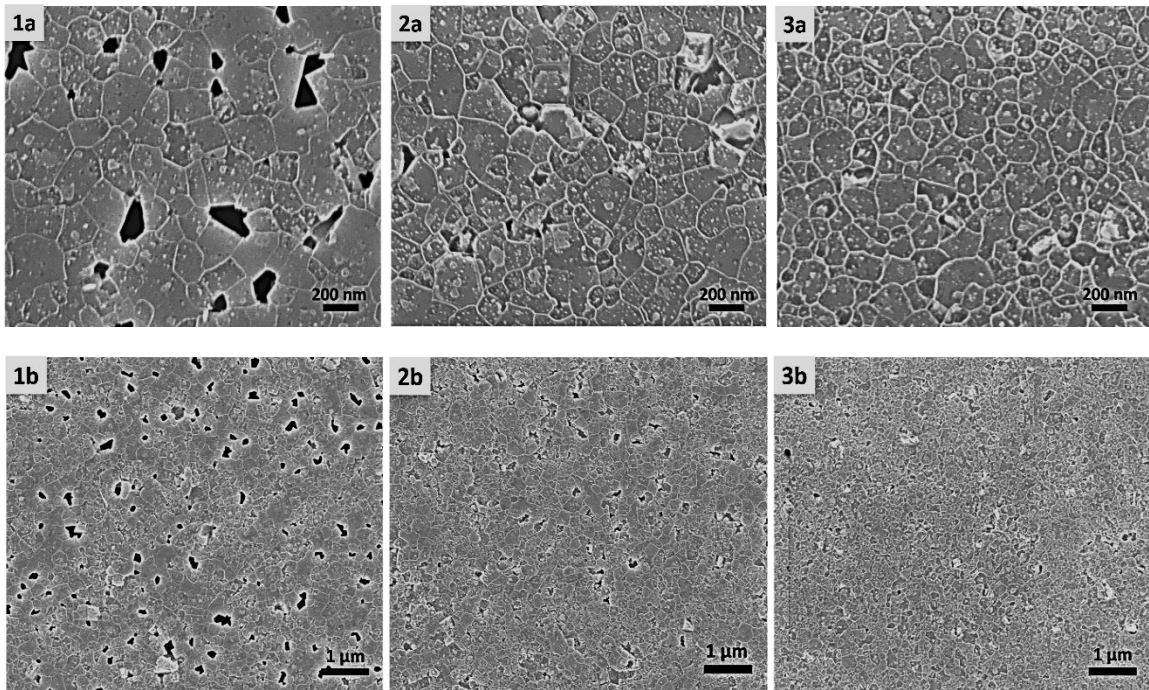


Figure 11: SEM images of differently prepared  $MA_{0.75}FA_{0.15}PEA_{0.1}SnI_3$  perovskite layers; image 1: one times AS dropping and substrate put on heating plate at RT and heated up to 70 °C, image 2: one time AS dropping and putting substrate on hot heating plate (70 °C), image 3: two times AS dropping and putting substrate on hot heating plate (70 °C); those images with a scale of 200 nm compared to those with b with a scale of 1  $\mu$ m

Figure 11 shows the SEM images of three differently prepared substrates. It can be observed that the perovskite layer shows holes (black dots in the image) when prepared with one AS dropping step and an annealing procedure where the substrates were put on the heating plate at RT and then heated up (1a & b). These pinholes are detrimental for the solar cell performance and can lead to short circuits. In addition it can be seen that this is not only the case for the small area in 1a but over a huger area displayed in 1b. The layer treated with one time AS dropping but being directly put on the hot heating plate immediately after the spin coating, exhibits less pinholes. The smoothest perovskite layer was obtained with a two time AS dropping and putting the substrate immediately on the heating plate as it can be seen in image 3 a and b. As the heating rate influences the crystallization of the perovskite layer and the grain sizes, the average grain size (see Table 8) was determined with the SEM images. As expected a slower heating rate leads to larger grains with an average grain size of 116-270 nm, compared to a faster crystallization when putting the substrates on the hot heating plate, leading to smaller average grain sizes of about 76-223 nm with one AS dropping step and even slightly smaller average grain sizes 75-206 nm for layers prepared with two AS dropping steps.

Table 8: Average grain size range of the differently prepared perovskite layer, calculated from measuring the size of the ten smallest and ten biggest grains each

	Average grain size / nm
Slow heating, 1 time AS dropping, (1)	116 - 270
Hot HP, 1 time AS dropping (2)	76 - 223
Hot HP, 2 times AS dropping (3)	75 - 206

Those investigations are in accordance with *JV*- measurements of solar cells, where the perovskite layers were prepared in the same way as described above. It can be observed in Figure 12 and in Table 9 that the best solar cell performance was reached with those substrates, which were put directly on the hot heating plate and received a two times AS dropping. All values increase from one time AS dropping to 2 times AS dropping and immediately putting the solar cells on the hot heating plate. This is in accordance with the investigation of the layers via SEM, as the surface of the perovskite layer was the best for two times AS dropping and a direct annealing step.

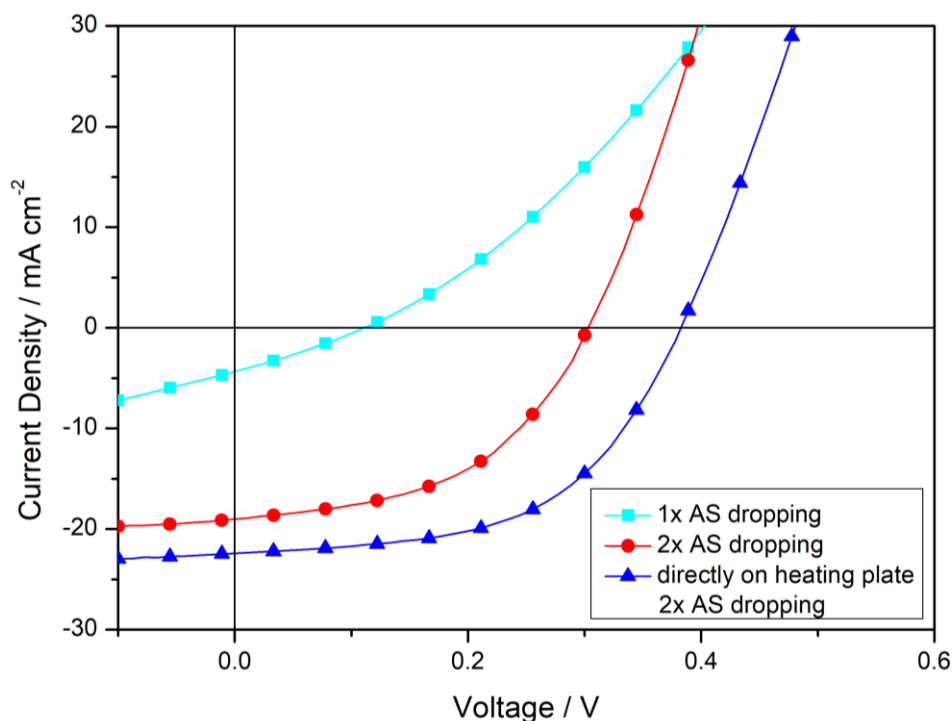


Figure 12: Performance of differently prepared solar cells, where the perovskite layer was prepared in three different ways, either it was treated with one time AS dropping and put on a heating plate at RT and was then heated up or one time AS dropping and putting the substrates on the hot HP or substrates which were treated with two times AS dropping and were directly put it on the HP

The best solar cell performance achieved within this study was with two times AS dropping and a direct annealing step on the hot heating plate with a PCE of 4.54%, a FF of 54.6%, a  $V_{OC}$  of 0.38 V and a  $J_{SC}$  of 22.4 mA cm<sup>-2</sup>.

*Table 9: Mean values and standard deviation of the  $V_{oc}$ ,  $J_{sc}$ , FF and PCE for the differently annealed solar cells and one time or two time AS dropping; the mean values were calculated out of the five best cells*

<b>Technique</b>	<b><math>V_{OC}</math> / V</b>	<b><math>J_{SC}</math> / mA cm<sup>-2</sup></b>	<b>FF / %</b>	<b>PCE / %</b>
Fast	0.09 ± 0.01	4.3 ± 0.5	27.6 ± 1.1	0.11 ± 0.01
<b>Best cell</b>	<b>0.11</b>	<b>4.34</b>	<b>28.0</b>	<b>0.14</b>
Fast 2x AS	0.29 ± 0.01	15.6 ± 2.1	41.9 ± 4.9	1.87 ± 40.54
<b>Best cell</b>	<b>0.30</b>	<b>19.0</b>	<b>49.2</b>	<b>2.77</b>
Directly HP 2x AS	0.38 ± 0.02	19.4 ± 2.9	54.6 ± 2.8	4.5 ± 0.34
<b>Best cell</b>	<b>0.38</b>	<b>22.4</b>	<b>54.6</b>	<b>4.54</b>

### 3.6 Optimization of the PC<sub>60</sub>BM layer

The influence of film thickness of the PC<sub>60</sub>BM layer on the solar cell performance was investigated. In addition two different filter sizes (0.2  $\mu\text{m}$  or 0.45  $\mu\text{m}$ ) were used to observe the influence on the performance of the solar cell, as previous experiments showed that using 0.45  $\mu\text{m}$  sized filters, comet like particles can be observed on the surface of the solar cell by the naked eye. The following four different spin coating rates for the PC<sub>60</sub>BM layer were used: 2000, 3000, 5000 and 6000 rpm and the impact on the performance was further investigated via *JV*- measurements.

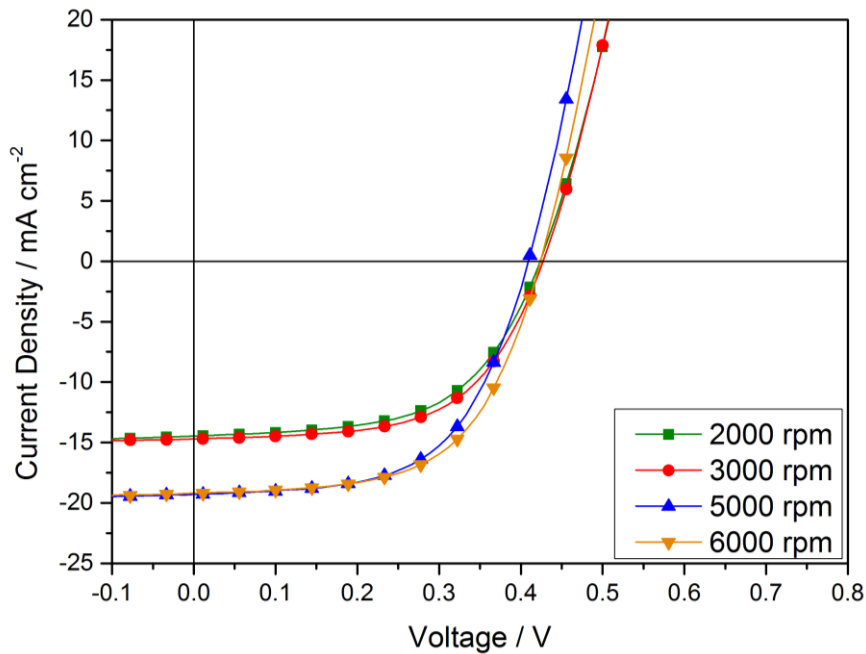


Figure 13: Solar cell performance for different spin coating rates of the PC<sub>60</sub>BM layer of the best cell for each

Figure 13 shows that the solar cell performance increases with a higher spin coating rate. It can be observed that using spin coating rates of 2000 rpm and 3000 rpm for the PC<sub>60</sub>BM layer the performance is similar for both, this is also the case for the spin coating rates of 5000 and 6000 rpm. In addition it can be observed that the above mentioned comet like particles on the surface of the PC<sub>60</sub>BM layer got reduced with an increase of the spin coating rate. The best solar cell performance was achieved with a spin coating rate of 6000 rpm with a PCE of 4.74%, a FF of 59.16%, a  $V_{OC}$  of 0.42 and a  $J_{SC}$  of 19.19  $\text{mA cm}^{-2}$ .

Table 10: Mean values and standard deviation of the  $V_{oc}$ ,  $J_{sc}$ , FF and PCE for four different spin coating rates of the  $PC_{60}BM$  layer, calculated out of the five best values

Spin coating rate	$V_{OC} / V$	$J_{SC} / mA\ cm^{-2}$	FF / %	PCE / %
2000 rpm	$0.41 \pm 0.04$	$14.92 \pm 1.80$	$55.4 \pm 3.9$	$3.35 \pm 0.17$
<b>Best cell</b>	<b>0.42</b>	<b>14.47</b>	<b>57.48</b>	<b>3.54</b>
3000 rpm	$0.43 \pm 0.01$	$14.78 \pm 0.86$	$57.8 \pm 2.7$	$3.65 \pm 0.02$
<b>Best cell</b>	<b>0.42</b>	<b>14.71</b>	<b>59.35</b>	<b>3.67</b>
5000 rpm	$0.42 \pm 0.02$	$17.61 \pm 1.76$	$58.8 \pm 1.5$	$4.23 \pm 0.23$
<b>Best cell</b>	<b>0.41</b>	<b>19.28</b>	<b>57.79</b>	<b>4.52</b>
6000 rpm	$0.43 \pm 0.01$	$17.96 \pm 1.27$	$59.6 \pm 0.9$	$4.55 \pm 0.15$
<b>Best cell</b>	<b>0.42</b>	<b>19.19</b>	<b>59.16</b>	<b>4.74</b>

Two different filter sizes were used for the filtration of the  $PC_{60}BM$  solution to observe the influence on the solar cell performance. Before the optimization of the  $PC_{60}BM$  layer, a  $45\mu m$  filter was used for the filtration of the  $PC_{60}BM$  solution, however after the application of this solution and the spin coating, small particles could be observed on the surface by the naked eye. So this was tried to be avoided by filtering the solution with a smaller filter size of  $0.2\ \mu m$ .

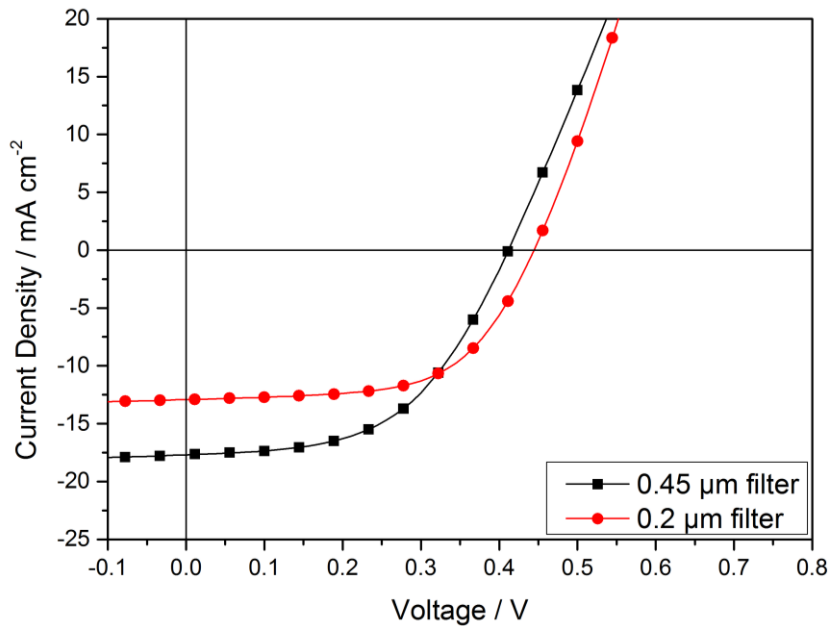


Figure 14: Best performance of solar cells with  $PC_{60}BM$  filtered either with a  $0.2\ \mu m$  (red) or a  $0.45\ \mu m$  filter (black)

Although still particles can be observed on the surface, the number of it decreased. The investigation of the performance (Figure 14 and

Table 11) shows that the mean values of all parameters are higher in the case for the solar cells which were built with a PC<sub>60</sub>BM solution that was filtered with 0.2 μm filter, in contrast to the ones filtered with 0.45 μm filter. However the best solar cell performance within this experiment was achieved with a 0.45 μm filtering step. This leads to the fact that no precise statement can be made, as the values are close to each other. Further investigation would be necessary. However it can be said that the distribution of the values when using the smaller filter is littler, therefor it is also more reproducible.

*Table 11: Mean values, standard deviation and best cells of solar cell performance parameters  $V_{OC}$ ,  $J_{SC}$ ,  $FF$  and  $PCE$  of solar cells where the PC<sub>60</sub>BM solution was either filtered with a 0.2 μm or a 0.45 μm filter, the values calculated out of the five best cells*

<b>PC<sub>60</sub>BM filter size</b>	<b><math>V_{OC}</math> / V</b>	<b><math>J_{SC}</math> / mA cm<sup>-2</sup></b>	<b>FF / %</b>	<b>PCE / %</b>
0.2 μm	$0.44 \pm 6.2 \cdot 10^{-17}$	$11.99 \pm 0.83$	$61.4 \pm 0.01$	$3.26 \pm 0.19$
<b>Best cell</b>	<b>0.44</b>	<b>12.91</b>	<b>59.9</b>	<b>3.43</b>
0.45 μm	$0.42 \pm 0.01$	$11.96 \pm 3.84$	$54.1 \pm 0.03$	$2.73 \pm 0.77$
<b>Best cell</b>	<b>0.41</b>	<b>17.69</b>	<b>52.3</b>	<b>3.82</b>

### **3.7 Influence of a PEAI-interlayer between the PEDOT:PSS and perovskite layer**

As it was reported that a phenylethylammonium bromide (PEABr) interlayer between the PEDOT:PSS and perovskite layer improves the interface<sup>129</sup>, we introduced a PEAI interlayer and observed the influence on the solar cell performance. Therefor the performance of solar cells with and without interlayer was compared. The perovskite layer was prepared with one time AS dropping and putting the solar cells directly on the hot heating plate (70 °C) for both solar cell types (with and without interlayer).

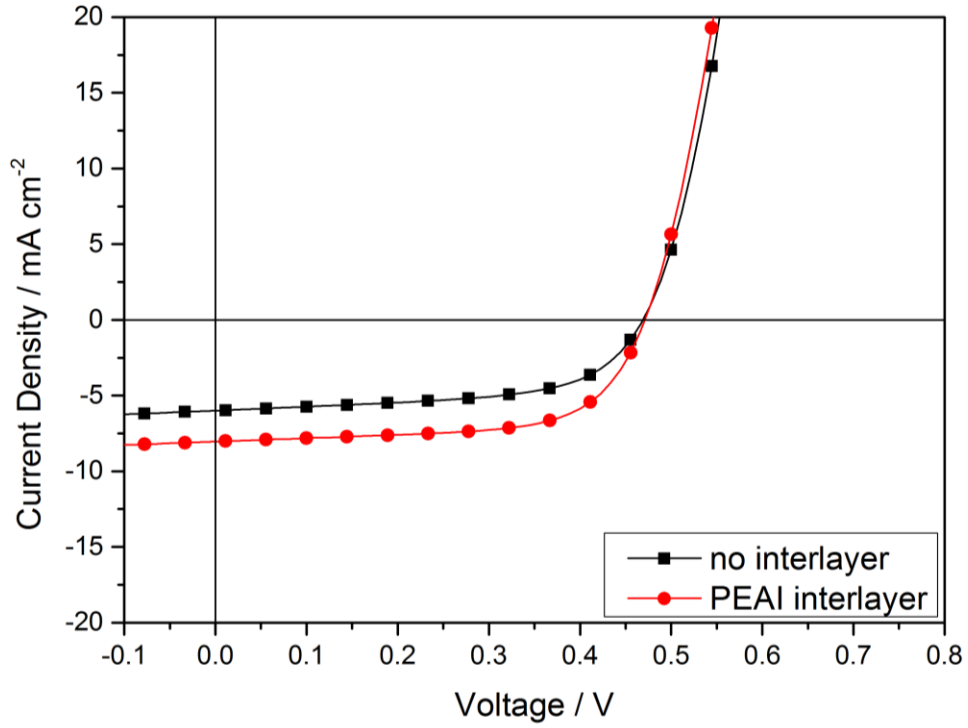


Figure 15: *JV*-curves of solar cells built in the device architecture glass/ITO/PEDOT:PSS/ $MA_{0.75}FA_{0.15}PEA_{0.1}SnI_3$ /PC<sub>60</sub>BM/Al, where a PEAI interlayer was introduced between PEDOT:PSS and  $MA_{0.75}FA_{0.15}PEA_{0.1}SnI_3$  layer; these curves show the best solar cell performance of each device

Observing the *JV*-curves (Figure 15) of a solar cell built with PEAI interlayer and without interlayer shows that the performance increases with introducing an interlayer. The  $V_{OC}$  remains the same with 0.47 V for both types, however an increase of the  $J_{SC}$  can be observed with a PEAI layer. Therefore also the FF and the PCE were higher for solar cells with an interlayer. It is assumed that an introduction of this low-dimensional interlayer, leads to an improvement of the film morphology and traps states are reduced as reported by Chen et al. The best solar cell performance with a PEAI interlayer achieved a PCE of 2.4%, a FF of 65.1%, a  $V_{OC}$  of 0.47 V and a  $J_{SC}$  of 8.04 mA cm<sup>-2</sup>.

Table 12: Mean values, standard deviation and best solar cell performance, for solar cells built in the device architecture glass/ITO/PEDOT:PSS/ $MA_{0.75}FA_{0.15}PEA_{0.1}SnI_3$ /PC<sub>60</sub>BM/Al and this device architecture with an interlayer of PEAI between PEDOT:PSS and  $MA_{0.75}FA_{0.15}PEA_{0.1}SnI_3$  layer

PEAI interlayer	$V_{OC}$ / V	$J_{SC}$ / mA cm <sup>-2</sup>	FF / %	PCE / %
No interlayer	0.47 ± 0.005	5.41 ± 0.44	58.8 ± 1.9	1.5 ± 0.11
<b>Best cell</b>	<b>0.47</b>	<b>5.99</b>	<b>59.3</b>	<b>1.7</b>
Interlayer	0.47 ± 0	7.23 ± 0.86	62.7 ± 2.6	2.1 ± 0.3
<b>Best cell</b>	<b>0.47</b>	<b>8.04</b>	<b>65.1</b>	<b>2.4</b>

### 3.8 Investigation of the influence of CuBr<sub>2</sub>

CuBr<sub>2</sub> was introduced into the perovskite precursor solution as studies showed that the perovskite crystallization is improved, as well as the stability towards air gets better and the defect concentration is lowered.<sup>131,132</sup> Therefore different amounts of  $y$  CuBr<sub>2</sub> were added to the perovskite precursor solution (10 mol% and 20 mol%) and the corresponding amount of  $x$  SnI<sub>2</sub> was decreased (90 mol% and 80 mol%) to receive a 1M solution with a MA<sub>0.75</sub>FA<sub>0.15</sub>PEA<sub>0.1</sub>Sn <sub>$x$</sub> Cu <sub>$y$</sub> I<sub>1+2 $x$</sub> Br<sub>2 $y$</sub>  perovskite. Solar cells prepared with those perovskites were compared with a MA<sub>0.75</sub>FA<sub>0.15</sub>PEA<sub>0.1</sub>SnI<sub>3</sub> perovskite solar cell prepared without any addition of CuBr<sub>2</sub>. It was investigated the absorption behaviour and the surface of the perovskite material as well as  $JV$ -behaviour.

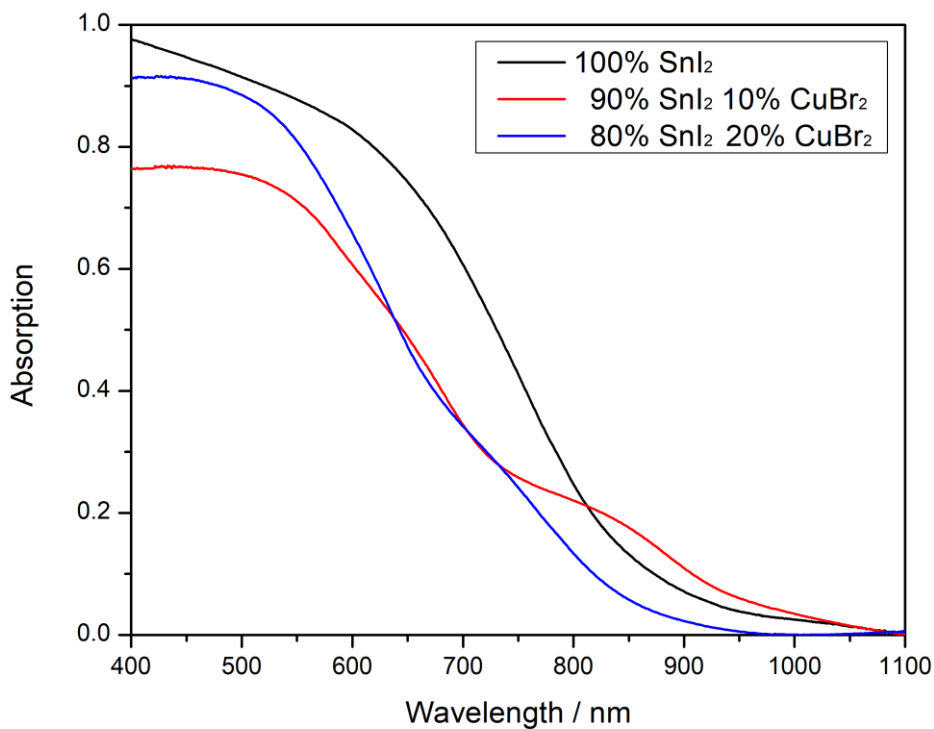


Figure 16: Absorption behaviour of a MA<sub>0.75</sub>FA<sub>0.15</sub>PEA<sub>0.1</sub>SnI<sub>3</sub> perovskite, as well as from perovskites with a mixture of 90 mol% SnI<sub>2</sub> with 10 mol% CuBr<sub>2</sub> and 80 mol% SnI<sub>2</sub> with 20 mol% CuBr<sub>2</sub>

The addition of CuBr<sub>2</sub> to the MA<sub>0.75</sub>FA<sub>0.15</sub>PEA<sub>0.1</sub>SnI<sub>3</sub> perovskite did not lead to a change in colour of the perovskite layer and it remained black. The absorption spectrum in Figure 16 shows that the absorption of the perovskite prepared with 100 mol% SnI<sub>2</sub> has a similar absorption onset as the one with 90 mol% SnI<sub>2</sub> and 10 mol% CuBr<sub>2</sub>, however with 80 mol% SnI<sub>2</sub> and 20 mol% CuBr<sub>2</sub> the absorption is shifted to lower wavelengths, to about 950 nm. The absorption with additional CuBr<sub>2</sub> was slightly higher than without CuBr<sub>2</sub>.

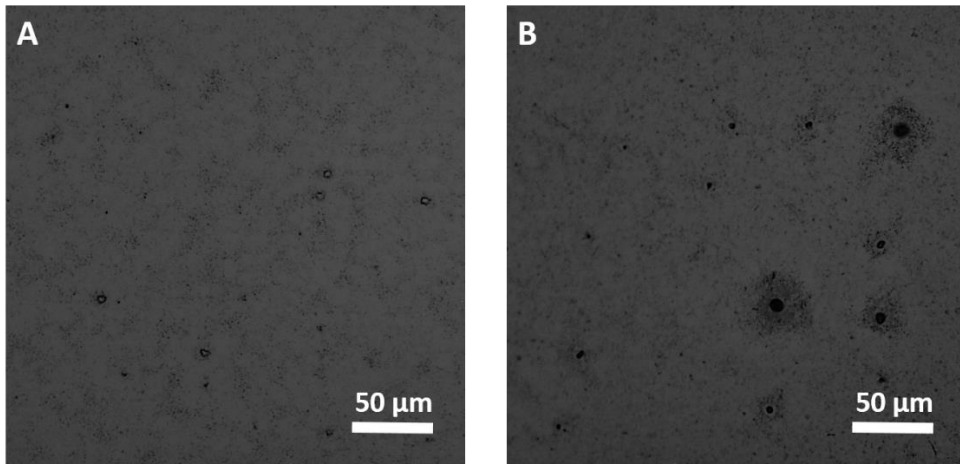


Figure 17: Optical light microscopy images of different perovskite layers, A: 90%  $\text{SnI}_2$  10%  $\text{CuBr}_2$ ; B: 80%  $\text{SnI}_2$  20%  $\text{CuBr}_2$

Furthermore the surface of the prepared perovskite layers was investigated via optical light microscopy. It can be observed that the addition of 10 mol% and 20 mol% of  $\text{CuBr}_2$  leads to small holes in the surface (Figure 17 image A and B), whereas for the perovskite without addition of  $\text{CuBr}_2$  nearly no holes can be observed (Figure 9 image C). This leads to the assumption that the solar cell performance is negatively influenced by the addition of  $\text{CuBr}_2$ .

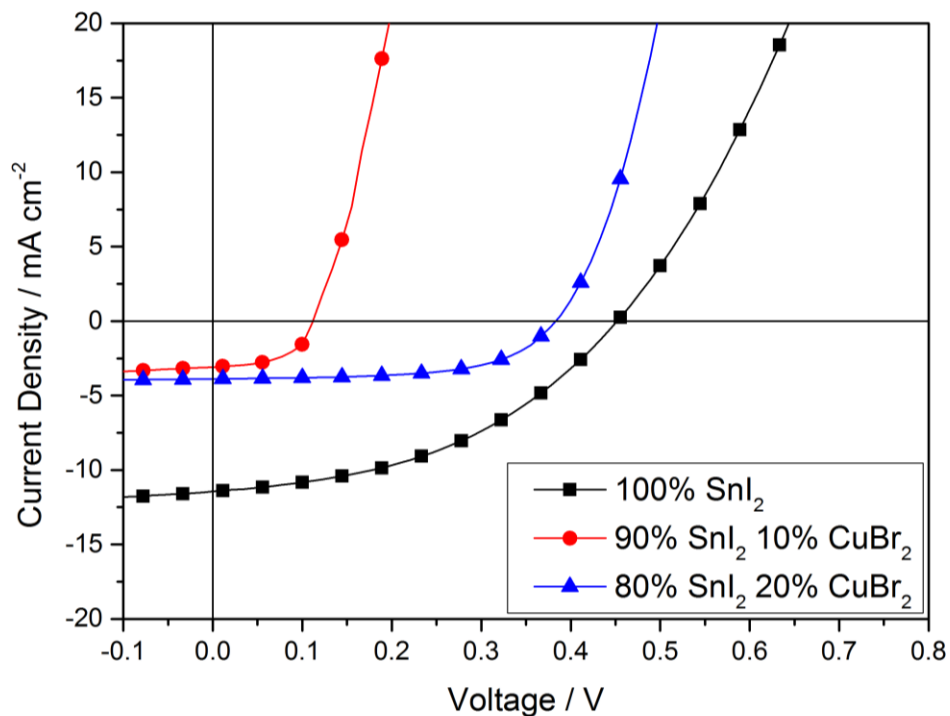


Figure 18: JV- curves of solar cells with different perovskite precursor solution, as  $\text{CuBr}_2$  was added; showing the best cells of each solar cell

The solar cell performance of the different perovskite solutions was observed. The  $V_{OC}$ , the  $J_{SC}$  and the PCE reach the highest values for the perovskite with 100 mol%  $SnI_2$ , whereas the values for the solar cells prepared with addition of 10 mol% and 20 mol%  $CuBr_2$  are below. This is maybe ascribed to the poorer film morphology of the perovskite surface and in accordance with the assumption above. However it can be observed in Table 13 that when adding 20 mol%  $CuBr_2$  the FF increases and is with 60.7 % the highest value. Nevertheless the overall best performance was reached with the solar cells prepared with 100 mol%  $SnI_2$  with a PCE of 2.22%, a FF of 42.8%, a  $V_{OC}$  of 0.46 V and a  $J_{SC}$  of 11.45  $mA\ cm^{-2}$ .

Table 13: Mean values, standard deviation and best solar cell performance of solar cells with varying perovskite precursor solutions via adding  $CuBr_2$  to the solution

Composition	$V_{OC} / V$	$J_{SC} / mA\ cm^{-2}$	FF / %	PCE / %
100% $SnI_2$ , 10% $SnF_2$	$0.44 \pm 0.01$	$10.91 \pm 0.49$	$40.8 \pm 2.9$	$1.96 \pm 0.17$
<b>Best cell</b>	<b>0.46</b>	<b>11.45</b>	<b>42.8</b>	<b>2.22</b>
90% $SnI_2$ , 10% $SnF_2$ , 10% $CuBr_2$	$0.11 \pm 0.01$	$2.86 \pm 0.17$	$49.1 \pm 3.1$	$0.15 \pm 0.02$
<b>Best cell</b>	<b>0.11</b>	<b>3.08</b>	<b>53.9</b>	<b>0.18</b>
80% $SnI_2$ , 10% $SnF_2$ , 20% $CuBr_2$	$0.38 \pm 0.01$	$3.74 \pm 0.19$	$59.7 \pm 1.1$	$0.85 \pm 0.03$
<b>Best cell</b>	<b>0.38</b>	<b>3.89</b>	<b>60.7</b>	<b>0.89</b>

## 4 Best solar cell performance & investigation of the stability

Via the optimization processes of the solar cell preparation of tin based perovskite solar cells a maximum performance was reached with the following device architecture: glass/ITO/PEDOT:PSS/MA<sub>0.75</sub>FA<sub>0.15</sub>PEA<sub>0.1</sub>SnI<sub>3</sub>/PC<sub>60</sub>BM/Al. As precursor purchased SnI<sub>2</sub> (99.99% purity) was further purified in the tube furnace, the AS dropping was carried out the optimized way (2 times AS dropping, fast) which is ascribed above and the solar cells were put immediately on the hot heating plate. The PC<sub>60</sub>BM layer was spin coated with the optimized spin coating rate and the solution was filtered with a 0.45  $\mu\text{m}$  filter. The best solar cell performance (Figure 19) reached a PCE of 6.4%, a FF of 62.4%, a  $V_{\text{OC}}$  of 0.48 V and a  $J_{\text{SC}}$  of 21.69  $\text{mA cm}^{-2}$ .

Additionally the performance of this solar cell was recorded with mask, which did not lead to a huge deterioration of the solar cell performance and still values of 5.1% for the PCE, 65.4% for the FF, 0.45 V for the  $V_{\text{OC}}$  and 17.4  $\text{mA cm}^{-2}$  for the  $J_{\text{SC}}$  were achieved.

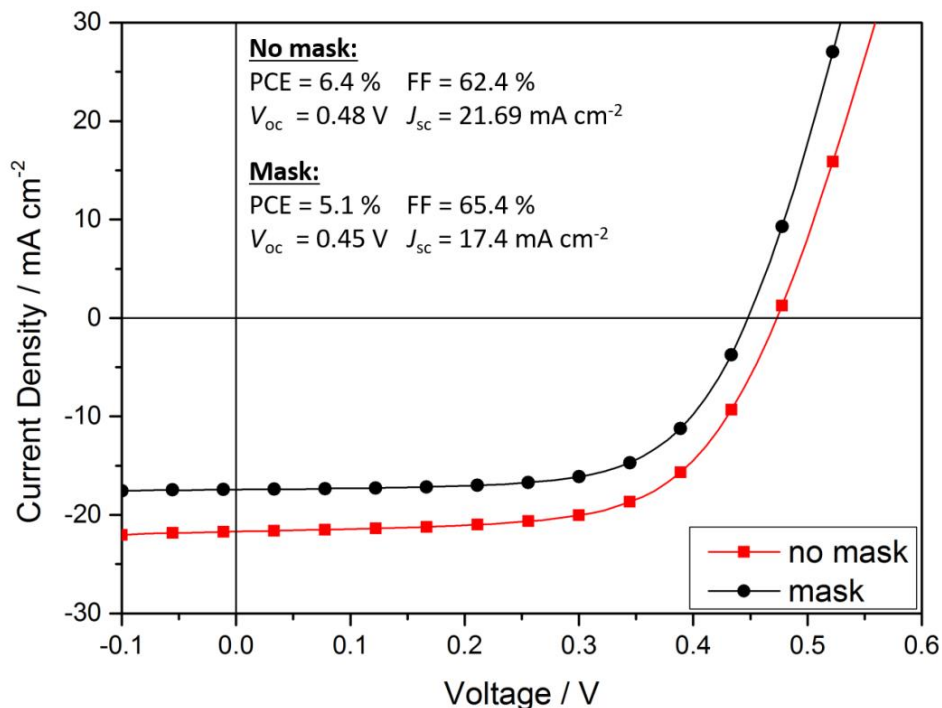


Figure 19: JV- curves and the received solar cell parameters (PCE, FF,  $V_{\text{OC}}$  and  $J_{\text{SC}}$ ) for the best solar cell performance reached within this study due to optimization processes, recorded without and with mask

*JV*- parameters of the best solar cell were recorded numerous times over 80 days stored in the glovebox which are illustrated in Figure 20. It can be observed that the solar cell performance increased in the first few days after solar cell preparation to a PCE of about 6%, a  $V_{OC}$  of about 0.46 V and a  $J_{SC}$  of about 22 mA cm<sup>-2</sup>, only the FF decreased from about 66% to 55%. These values have then been stabilized and remain relatively constant over 80 days, which shows that this solar cell is quiet stable. It can also be observed that the  $V_{OC}$  even increases after 80 days.

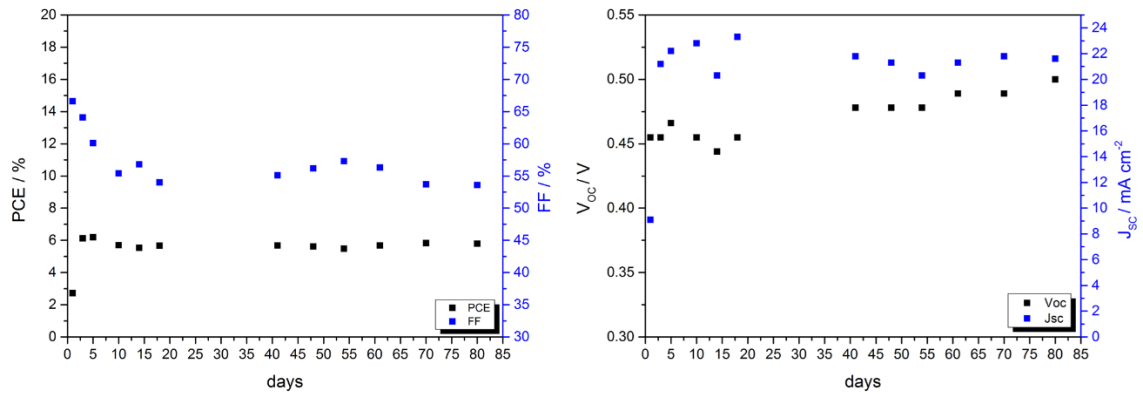


Figure 20: Stability measurement of the best solar cell measured by the PCE, FF,  $V_{OC}$  and  $J_{SC}$  values

It is known that Sn-based perovskite solar cells can show a hysteretic effect. This *JV*-hysteresis is the phenomena that the *JV*- curve depends on the direction of the scan (forward or backward) and therefore no reliable statement about the received *JV*-parameters can be made. Therefore the method of maximum power point tracking was used in order to determine stabilized PCE values, as well as forward and backward scans are recorded to see if there is any hysteresis phenomena. In Figure 21 it is shown the *JV*-hysteresis of the above described best solar cell measured on different days. On the day of preparation the solar cell shows hysteresis but after 5 days there is no hysteresis. After 80 days nearly no hysteresis can be observed.

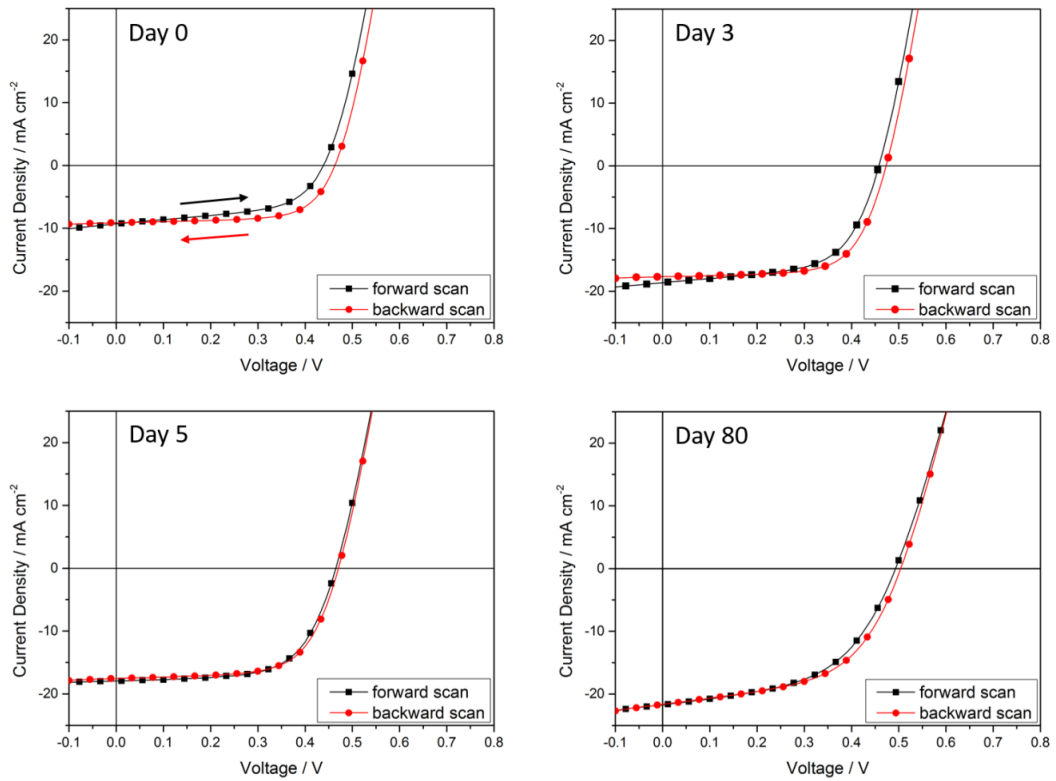


Figure 21: Evolution of the hysteresis with days displayed via JV-curves in the forward and backward scan of the solar cell measured on the day of preparation after three, five and 80 days

As hysteresis can be observed in some parts, it is used the method of tracking the MPP so a stabilized value is received through which the maximum PCE can be obtained.

The MPP tracking is shown in Figure 22 and it is received a PCE value of about 4.1 %, which is quite similar to the received PCE value of 4.26% from the JV- curve. The values are received from the measurement after five days, where no hysteresis is shown for the forward and backward scan. If there would be hysteresis the received PCE value from the MPP tracking can differ from the measured PCE value from the JV- curve.

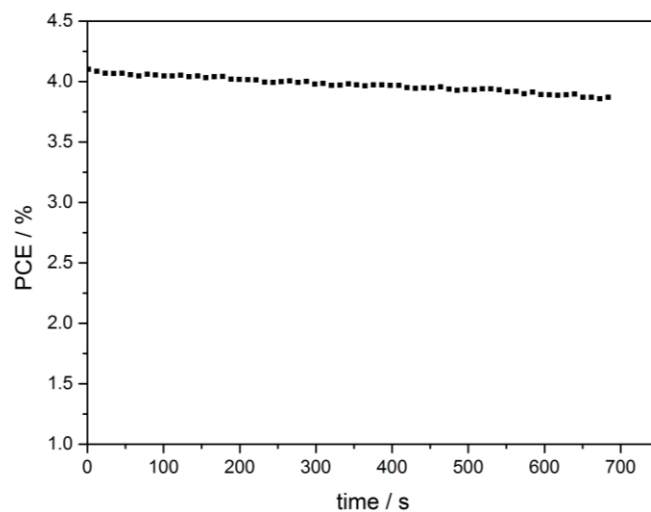


Figure 22: MPP-tracking of the best solar cell to receive the PCE without the influence of hysteresis

# 5 Experimental

## 5.1 Chemicals

SnI<sub>2</sub> anhydrous beads with a purity of 99.99% trace metal basis were obtained from Sigma Aldrich. SnF<sub>2</sub>, MAI and FAI were both purchased from Sigma Aldrich with a purity of 99%, 98% and  $\geq 98\%$  (H-NMR). PEAI was purchased from Dyesol. The used toluene and 2-propanol Rotipuran® were purchased from Roth with a purity of  $\geq 99.5\%$  (for synthesis) and  $\geq 99.8\%$ . Anhydrous chlorobenzene and CuBr<sub>2</sub> with a purity of 99.8% and 99.999% trace metals basis were obtained from Sigma Aldrich. DMF was used from SeccoSolv® with a purity  $\geq 99.9\%$  dried and PC<sub>60</sub>BM from Solenne with a purity of 99.5%. Dried DMSO was used with a water content  $\leq 0.02\%$  and PEDOT:PSS was purchased from Clevios P VP.AI 4083.

## 5.2 Characterisation

### 5.2.1 XRD analysis

The XRD measurements were performed on a PANalytical Empyrean diffractometer in a Bragg-Brentano configuration, that was operated at 40 mA and 40 kV with an Cu K $\alpha$  radiation ( $\lambda = 1.5418 \text{ \AA}$ ). The XRD measurements were carried out by Birgit Kunert at the institute of Solid-State Physics.

XRD patterns were recorded of the MA<sub>0.75</sub>FA<sub>0.15</sub>PEA<sub>0.1</sub>SnI<sub>3</sub> perovskite, the purified and the purchased SnI<sub>2</sub>. The perovskite precursor solution was prepared the same way as described in 5.6 for the measurement of the perovskite. This solution was then applied on a glass substrate (2.5 cm x 2.5 cm) and the excess solvent was evaporated at 80 °C on the heating plate. Another PMMA layer was spin coated on the perovskite layer, to make the sample more stable during measurement. A 10 mg/ml PMMA solution in chlorobenzene was prepared for the PMMA (protective) layer and spin coated at 5000 rpm with an acceleration of 2000 rpm/s.

The purchased and purified SnI<sub>2</sub> was pulverized with a mortar for the powder XRD.

### 5.2.2 Optical characterisation of perovskite $\text{MA}_{0.75}\text{FA}_{0.15}\text{PEA}_{0.1}\text{SnI}_3$

The UV-VIS measurements were performed on a PerkinElmer UV-VIS Spectrometer Lambda 35. The measurement was carried out in a wavelength scan range from 350 nm to 1100 nm with a slit width of 2 nm and a scan rate of 480 nm. The absorption, transmission and reflection measurement was carried out with a labsphere certified reflection standard.

The perovskite precursor solution was spin coated on a glass substrate for 60 s with a spin coating rate of 5000 rpm and an acceleration of 2000 rpm/s for the absorption measurement. After 20 s an AS drooping was applied with toluene. The perovskite precursor solution consisted of a 1 M  $\text{SnI}_2$  solution (purchased  $\text{SnI}_2$  with 99.99% purity; further purified in tube furnace) with DMF:DMSO 4:1, where for the cations the following agents were dissolved in a manner that a 1 M solution was received for the  $\text{MA}_{0.75}\text{FA}_{0.15}\text{PEA}_{0.1}\text{SnI}_3$  with 75 mol% MAI, 15 mol% FAI, 10 mol% PEAI and 10 mol%  $\text{SnF}_2$ . After the application of the perovskite layer, the substrate was annealed at 70 °C.

### 5.2.3 *JV*- measurements

The data for the *JV*- curves were recorded with a Keithley 2400 source meter and a costume-made LabVIEW software. The illumination was carried out with a Dedolight DLH400D lamp. The *JV*- curves were recorded at a light intensity of 100  $\text{mW}/\text{cm}^2$  at a voltage range from -100 mV to 1000 mV with maximum compliance of 100 mA, delay of 100 ms and scan rate of 200 mV/s.

### 5.2.4 Layer Thickness

The layer thickness was determined with a DektakXT Bruker profilometer.

### 5.2.5 SEM

The SEM images were recorded with a Supra 40 scanning electron microscope (Carl Zeiss) equipped with a field emission electron source with an acceleration voltage of 5 kV using an inlens secondary electron detector. The SEM measurements were carried out by Dr. Theodoros Dimopoulos at the Austrian Institute of Technology.

For SEM measurements, the following deposition parameters for MA<sub>0.75</sub>FA<sub>0.15</sub>PEA<sub>0.1</sub>SnI<sub>3</sub> perovskite layers were used. The perovskite precursor solution was prepared in a solution with the ratio 4:1 and 1:1 DMF:DMSO. After spin coating the substrates with the perovskite precursor solution and AS dropping treatment, 3 were immediately put on the 70 °C heating plate for 20 min and one substrate was put afterwards on the heating plate, with a slow heating rate from RT to 70 °C. One substrate was treated 2 times with an AS dropping. The prepared substrates are listed in Table 14.

*Table 14: Listed preparation methods of the substrates according to the DMF: DMSO solvent ratio, the AS treatment and the annealing step*

<b>Substrate</b>	<b>DMF : DMSO</b>	<b>Heating plate</b>	<b>AS treatment</b>
<b>1</b>	4 : 1	Immediately put on hot HP	1 time
<b>2</b>	4 : 1	Immediately put on hot HP	2 times
<b>3</b>	4 : 1	Put on cold HP, then heated	1 time
<b>4</b>	1 : 1	Immediately put on hot HP	1 time

### 5.2.6 Optical Microscopy

The optical microscopy measurements were carried out with an Olympus BX60 microscope and the images were taken with an Olympus E-520 camera.

## 5.3 Purification of SnI<sub>2</sub>

The purchased SnI<sub>2</sub> (99.99%) was purified via the following purification methods: sublimation, bulb-to-bulb- distillation, recrystallization and purification in the tube furnace. These purification methods are described in more detail in the following parts.

### 5.3.1 Sublimation

Purification of SnI<sub>2</sub> with a purity of 99.99 % was carried out via sublimation according to literature.<sup>139</sup> In the first step it was tried to remove SnI<sub>4</sub> residues at about 140 °C and 2.1 mbar. Heating was achieved with a heating mantle. A yellow fraction was on the sublimation finger and removed. The residue should be SnI<sub>2</sub> and SnO. To separate these two materials another sublimation step was carried out at 200 °C and 2.1 mbar. An orange product was produced, which deposited on the wall of the flask, in addition further yellowish product was formed.

During the sublimation a lot of yellowish product was formed. Due to no improvement of the solar cell performance, it was assumed that the product did not lead to pure  $\text{SnI}_2$ .

### 5.3.2 Bulb-to-bulb distillation

Purification of  $\text{SnI}_2$  with a purity of 99.99% was carried out via bulb-to-bulb distillation at 150 °C and 1.9 mbar. The purification did not seem to be successful as the  $\text{SnI}_2$  remained in the last bulb and no other phase could be separated. This purification technique did not lead to a better performance of the solar cells, therefore it was assumed that the purification was not successful.

### 5.3.3 Recrystallization - $\text{SnI}_2(\text{DMF})$ complex

Another purification technique should be achieved via recrystallization of  $\text{SnI}_2$  in DMF to receive purer  $\text{SnI}_2(\text{DMF})$  complexes.<sup>139</sup> Therefore 1 g of  $\text{SnI}_2$  (99.99%) was dissolved in 700  $\mu\text{l}$  DMF at 50 °C for 1h. The solution was then cooled down to room temperature and filtered with a 0.45  $\mu\text{m}$  PTFE filter into a 20 ml vial. The vial was tilted to receive a huger surface of the solution. Inert toluene was slowly added on the solution with a syringe. These layered solutions stood for 2 days, after which yellowish needles could be observed, which were filtered and dried under vacuum for 1h.



Figure 23: Set up of the crystallization, tilted vial with crystallized yellowish  $\text{SnI}_2(\text{DMF})$  complexes

### 5.3.4 Tube furnace

The purchased SnI<sub>2</sub> (99.99 %) was purified in tube furnace. Therefore a certain amount of SnI<sub>2</sub> was weighed into a vial, which was put into a Schlenk tube inside the glovebox. The Schlenk tube was closed in nitrogen atmosphere and put outside the glovebox into the tube furnace. Under excess pressure of nitrogen the Schlenk tube was heated up to 380 °C within 30 minutes and held at this temperature for two hours. After cooling down the purified SnI<sub>2</sub> was put back again into the glovebox.

A yellowish orange residue could be observed on the wall of the Schlenk tube, which was thought to be SnI<sub>4</sub>, whereas the purified SnI<sub>2</sub> was dark red.

## 5.4 General solar cell preparation

### 5.4.1 Device Fabrication

The solar cells were built in the same inverted planar device stack: glass/ITO/PEDOT:PSS/Sn-Perovskite/PC<sub>60</sub>BM/Al illustrated in Scheme 8.

## 5.5 General solar cell preparation

The solar cells were always built in the same device architecture. The cleaning procedure for the substrates and the application of PEDOT:PSS were carried out the same way for all substrates. The following preparation steps are the ideal ones that were received out of the optimization processes. Therefore some parameters were varied during the optimization experiments. These variations are described in more detail in the following points.

The glass/ITO substrates (ITO patterned  $R_s = 15\Omega$ , 15 x 15 x 1.1 mm) were cleaned at first with acetone and further by sonification in isopropanol for 30 min at 40 °C. The substrates were then dried under a N<sub>2</sub> gas stream and further an oxygen plasma etching (FEMTO, Diener electronic) was performed for 3 min. The PEDOT:PSS (Clevios P VP.Al 4083, Heraeus) was spin coated at 3000 rpm for 30 seconds (Spin coated Model XW-4A 220 Volts) on the cleaned glass/ITO substrates and then annealed for 20 min at 120 °C. PEDOT: PSS was applied with a 0.45 µm filter (PVDF-45/25 Chromafil Xtra). Subsequent steps were carried out in the nitrogen filled glovebox. 30 µl of the perovskite precursor solution (preparation see 5.6) was spin coated at 5000 rpm with an acceleration of 2000 rpm/s for 60 s (spin coater: Model WS 650 MZ-23NPPB).

After 20 s of spin coating an AS treatment was applied, therefore 50  $\mu\text{l}$  of chlorobenzene were applied, through which the colour changed from yellow to black. This was followed by an annealing step for 20 min at 70  $^{\circ}\text{C}$  (programmable heating plate: MCS 66, CAT Ingenieurbüro M. Zipperer GmbH). The applied perovskite precursor solution was filtered before with a 0.45  $\mu\text{m}$  filter (PTFE, 13 mm Syringe Filter). For the PC<sub>60</sub>BM layer 30  $\mu\text{l}$  of a 20 mg/ml PC<sub>60</sub>BM in chlorobenzene solution was applied and spin coated at 4000 rpm with an acc. of 1000 rpm/s. PC<sub>60</sub>BM was always filtered before spin coating (either with a 0.2  $\mu\text{m}$  or 0.45  $\mu\text{m}$  filter size). The aluminium electrodes were thermally evaporated using a thermal evaporation chamber MB-EVAP mounted inside the glovebox. It is tried to hold the rate between 1-5  $\text{\AA}/\text{s}$  under a pressure of  $1 \cdot 10^{-5}$  mbar with rotation of the substrates during the evaporation for the thermal evaporation. The electrodes were evaporated on the substrates with an area of 0.09  $\text{cm}^2$  and 100 nm layer thickness for each electrode.

## 5.6 Perovskite precursor solution preparation

The perovskite precursor solutions were prepared under nitrogen atmosphere in the MBraun glovebox. SnI<sub>2</sub> was dissolved in a solution of DMF: DMSO in a 4:1 ratio that a 1 M solution was obtained. In addition 10 mol% of SnF<sub>2</sub> were added. The cations were added in a ratio that a 1 M solution concerning the cations was obtained. In the case of MA<sub>0.75</sub>FA<sub>0.15</sub>PEA<sub>0.1</sub>SnI<sub>3</sub> there were added 75 mol% of MAI, 15 mol% FAI and 10 mol% PEAI. The prepared precursor solution was then stirred over night at RT.

## 5.7 Optimization of the solar cell performance

### 5.7.1 Optimization of the perovskite layer

The perovskite precursor solution was prepared with purified SnI<sub>2</sub> and a 1 M solution was prepared in 4:1 DMF:DMSO. The PC<sub>60</sub>BM solution was a 20 mg/ml solution dissolved in CB with a spin coating rate of 2000 rpm and 1000 rpm/s. CB was used for the AS dropping. The spin coating rate for the perovskite layer was varied as it is described in Table 15 and the influence on the layer thickness was investigated.

Table 15: Listed spin coating rate and acceleration for the perovskite layer preparation

Spin coating rate / rpm	Acceleration / rpm/s
4500	1000
5000	2000
5500	2000
6000	2000

In addition the concentration of the perovskite precursor solution was varied. Therefore SnI<sub>2</sub> was dissolved in DMF: DMSO (4:1) to reach a 0.5, 0.8, 1, 1.5 or 2 M solution. The equivalent amount of MAI, FAI, PEAI and 10 mol% SnF<sub>2</sub> were in addition to that dissolved, to receive a MA<sub>0.75</sub>FA<sub>0.15</sub>PEA<sub>0.1</sub>SnI<sub>3</sub> perovskite.

### 5.7.2 Optimization of the AS dropping

1 M perovskite precursor solution in 4:1 DMF:DMSO spin coating at 5000 rpm and 2000 rpm/s. A 20 mg/ml solution of PC<sub>60</sub>BM in CB was spin coated 2000 rpm and an acceleration of 1000 rpm/s. The parameters concerning the AS dropping and annealing step were varied and are further described in Table 16.

Table 16: Listed AS technique parameters that were varied and corresponding parameters which remained the same

AS technique parameters	Opt. Distance	Opt. Speed	Opt. 1 or 2 times AS dropping	Opt. Annealing	Opt. AS
Distance	varied	far	far	far	far
Speed	Fast	varied	fast	fast	fast
1 or 2 times AS dropping	1 time	1 time	varied	2 times	2 times
Annealing	HP RT, slow heating	HP RT, slow heating	HP RT, slow heating	varied	Hot HP
AS	toluene	toluene	toluene	toluene	varied

The varied parameters to optimize the solar cell performance are further described in the following.

### **Distance**

The influence of the AS dropping distance on the solar cell performance was investigated. Therefore three different distances for the AS dropping were applied: distance between pipette tip and substrate was about 1 cm (near), 2.5 cm (middle) or 4.5 cm (far).

### **AS dropping speed**

The speed of how fast the AS was applied was varied. The AS was either dropped fast on the substrate or slowly dropwise.

### **AS dropping number**

The AS dropping was applied either one time or two times. For the one time AS dropping step the solar cell was treated during the spin coating after 20 s with an AS. The whole procedure as for the one time AS dropping was repeated for the 2 times AS dropping step. So the whole spin coating procedure took two minutes with AS treatment after 20 seconds and 80 seconds.

### **Annealing**

Two different annealing techniques were observed. The substrates were either put directly on the hot heating plate (70 °C) for 20 minutes or on the heating plate at room temperature and then heated up to 70 °C and hold at this temperature for 20 minutes.

### **AS variation**

The influence of the AS on the solar cell performance was observed, therefore it was either used toluene or chlorobenzene as AS.

### **5.7.3 Optimization of the PC<sub>60</sub>BM layer**

A 1 M perovskite precursor solution with purified SnI<sub>2</sub> in 4:1 DMF:DMSO were prepared and spin coated with 5000 rpm and 2000 rpm/s. Chlorobenzene was used as anti-solvent. For PC<sub>60</sub>BM a 20 mg/ml solution dissolved in chlorobenzene was used. The optimization of the PC<sub>60</sub>BM layer includes the variation of spin coating rate of the PC<sub>60</sub>BM layer and the filter technique. The varied spin coating rates and accelerations for the PC<sub>60</sub>BM layer are listed in Table 17.

Table 17: Spin coating rate and acceleration for the spin coating process of the PC<sub>60</sub>BM layer

<b>PC<sub>60</sub>BM spin coating rate</b>	<b>Acceleration</b>
2000 rpm	1000 rpm/s
3000 rpm	1000 rpm/s
5000 rpm	2000 rpm/s
6000 rpm	2000 rpm/s

The PC<sub>60</sub>BM solution was either filtered with a 0.2 μm or a 0.45 μm filter.

#### **5.7.4 PEAI interlayer between the PEDOT: PSS and perovskite layer**

For the PEAI interlayer, a solution of PEAI 20 mg/ml were dissolved in DMF and stirred over night at RT. This solution (30 μl) was spin coated on the PEDOT: PSS layer at 3000 rpm with an acceleration of 1000 rpm/s for 30 s. Subsequently the perovskite layer was then spin coated on this layer.

#### **5.7.5 Influence of CuBr<sub>2</sub> on the solar cell performance**

CuBr<sub>2</sub> was added to the perovskite precursor solution to investigate the influence on the solar cell performance. Four different precursor solutions were prepared. One solution was prepared the same way as it is described in point 5.6. The other two solutions were prepared the same way, but with either 90 mol% or 80 mol% of SnI<sub>2</sub> and 10 mol% or 20 mol% of CuBr<sub>2</sub>. The solar cells were prepared the same way as described in 5.5.

## 6 Conclusion and Outlook

It is known that tin based perovskite solar cells are a promising alternative to lead based perovskite solar cells. Therefore  $\text{MA}_{0.75}\text{FA}_{0.15}\text{PEA}_{0.1}\text{SnI}_3$  perovskite based solar cells were investigated in more detail with the following device architecture: glass/ITO/PEDOT:PSS/Sn-Perovskite/ $\text{PC}_{60}\text{BM}/\text{Al}$ . The fabrication of the different layers was optimized to improve the solar cell performance. Additionally the purification of commercial  $\text{SnI}_2$  (99.99% purity) was observed in more detail, as well as the influence of an interlayer between the PEDOT:PSS and perovskite layer and the influence of adding  $\text{CuBr}_2$  to the perovskite precursor solution on the solar cell performance.

In summary it was shown that only with optimizing the preparation steps of the Sn-based perovskite solar cell, the performance is strongly influenced. This shows the necessity to first improve the fabrication of tin based perovskite solar cells before varying for example cations, as the reproducibility of those solar cells is a major problem. One huge factor that influences the solar cell performance is the easy oxidation of  $\text{SnI}_2$  from  $\text{Sn}^{2+}$  to  $\text{Sn}^{4+}$ . So the purity of the purchased  $\text{SnI}_2$  is a key issue for the solar cell performance and it is suggested to use  $\text{SnI}_2$  with a purity  $\geq 99.99\%$ . The purification of the purchased  $\text{SnI}_2$  in a tube furnace led to a better solar cell performance in most cases. However the usage of purified  $\text{SnI}_2$  sometimes also showed no enhancement in the performance which leads to the assumption that the different charges used within this study, possibly varied in purity. The XRD measurement also showed that neither in the purchased nor in the purified  $\text{SnI}_2$ , contents of  $\text{SnI}_4$  were found, so it is assumed that the amount of  $\text{Sn}^{4+}$  is also rather small in the commercial product. However it would be essential to further investigate the purchased and purified  $\text{SnI}_2$  with regard to the  $\text{Sn}^{4+}$  content with other methods than XRD.

Furthermore it was found that a formation of a smooth perovskite layer is essential for the performance of the solar cell. So the AS dropping and the annealing step are important for the crystallization of the perovskite layer, therefore the optimization contributes greatly to the formation of homogenous perovskite layers, without holes. It was found that the AS dropping should be applied in a proper speed (not too fast then holes will form and not too slow) and from a distance of about 4.5 cm. The annealing should occur directly after the perovskite layer is applied on a hot heating plate for 20 minutes. Best results are achieved with a 1M perovskite precursor solution and a film thickness of  $323.5\text{nm} \pm 45.1\text{nm}$ .

For the PC<sub>60</sub>BM layer it was found that a faster spin coating rate leads to a smoother surface with less particles. A maximum PCE of 6.4% can be achieved with a FF of 62.4%, a  $V_{OC}$  of 0.48 V and a  $J_{SC}$  of 21.69 mA cm<sup>-2</sup> via the optimization of the solar cell fabrication without any changes of the perovskite composition and the device stack. It was used an inverted device architecture with MA<sub>0.75</sub>FA<sub>0.15</sub>PEA<sub>0.1</sub>SnI<sub>3</sub> as perovskite material. In addition it was found that solar cells with good performances can be quiet stable as it was demonstrated that the best solar cells were still stable after 80 days.

For this solar cell also hysteresis was observed and it is found that a hysteretic effect can be observed on the first day of measurement, which then vanishes after some days.

An additional PEAI interlayer between the PEDOT:PSS and perovskite layer leads to an improvement of the solar cell performance as it is also described by Chen et al.<sup>129</sup> It is suggested to further investigate the influence of this interlayer to improve the interface between the HTL and the perovskite layer. The addition of CuBr<sub>2</sub> to the perovskite neither led to a better stability nor to an improvement of the solar cell performance. Therefor it is suggested to further research the influence of CuBr<sub>2</sub> as additive in Sn based perovskites for solar cells and vary the amounts of addition and record a XRD for having a closer look on how the CuBr<sub>2</sub> incorporates in the MA<sub>0.75</sub>FA<sub>0.15</sub>PEA<sub>0.1</sub>SnI<sub>3</sub> structure. Further improvement of the solar cell performance can be achieved by varying the cations to influence the dimensionality or by variation of the halide anions.

# 7 Index of Schemes

Scheme 1: Renewable Energy Share of global electricity production (End – 2017); data used from reference .....	1
Scheme 2: Illustration of the Fermi levels and energy levels of a p- and n-doped material (1); formation of a depletion region via joining the p- and n-doped material and the corresponding energy levels and Fermi level (2); drawn based on reference 12.....	4
Scheme 3: Charge carrier formation for perovskite solar cells: 1 Free charge generation via absorption of light 2. Transport of charges 3.Extraction of charges.....	5
Scheme 4: Illustration of a characteristic JV- curve with corresponding parameters like the $J_{SC}$ , $V_{OC}$ , $J_{mpp}$ and $V_{mpp}$ , this schematic contains the curve resulting from illuminated (blue curve), dark conditions (black curve) and the generated power curve (red); self-designed based on reference .....	6
Scheme 5: Illustration of the device set up and working principle of a dye-sensitized solar cell; self-designed based on reference 24 .....	9
Scheme 6: 3D structure of $ABX_3$ ; mixture of 2D/3D structure of perovskite with smaller and bigger cations; 2D structure of perovskite .....	11
Scheme 7: Device architecture of perovskite solar cells; regular set up perovskite solar cell with mesoporous (left) or planar (middle) $TiO_2$ scaffold; inverted device set up with planar $TiO_2$ scaffold (right); self-designed based on refernces 42, 43, 44 .....	11
Scheme 8: Illustration of the device architecture for the prepared solar cells; glass/ITO/PEDOT:PSS/Sn based perovskite/ $PC_{60}BM/Al$ .....	28

# 8 Index of Figures

Figure 1: JV- curves of the best solar cell performance when using the purchased $SnI_2$ and $SnI_2$ of each purification method for the preparation of the solar cells .....	22
Figure 2: Boxplot of the mean values and standard deviation of the $V_{OC}$ , the $J_{SC}$ , the FF and the PCE for the purchased $SnI_2$ and the purified $SnI_2$ via bulb-to-bulb distillation, recrystallization, sublimation and purification in the tube furnace .....	24
Figure 3: XRD diffractograms of the purchased $SnI_2$ (black), purified $SnI_2$ (red), reference $SnI_2$ (blue) and reference $SnI_4$ (green); the Miller indices are assigned to the corresponding diffraction patterns of the purchased $SnI_2$ ; the reference for $SnI_2$ and $SnI_4$ are obtained from ICSD ID 1749 and 69631 .....	25
Figure 4: XRD diffractogram of the perovskite with the assigned Miller indices to the corresponding diffraction patterns .....	26
Figure 5: Absorption spectrum of $MA_{0.75}FA_{0.15}PEA_{0.1}SnI_3$ perovskite (left graph); Calculation of the band gap for $MA_{0.75}FA_{0.15}PEA_{0.1}SnI_3$ perovskite via the Tauc-Plot with a band gap energy of 1.33 eV (right graph).....	27
Figure 6: Left: solar cell performance of differently spin coated perovskite layers, with spin coating rates of 4500, 5000, 5500 and 6000 rpm; it is shown the best solar cell performance of each spin coating rate; right: variation of the PCE in dependence of the film thickness.....	29
Figure 7: Left: JV- curves of the best performance of the solar cells built with differently concentrated perovskite precursor solutions, with a concentration range from	

0.5, 0.8, 1, 1.5 and 2 M; right: PCE in dependence of differently concentrated perovskite precursor solutions .....	30
Figure 8: Best solar cell performance of solar cells prepared with different anti-solvent dropping distances (near, middle & far) .....	33
Figure 9: Optical microscope images of glass substrates spin coated with the perovskite layer with different AS dropping distances between the pipette tip and the substrate; magnification 50 times onlight; image <b>A</b> with a near distance, <b>B</b> with a middle distance and <b>C</b> with a distance far; image <b>D</b> and <b>E</b> show prepared glass/ITO substrates with the perovskite layer on it with a near AS dropping distance in <b>D</b> and a far distance for image <b>E</b> .....	34
Figure 10: Best solar cell performance of solar cells prepared with different AS dropping speed (fast or slow) and number (one time or two times AS dropping) .....	35
Figure 11: SEM images of differently prepared MA <sub>0.75</sub> FA <sub>0.15</sub> PEA <sub>0.1</sub> SnI <sub>3</sub> perovskite layers; image 1: one times AS dropping and substrate put on heating plate at RT and heated up to 70 °C, image 2: one time AS dropping and putting substrate on hot heating plate (70 °C), image 3: two times AS dropping and putting substrate on hot heating plate (70 °C); those images with a scale of 200 nm compared to those with b with a scale of 1 µm.....	37
Figure 12: Performance of differently prepared solar cells, where the perovskite layer was prepared in three different ways, either it was treated with one time AS dropping and put on a heating plate at RT and was then heated up or one time AS dropping and putting the substrates on the hot HP or substrates which were treated with two times AS dropping and were directly put it on the HP .....	38
Figure 13: Solar cell performance for different spin coating rates of the PC <sub>60</sub> BM layer of the best cell for each .....	40
Figure 14: Best performance of solar cells with PC <sub>60</sub> BM filtered either with a 0.2 µm (red) or a 0.45 µm filter (black) .....	41
Figure 15: JV- curves of solar cells built in the device architecture glass/ITO/PEDOT:PSS/ MA <sub>0.75</sub> FA <sub>0.15</sub> PEA <sub>0.1</sub> SnI <sub>3</sub> /PC <sub>60</sub> BM/Al, where a PEAI interlayer was introduced between PEDOT:PSS and MA <sub>0.75</sub> FA <sub>0.15</sub> PEA <sub>0.1</sub> SnI <sub>3</sub> layer; these curves show the best solar cell performance of each device .....	43
Figure 16: Absorption behaviour of a MA <sub>0.75</sub> FA <sub>0.15</sub> PEA <sub>0.1</sub> SnI <sub>3</sub> perovskite, as well as from perovskites with a mixture of 90 mol% SnI <sub>2</sub> with 10 mol% CuBr <sub>2</sub> and 80 mol% SnI <sub>2</sub> with 20 mol% CuBr <sub>2</sub> .....	44
Figure 17: Optical light microscopy images of different perovskite layers, A: 90% SnI <sub>2</sub> 10% CuBr <sub>2</sub> ; B: 80% SnI <sub>2</sub> 20% CuBr <sub>2</sub> .....	45
Figure 18: JV- curves of solar cells with different perovskite precursor solution, as CuBr <sub>2</sub> was added; showing the best cells of each solar cell .....	45
Figure 19: JV- curves and the received solar cell parameters (PCE, FF, V <sub>OC</sub> and J <sub>SC</sub> ) for the best solar cell performance reached within this study due to optimization processes, recorded without and with mask.....	47
Figure 20: Stability measurement of the best solar cell measured by the PCE, FF, V <sub>OC</sub> and J <sub>SC</sub> values.....	48
Figure 21: Evolution of the hysteresis with days displayed via JV-curves in the forward and backward scan of the solar cell measured on the day of preparation after three, five and 80 days .....	49
Figure 22: MPP-tracking of the best solar cell to receive the PCE without the influence of hysteresis .....	49

Figure 23: Set up of the crystallization, tilted vial with crystallized yellowish SnI <sub>2</sub> (DMF) complexes .....	53
--	----

## 9 Index of Tables

Table 1: Mean values and standard deviation of the Voc, Jsc, FF and PCE for differently purified SnI <sub>2</sub> , purified via sublimation, bulb-to-bulb distillation, recrystallization and tube furnace, the values are calculated out of five values .....	23
Table 2: Mean values and standard deviation of the film thickness and roughness for the differently spin coated perovskite layers .....	29
Table 3: Mean value and standard deviation for the performance parameters V <sub>OC</sub> , J <sub>SC</sub> , FF and PCE calculated out of the best 5 values for the different spin coating rates of the perovskite layer.....	30
Table 4: Mean values, standard deviation and best performance of the solar cells with differently concentrated perovskite precursor solutions with 0.5, 0.8, 1, 1.5 and 2 M solutions, the mean values and the standard deviation were calculated with the best five performance values .....	31
Table 5: Mean values and standard deviation for the performance of solar cells prepared with an anti-solvent either with chlorobenzene or toluene; the values were calculated out of the five best cells .....	32
Table 6: Mean values and standard deviation of the solar cell performance with three different anti-solvent dropping distances (near, middle & far); the mean values and standard deviations were calculated out of the best five values .....	33
Table 7: Mean values and standard deviation of the Voc, Jsc, FF and PCE for the different AS dropping speeds (fast or slow) and one time or two time AS dropping ....	36
Table 8: Average grain size range of the differently prepared perovskite layer, calculated from measuring the size of the ten smallest and ten biggest grains each .....	38
Table 9: Mean values and standard deviation of the Voc, Jsc, FF and PCE for the differently annealed solar cells and one time or two time AS dropping; the mean values were calculated out of the five best cells .....	39
Table 10: Mean values and standard deviation of the Voc, Jsc, FF and PCE for four different spin coating rates of the PC <sub>60</sub> BM layer, calculated out of the five best values	41
Table 11: Mean values, standard deviation and best cells of solar cell performance parameters V <sub>OC</sub> , J <sub>SC</sub> ; FF and PCE of solar cells where the PC <sub>60</sub> BM solution was either filtered with a 0.2 μm or a 0.45 μm filter, the values calculated out of the five best cells .....	42
Table 12: Mean values, standard deviation and best solar cell performance, for solar cells built in the device architecture glass/ITO/PEDOT:PSS/MA <sub>0.75</sub> FA <sub>0.15</sub> PEA <sub>0.1</sub> SnI <sub>3</sub> /PC <sub>60</sub> BM/Al and this device architecture with an interlayer of PEAI between PEDOT:PSS and MA <sub>0.75</sub> FA <sub>0.15</sub> PEA <sub>0.1</sub> SnI <sub>3</sub> layer .....	43
Table 13: Mean values, standard deviation and best solar cell performance of solar cells with varying perovskite precursor solutions via adding CuBr <sub>2</sub> to the solution .....	46
Table 14: Listed preparation methods of the substrates according to the DMF: DMSO solvent ratio, the AS treatment and the annealing step.....	52
Table 15: Listed spin coating rate and acceleration for the perovskite layer preparation .....	56

Table 16: Listed AS technique parameters that were varied and corresponding parameters which remained the same .....	56
Table 17: Spin coating rate and acceleration for the spin coating process of the PC <sub>60</sub> BM layer .....	58

# 10 References

- <sup>1</sup> International Energy Agency <<https://www.iea.org/newsroom/news/2018/march/global-energy-demand-grew-by-21-in-2017-and-carbon-emissions-rose-for-the-firs.html>> cited on: 27<sup>th</sup> June 2018
- <sup>2</sup> International Energy Agency, <https://www.iea.org/newsroom/news/2017/november/a-world-in-transformation-world-energy-outlook-2017.html>, cited on 27<sup>th</sup> June 2018
- <sup>3</sup> REN21 Renewables 2018 Global Status Report, 2018
- <sup>4</sup> IEA, Report IEA-PVPS T9, 2018
- <sup>5</sup> International Energy Agency <<https://www.iea.org/topics/renewables/solar/>>, cited on: 28<sup>th</sup> June 2018
- <sup>6</sup> Brédas, J.L.; Norton, J.E.; Cornil, J., Coropceanu, V., *Acc. Chem. Res.* **2009**, *42*, 1691–1699.
- <sup>7</sup> Mazziro, K.A.; Luscombe, C.K. *Chem. Soc. Rev.* **2015**, *44*, 78–90.
- <sup>8</sup> <<http://solarlove.org/how-solar-cells-work-components-operation-of-solar-cells/>>, cited on: 2<sup>nd</sup> May 2018
- <sup>9</sup> <[https://ocw.tudelft.nl/wp-content/uploads/solar\\_energy\\_section\\_3.pdf](https://ocw.tudelft.nl/wp-content/uploads/solar_energy_section_3.pdf)> 5.6.2018
- <sup>10</sup> <<http://www.pveducation.org/pvcdrom/solar-cell-operation/light-generated-current>> 5<sup>th</sup> June 2018
- <sup>11</sup> <[http://www.chemistry.wustl.edu/~edudev/LabTutorials/CourseTutorials/Tutorials/LED/151\\_T2\\_bonds.htm](http://www.chemistry.wustl.edu/~edudev/LabTutorials/CourseTutorials/Tutorials/LED/151_T2_bonds.htm)> 30<sup>th</sup> April 2018
- <sup>12</sup> <<http://web.ift.uib.no/AMOS/PHYS208/larsP-N/p-n-slide-lars.pdf>> 5<sup>th</sup> June 2018
- <sup>13</sup> Skvarenina, T. L.; The Power Electronics Handbook, *CRC Press*, **2002**.
- <sup>14</sup> Mao, G.-P.; Wang, W.; Shao, S.; Sun, X.-J.; Chen, S.-A.; Li, M.-H., Li, H.-M. *Rare Met.*, **2018**, *37* (2), 96-106
- <sup>15</sup> Pearsall, N., The Performance of Photovoltaic (PV) Systems; Modelling, Measurement and Assessment: *Woodhead Publishing Series in Energy Number 2017*, 105.
- <sup>16</sup> White, S.; *Solar Photovoltaic Basics*, Routledge, **2015**.
- <sup>17</sup> <<https://www.pveducation.org>> cited on 9<sup>th</sup> July 2018
- <sup>18</sup> Luque, A., Hegedus, S.; Handbook of Photovoltaic Science and Engineering Second Edition, *John Wiley & Sons*, **2011**.
- <sup>19</sup> <<https://www.pveducation.org/pvcdrom/short-circuit-current>> cited on 9<sup>th</sup> July 2018
- <sup>20</sup> <<https://www.pveducation.org/pvcdrom/solar-cell-operation/impact-of-both-series-and-shunt-resistance>> cited on 7<sup>th</sup> August 2018
- <sup>21</sup> Messenger, R. A.; Abtahi, A.; Photovoltaic Systems Engineering, Fourth Edition, *CRC Press* **2017**.
- <sup>22</sup> <<https://www.pveducation.org/pvcdrom/solar-cell-operation/solar-cell-efficiency>> cited on 9<sup>th</sup> July 2018.
- <sup>23</sup> Miller, F. P.; Vandome, A. F.; McBrewster, J.; Dye-Sensitized Solar Cell; *VDM Publishing* **2009**.
- <sup>24</sup> Kawashima, T.; Ezure, T.; Okada, K.; Matsui, H.; Goto, K.; Tanabe, N. *J. of Photochem. and Photobiol. A Chem.* **2004**, *164*, 199-202.
- <sup>25</sup> Nazeeruddin, M. K.; Baranoff, E.; Grätzel, M. *Solar Energy* **2011**, *85*, 1172-1178.
- <sup>26</sup> <http://www.greenworldinvestor.com/2011/07/04/dye-sensitised-solar-cells-dscc-processadvantages-and-disadvantages/>
- <sup>27</sup> Gong, J. Sumathy, K.; Qiao, Q.; Zhou, Z. *Renewable and Sustainable Energy Reviews* **2017**, *68*, 234-246.
- <sup>28</sup> Kakiage, K.; Aoyama, Y.; Yano, T.; Oya, K.; Fujisawa, J.; Hanaya, M. *Chem. Commun.* **2015**, *51*, 15869-16002.
- <sup>29</sup> O'Regan, B.; Grätzel, M. *Nature* **1991**, *353*, 737–740.
- <sup>30</sup> Hardin, B. E.; Snaith, H. J.; McGehee, M. D. *Nat. Photonics* **2012**, *6*, 162–169.
- <sup>31</sup> A. Kojima, K. Teshima, Y. Shirai and T. Miyasaka, *J. Am. Chem. Soc.* **2009**, *131*, 6050–6051.
- <sup>32</sup> NREL, Best Research-Cell Efficiencies, <http://www.nrel.gov>, accessed: November 2016.
- <sup>33</sup> Weber, D. Z. *Natural Science* **33b**, 1978a. 1443–1445.
- <sup>34</sup> Weber, D., *Z. Natural Science* **33**, 1978b. 862–865.

- <sup>35</sup> Roy, J. N.; Bose D. N.; Photovoltaic Science and Technology, Cambridge University Press, **2018**.
- <sup>36</sup> Mitzi, D. B.; Wang, S.; Feild, C. A.; Chess, C. A.; Guloy, A. M. *Science* **1995**, *267*, 1473–1476.
- <sup>37</sup> Calabrese, J.; Jones, N. L.; Harlow, R. L.; Herron, N.; Thorn, D. L.; Wang, Y. *J. Am. Chem. Soc.* **1991**, *113*, 2328–2330.
- <sup>38</sup> Wang, S. M.; Mitzi, D. B.; Field, C. A.; Guloy, A. *J. Am. Chem. Soc.* **1995**, *117*, 5297–5302.
- <sup>39</sup> Tsai, H.; Nie, W.; Blancon, J.-C.; Stoumpos, C. C.; Asadpour, R.; Harutyunyan, B.; Neukirch, A. J.; Verduzco, R.; Crochet, J. J.; Tretiak, S.; Pedesseau, L.; Even, J.; Alam, M. A.; Gupta, G.; Lou, J.; Ajayan, P. M.; Bedzyk, M. J.; Kanatzidis, M. G.; Mohite, A. D. *Nature* **2016**, *536*, 312–316.
- <sup>40</sup> Smith, I. C.; Hoke, E. T.; Solis-Ibarra, D.; McGehee, M. D.; Karunadasa, H. I. *Angew. Chem.* **2014**, *126*, 11414–11417
- <sup>41</sup> Hoefler, S. F.; Trimmel, G.; Rath, T. *Chemical Monthly* **2017**, *148*, 795-826.
- <sup>42</sup> Correa-Baena, J.-P.; Abate, A.; Saliba, M.; Tress, W.; Jacobsson, T. J.; Graetzel, M.; Hagfeldt, A. *Energy Environ. Sci.* **2017**, *10*, 710-727.
- <sup>43</sup> Jung, H. S.; Park, N.-G.; *Small* **2015**, *11 No. 1*, 10-25.
- <sup>44</sup> Graetzel, M.; *Nature Materials* **2014**, *Vol 13*, 838-842.
- <sup>45</sup> Liu, Y. C.; Yang, Z.; Cui, D.; Ren, X. D.; Sun, J. K.; Liu, X. J.; Zhang, J. R.; Wei, Q. B.; Fan, H. B.; Yu, F. Y.; Zhang, X.; Zhao, C. M.; Liu, S. Z. *Adv. Mater.* **2015**, *27*, 5176–5183.
- <sup>46</sup> Xing, G.; Mathews, N.; Sun, S.; Lim, S. S.; Lam, Y. M.; Graetzel, M.; Mhaisalkar, S.; Sum, T. C. *Science* **2013**, *342*, 344.
- <sup>47</sup> Dong, Q.; Fang, Y.; Shao, Y.; Mulligan, P.; Qiu, J.; Cao, L.; Huang, J.; *Science* **2015**, *347*, 967.
- <sup>48</sup> Ishihara, T. *J. Lumin.* **1994**, *60*, 269-274.
- <sup>49</sup> Zhang, W.; Saliba, M.; Stranks, S. D.; Sun, Y.; Shi, X.; Wiesner, U.; Snaith, H. J. *Nano Lett.* **2013**, *13*, 4505.
- <sup>50</sup> Sun, S. Y.; Salim, T.; Mathews, N.; Duchamp, M.; Boothroyd, C.; Xing, G. C.; Sum, T. C.; Lam, Y. M. *Energy Environ. Sci.* **2014**, *7*, 399.
- <sup>51</sup> Park, N. G. *Mater. Today* **2015**, *18*, 65.
- <sup>52</sup> Im, J.-H.; Lee, C.-R.; Lee, J.-W.; Park, S.-W.; Park, N.-G. *Nanoscale* **2011**, *3*, 4088–4093.
- <sup>53</sup> Lee, M. M.; Teuscher, J.; Miyasaka, T.; Murakami, T. N.; Snaith, H. J. *Science* **2012**, *338*, 643–647.
- <sup>54</sup> Kim, H.-S.; Lee, C.-R.; Im, J.-H.; Lee, K.-B.; Moehl, T.; Marchioro, A.; Moon, S.-J.; Humphry-Baker, R.; Yum, J.-H.; Moser, J. E.; Graetzel M.; Park, N.-G. *Sci. Rep.* **2012**, *2*, 591.
- <sup>55</sup> Jeon, N. J.; Noh, J. H.; Kim, Y. C.; Yang, W. S.; Ryu, S.; Il Seol, S. *Nat. Mater.* **2014**, *13*, 897–903.
- <sup>56</sup> Jeon, N. J.; Noh, J. H.; Yang, W. S.; Kim, Y. C.; Ryu, S.; Seo, J.; Seok, S. I. *Nature* **2015**, *517*, 476–480.
- <sup>57</sup> Yang, W. S.; Noh, J. H.; Jeon, N. J.; Kim, Y. C.; Ryu, S.; Seo, J.; Seok, S. I. *Science* **2015**, *348*, 1234–1237.
- <sup>58</sup> Bi, D.; Yi, C.; Luo, J.; De'coppet, J.-D.; Zhang, F.; Zakeeruddin, S. M.; Li, X.; Hagfeldt, A.; Graetzel, M. *Nat. Energy* **2016**, *1*, 16142.
- <sup>59</sup> Yi, C.; Luo, J.; Meloni, S.; Boziki, A.; Ashari-Astani, N.; Graetzel, C.; Zakeeruddin, S. M.; Rothlisberger, U.; Graetzel, M. *Energy Environ. Sci.* **2016**, *9*, 656–662.
- <sup>60</sup> Lee, J.-W.; Kim, D.-H.; Kim, H.-S.; Seo, S.-W.; Cho, S. M.; Park, N.-G. *Adv. Energy Mater.* **2015**, *5*, 1501310.
- <sup>61</sup> McMeekin, D. P.; Sadoughi, G.; Rehman, W.; Eperon, G. E.; Saliba, M.; Hoerantner, M. T.; Haghighirad, A.; Sakai, N.; Korte, L.; Rech, B.; Johnston, M. B.; Herz, L. M.; Snaith, H. J.; *Science* **2016**, *351*, 151–155.
- <sup>62</sup> Saliba, M.; Matsui, T.; Seo, J.-Y.; Domanski, K.; CorreaBaena, J.-P.; Nazeeruddin, M. K.; Zakeeruddin, S. M.; Tress, W.; Abate, A.; Hagfeldt A.; Gratzel, M.; *Energy Environ. Sci.* **2016**, *9*, 1989–1997.
- <sup>63</sup> Saliba, M.; Matsui, T.; Domanski, K.; Seo, J.-Y.; Ummadisingu, A.; Zakeeruddin, S. M.; Correa-Baena, J.-P.; Tress, W. R.; Abate, A.; Hagfeldt, A.; Graetzel, M. *Science* **2016**, *354*, 206–209.

- <sup>64</sup> Liu, M.; Johnston, M. B.; Snaith, H. J. *Nature* **2013**, *501*, 395-398.
- <sup>65</sup> H. Zhou, Q. Chen, G. Li, S. Luo, T.-b. Song, H.-S. Duan, Z. Hong, J. You, Y. Liu and Y. Yang, *Science*, **2014**, *345*, 542-546.
- <sup>66</sup> Correa Baena, J. P.; Steier, L.; Tress, W.; Saliba, M.; Neutzner, S.; Matsui, T.; Giordano, F.; Jacobsson, T. J.; Srimath Kandada, A. R.; Zakeeruddin, S. M.; Petrozza, A.; Abate, A.; Nazeeruddin, M. K.; Gratzel, M.; Hagfeldt, A. *Energy Environ. Sci.*, 2015, *8*, 2928-2934.
- <sup>67</sup> Zhu, Z.; Bai, Y.; Liu, X.; Chueh, C.-C.; Yang, S.; Jen, A. K. Y.; *Adv. Mater.* **2016**, *28*, 6478-6484.
- <sup>68</sup> Seo, J.-Y.; Matsui, T.; Luo, J.; Correa-Baena, J.-P.; Giordano, F.; Saliba, M.; Schenk, K.; Ummadisingu, A.; Domanski, K.; Hadadian, M.; Hagfeldt, A.; Zakeeruddin, S. M.; Steiner, U.; Gratzel, M.; Abate, A. *Adv. Energy Mater.* **2016**, *6*, 1600767.
- <sup>69</sup> Anaraki, E. H.; Kermanpur, A.; Steier, L.; Domanski, K.; Matsui, T.; Tress, W.; Saliba, M.; Abate, A.; Gratzel, M.; Hagfeldt, A.; Correa-Baena, J.-P. *Energy Environ. Sci.* **2016**, *9*, 3128-3134.
- <sup>70</sup> Papanikolaou, N. C.; Hatzidaki, E. G.; Belivanis, S.; Tzanakakis, G. N.; Tsatsakis, A.M. *Med Sci Monit* **2005**, *11*, 329-336.
- <sup>71</sup> <<http://www.who.int/news-room/fact-sheets/detail/lead-poisoning-and-health>> cited on: 8<sup>th</sup> August 2018
- <sup>72</sup> Shannon, R. D. *Acta Crystallogr. Sect. A* **1976**, *32*, 751-767.
- <sup>73</sup> Chen, Q.; De Marco, N.; Yang, Y.; Bin Song, T.; Chen, C. C.; Zhao, H.; Hong, Z.; Zhou, H.; Yang, Y. *Nano Today* **2015**, *10*, 355-396.
- <sup>74</sup> Krishnamoorthy, T.; Ding, H.; Yan, C.; Leong, W. L.; Baikie, T.; Zhang, Z.; Sherburne, M.; Li, S.; Asta, M.; Mathews, Mhaisalkar, S. G. *J. Mater. Chem. A* **2015**, *3*, 23829-23832.
- <sup>75</sup> Stoumpos, C. C.; Frazer, L.; Clark, D. J.; Kim, Y. S.; Rhim, S. H.; Freeman, A. J.; Ketterson, J. B.; Jang, J. I.; Kanatzidis, M. G. *J. Am. Chem. Soc.* **2015**, *137*, 6804-6819.
- <sup>76</sup> Kopacic, I.; Friesenbichler, B.; Hoefler, S. F.; Kunert, B.; Plank, H.; Rath, T.; Trimmel, G. *ACS Appl. Energy Mater.* **2018**, *1*, 343-347.
- <sup>77</sup> Lyu, M.; Yun, J.-H.; Cai, M.; Jiao, Y.; Bernhardt, P. V.; Zhang, M.; Wang, Q.; Du, A.; Wang, H.; Liu, G.; Wang, L. *Nano Res.* **2016**, *9*, 692-702.
- <sup>78</sup> Ran, C.; Wu, Z.; Xi, J.; Yuan, F.; Dong, H.; Lei, T.; He, X.; Hou, X. *J. Phys. Chem. Lett.* **2017**, *8*, 394-400.
- <sup>79</sup> Zhang, X.; Wu, G.; Gu, Z.; Guo, B.; Liu, W.; Yang, S.; Ye, T.; Chen, C.; Tu, W.; Chen, H. *Nano Res* **2016**, *9*, 2921.
- <sup>80</sup> Park, B.-W.; Philippe, B.; Zhang, X.; Rensmo, H.; Boschloo, G.; Johansson, E. M. J. *Adv. Mater. (Weinheim, Ger.)* **2015**, *27*, 6806-6813.
- <sup>81</sup> Lehner, A. J.; Fabini, D. H.; Evans, H. A.; Hebert, C.-A.; Smock, S. R.; Hu, J.; Wang, H.; Zwanziger, J. W.; Chabynyc, M. L.; Seshadri, R. *Chem. Mater.* **2015**, *27*, 7137-7148.
- <sup>82</sup> Saparov, B.; Hong, F.; Sun, J.-P.; Duan, H.-S.; Meng, W.; Cameron, S.; Hill, I. G.; Yan, Y.; Mitzi, D. B. *Chem Mater.* **2015**, *27*, 5622-5632.
- <sup>83</sup> Harikesh, P. C.; Mulmudi, H. K.; Ghosh, B.; Goh, T. W.; Ting Teng, Y.; Thirumal, K.; Lockrey, M.; Weber, K.; Koh, T. M.; Li, S.; Mhaisalkar, S.; Mathews, N. *Chem. Mater.* **2016**, *28*, 7496-7504.
- <sup>84</sup> Hebig, J.-C.; Kühn, I.; Flohre, J.; Kirchartz, T.; *ACS Energy Lett.* **2016**, *1*, 309-314
- <sup>85</sup> Mitzi, D. B. *Inorg. Chem.* **2000**, *39*, 6107-6113.
- <sup>86</sup> Mitzi, D. B. *J. Chem. Soc., Dalton Trans.* **2001**, 1-12.
- <sup>87</sup> Jakubas, R.; Sobczyk, L. *Phase Transitions* **1990**, *20*, 163-193.
- <sup>88</sup> Zaleski, J.; Jakubas, R.; Sobczyk, L.; Mroz, J. *Ferroelectrics* **1990**, *103*, 83-90.
- <sup>89</sup> Jakubas, R.; Decressain, R.; Lefebvre, J. *Phase Crystals J. Phys. Chem. Solids* **1992**, *53*, 755-759.
- <sup>90</sup> Pawlaczyk, C.; Jakubas, R.; Unruh, H. G. *Solid State Commun.* **1998**, *108*, 247-250.
- <sup>91</sup> Brandt, R. E.; Stevanović, V.; Ginley, D. S.; Buonassisi, T. *MRS Commun.* **2015**, *5*, 265-275.
- <sup>92</sup> Stoumpos, C.C.; Malliakas, C.D.; Kanatzidis, M.G. *Inorg. Chem.* **2013**, *52*, 9019
- <sup>93</sup> Hao, F.; Stoumpos, C. C.; Chang, R. P.; Kanatzidis, M. G. *J. Am. Chem. Soc.* **2014**, *136*, 8094.
- <sup>94</sup> Yang, Z.; Rajagopal, A.; Chueh, C. C.; Jo, S. B.; Liu, B.; Zhao, T.; Jen, A. K. *Adv. Mater.* **2016**, *28*, 8990.
- <sup>95</sup> Shockley, W.; Queisser, H. J. *J. Appl. Phys.* **1961**, *32*, 510.

- <sup>96</sup> Rühle, S. *Solar Energy* **2016**, *130*, 139-147.
- <sup>97</sup> Wu, B.; Zhou, Y.; Xing, G.; Xu, Q.; Garces, H. F.; Solanki, A.; Goh, T. W.; Padture, N. P.; Sum, T. C. *Adv. Funct. Mater.* **2017**, *27*, 1604818.
- <sup>98</sup> Noel, N. K.; Stranks, S. D.; Abate, A.; Wehrenfennig, C.; Guarnera, S.; Haghighirad, A.-A.; Sadhanala, A.; Eperon, G. E.; Pathak, S. K.; Johnston, M. B.; Petrozza, A.; Herz, L. M.; Snaith, H. J. *Energy Environ. Sci.* **2014**, *7*, 3061.
- <sup>99</sup> Liao, W. Zhao, D. Yu, Y. Grice, C. R. Wang, C. Cimardi, A. J. Schulz, P. Meng, W. Zhu, K. Xiong, R.-G. Yan, Y. *Adv. Mater.* **2016**, *28*, 9333.
- <sup>100</sup> Hao, F.; Stoumpos, C.C.; Guo, P.; Zhou, N.; Marks, T.J.; Chang, R.P.H.; Kanatzidis, M.G. *J. Am. Chem. Soc.* **2015**, *137*, 11445.
- <sup>101</sup> Shao, S.; Liu, J.; Portale, G.; Fang, H. H.; Blake, G. R.; Brink, G. H. ten; Koster, L. J. A.; Loi, M. A. *Adv. Energy Mater.* **2018**, *8*, 1702019 (1-10).
- <sup>102</sup> Wang, N.; Zhou, Y.; Ju, M.-G.; Garces, H.F.; Ding, T.; Pang, S.; Zeng, X.C.; Padture, N.P.; Sun, X.W. *Adv. Energy Mater.* **2016**, *6*, 1601130.
- <sup>103</sup> Hao, F.; Stoumpos, C.C.; Cao, D.H.; Chang, R.P.H.; Kanatzidis, M.G.; *Nat. Photonics* **2014**, *8*, 489.
- <sup>104</sup> Zhao, Z.; Gu, F.; Li, Y.; Sun, W.; Ye, S.; Rao, H.; Liu, Z.; Bian, Z.; Huang, C. *Adv. Sci.* **2017**, *4*, 1700204 (1-7).
- <sup>105</sup> Ke, W.; Stoumpos, C. C.; Spanopoulos, I.; Mao, L.; Chen, M.; Wasielewski, M. R.; Kanatzidis, M. G. *J. Am. Chem. Soc.* **2017**, *139*, 14800-14806.
- <sup>106</sup> Kumar, M.H.; Dharani, S.; Leong, W.L.; Boix, P.P.; Prabhakar, R.R.; Baikie, T.; Shi, C.; Ding, H.; Ramesh, R.; Asta, M.; Graetzel, M.; Mhaisalkar, S.G.; Mathews, N. *Adv. Mater.* **2014**, *26*, 7122–7127.
- <sup>107</sup> Lee, S. J.; Shin, S. S.; Kim, Y. C.; Kim, D.; Ahn, T. K.; Noh, J. H.; Seo, J.; Seok, S. I. *J. Am. Chem. Soc.* **2016**, *138* (12), 3974–3977.
- <sup>108</sup> Marshall, K.; Walker, M.; Walton, R.I.; Hatton, R. *Nat. Energy* **2016**, *1*, 16178.
- <sup>109</sup> Song, T.-B.; Yokoyama, T.; Stoumpos, C.C.; Logsdon, J.; Cao, D.H.; Wasielewski, M.R.; Aramaki, S.; Kanatzidis, M.G. *J. Am. Chem. Soc.* **2017**, *139*, 836.
- <sup>110</sup> Xi, J.; Wu, Z.; Jiao, B.; Dong, H.; Ran, C.; Piao, C.; Lei, T.; Song, T.-B.; Ke, W.; Yokoyama, T.; Hou, X.; Kanatzidis, M.G. *Adv. Mater.* **2017**, *29*, 1606964.
- <sup>111</sup> Zhu, Z.; Chueh, C.-C.; Li, N.; Mao, C.; Jen, A. *Adv. Mater.* **2018**, *30*, 1703800.
- <sup>112</sup> Ke, W.; Priyanka, P.; Vegiraju, S.; Stoumpos, C. C.; Spanopoulos, I.; Soe, C. M. M.; Marks, T. J.; Chen, M.-C.; Kanatzidis, M. G. *J. Am. Chem. Soc.* **2018**, *140*, 388-393.
- <sup>113</sup> Ke, W.; Stoumpos, C.C.; Logsdon, J.L.; Wasielewski, M.R.; Yan, Y.; Fang, G.; Kanatzidis, M.G. *J. Am. Chem. Soc.* **2016**, *138*, 14998.
- <sup>114</sup> Feng, J.; Xiao, B. *J. Phys. Chem.* **2014**, *118*, 19655–19660.
- <sup>115</sup> Eperon, G.E.; Stranks, S.D.; Menelaou, C.; Johnston, M.B.; Herz, L.M.; Snaith, H.J. *Energy Environ. Sci.* **2014**, *7*, 982–988.
- <sup>116</sup> Koh, T. M.; Krishnamoorthy, T.; Yantara, N.; Shi, C.; Leong, W. L.; Boix, P. P.; Grimsdale, A. C.; Mhaisalkar, S. G.; Mathews, N. *J. Mater. Chem. A* **2015**, *3*, 14996–15000.
- <sup>117</sup> Yang, J.; Siempelkamp, B. D.; Liu, D.; Kelly, T. L. *ACS Nano* **2015**, *9*, 1955–1963.
- <sup>118</sup> Christians, J. A.; Miranda Herrera, P. A.; Kamat, P. V. *J. Am. Chem. Soc.* **2015**, *137*, 1530–1538.
- <sup>119</sup> Leguy, A. M. A.; Hu, Y.; Campoy-Quiles, M.; Alonso, M. I.; Weber, O. J.; Azarhoosh, P.; Van Schilfhaarde, M.; Weller, M. T.; Bein, T.; Nelson, J.; Docampo, P.; Barnes, P. R. F. *Chem. Mater.* **2015**, *27*, 3397–3407.
- <sup>120</sup> Zhao, L.; Kerner, R. A.; Xiao, Z.; Lin, Y. L.; Lee, K. M.; Schwartz, J.; Rand, B. P. *ACS Energy Lett.* **2016**, *1*, 595–602.
- <sup>121</sup> Liu, Z.; Sun, B.; Shi, T.; Tang, Z.; Liao, G. *J. Mater. Chem. A* **2016**, *4*, 10700–10709.
- <sup>122</sup> Mitzi, D. B.; Feild, C.; Harrison, W.; Guloy, A. *Nature* **1994**, *369*, 467–469.
- <sup>123</sup> Kagan, C. R.; Mitzi, D. B.; Dimitrakopoulos, C. D. *Science* **1999**, *286*, 945–947.
- <sup>124</sup> Cao, D. H.; Stoumpos, C. C.; Farha, O. K.; Hupp, J. T.; Kanatzidis, M. G. *J. Am. Chem. Soc.* **2015**, *137*, 7843–7850.
- <sup>125</sup> Liao, Y.; Liu, H.; Zhou, W.; Yang, D.; Shang, Y.; Shi, Z.; Li, B.; Jiang, X.; Zhang, L.; Quan, L. N.; Quintero-Bermudez, R.; Sutherland B. R.; Mi, Q.; Sargent, E. H.; Ning, Z. *J. Am. Chem. Soc.* **2017**, *139*, 6693 – 6699.

- 
- <sup>126</sup> Ke, W.; Stoumpos, C. C.; Zhu, M.; Mao, L.; Spanopoulos, I.; Liu, J.; Kontsevoi, O. Y.; Chen, M.; Sarma, D.; Zhang, Y.; Wasielewski, M. R.; Kanatzidis, M. G. *Sci. Adv.* **2017**, *3*, 1701293.
- <sup>127</sup> Liu, J.; Wu, Y.; Qin, C.; Yang, X.; Yasuda, T.; Islam, A.; Zhang, K.; Peng, W.; Chen, W.; Han, L. *Energy Environ. Sci.* **2014**, *7*, 2963.
- <sup>128</sup> Yokoyama, T.; Cao, D. H.; Stoumpos, C. C.; Song, T. B.; Sato, Y.; Aramaki, S.; Kanatzidis, M. G. *J. Phys. Chem. Lett.* **2016**, *7*, 776.
- <sup>129</sup> Chen, K.; Wu, P.; Yang, W.; Su, R.; Luo, D.; Yang, X.; Tu, Y.; Zhu, R.; Gong, Q. *Nano Energy*, **2018**, *49*, 411-418.
- <sup>130</sup> Friesenbichler, B. Investigation of different cations in organic/inorganic tin halide perovskites for solar cell applications. Master Thesis, Technical University, Graz, **2017**.
- <sup>131</sup> Li, M.; Wang, Z.-K.; Zhuo, M.-P.; Hu, Y.; Hu, K.-H.; Ye, Q.-Q.; Jain, S. M.; Yang, Y.-G.; Gao, X.-Y.; Liao, L.-S. *Adv. Mater.* **2018**, 1800258 (1-7).
- <sup>132</sup> Lee, S. J.; Shin, S. S.; Im, J.; Ahn, T. K.; Noh, J. H.; Jeon, N. J.; Seok, S. I.; Seo, J. *ACS Energy Lett.* **2018**, *3*, 46-53.
- <sup>133</sup> <[http://www.chemicalbook.com/ChemicalProductProperty\\_US\\_CB7479195.aspx](http://www.chemicalbook.com/ChemicalProductProperty_US_CB7479195.aspx)> cited on 3<sup>rd</sup> May 2018
- <sup>134</sup> <<https://www.sigmaaldrich.com/catalog/product/aldrich/466352?lang=de&region=AT>> cited on 3<sup>rd</sup> May 2018
- <sup>135</sup> Holleman, A. F., Wiberg, E., W., Wiberg, N.: *Lehrbuch der Anorganische Chemie*, Walter de Gruyter, **2007**
- <sup>136</sup> Howie, R. A.; Moser, W.; Trevena, I. C. *Acta Cryst. B* **28**, **1972**, 2965-2971.
- <sup>137</sup> Reuter, H.; Pawlak, R. *Cryst. Mater.* **2009**, *216 (1)*, 34-38.
- <sup>138</sup> Baloch, A. A. B., Hossain, M. I., Tabet, N., Alharbi, F. H. *J. Phys. Chem. Lett.* **2018**, *9*, 426-434.
- <sup>139</sup> Ozaki, M.; Katsuki, Y.; Liu, J.; Handa, T.; Nishikubo, R.; Yakumar, S.; Hashikawa, Y.; Murata, Y.; Saito, T.; Shimakawa, Y.; Kanemitsu, Y.; Saeki, A.; Wakamiya, A. *ACS Omega* **2017**, *2*, 7016-7021.